Modelling of Multi-antenna Wireless Channels and Relay Based Communication Systems

BABU SENA PAUL

Modelling of Multi-antenna Wireless Channels and Relay Based Communication Systems

A

Thesis Submitted

in Partial Fulfillment of the Requirements

for the Degree of

DOCTOR OF PHILOSOPHY

By

BABU SENA PAUL

Department of Electronics and Communication Engineering

Indian Institute of Technology Guwahati

Guwahati - 781 039, INDIA.

December, 2009

Modelling of Multi-antenna Wireless Channels and Relay Based Communication Systems

A

Thesis Submitted

in Partial Fulfillment of the Requirements

for the Degree of

DOCTOR OF PHILOSOPHY

By

BABU SENA PAUL

Department of Electronics and Communication Engineering

Indian Institute of Technology Guwahati

Guwahati - 781 039, INDIA.

December, 2009

Certificate

This is to certify that the thesis entitled "**Modelling of Multi-antenna Wireless Channels and Relay Based Communication Systems**", submitted by Babu Sena Paul, a research student in the *Department of Electronics and Communication Engineering , Indian Institute of Technology Guwahati*, for the award of the degree of **Doctor of Philosophy**, is a record of an original research work carried out by him under my supervision and guidance. The thesis has fulfilled all requirements as per the regulations of the Institute and in my opinion has reached the standard needed for submission. The results embodied in this thesis have not been submitted to any other University or Institute for the award of any degree or diploma.

Dated:
Guwahati.

Dr. Ratnajit Bhattacharjee
Associate Professor
Dept. of Electronics and Communication Engg.
Indian Institute of Technology
Guwahati - 781 039
India.

THIS WORK IS DEDICATED TO

MY MOM AND DAD

Acknowledgements

I feel it is a great privilege to express my deepest and most sincere gratitude to my supervisor, Dr. Ratnajit Bhattacharjee for his suggestions, constant encouragement and support during the course of the thesis work. I am also grateful to the other members of my doctoral committee, namely Prof. Anil Mahanta, Dr. H. Nemade and Dr. A. Mitra for their valuable comments on my work. I take this opportunity to thank Prof. S. Majhi, the head of the department for his kindness in allowing me to use various computing facilities of the department. I would also like to thank the other faculty members of the department, namely Prof. P. K. Bora, Prof. S. Dandapat, Dr. A. Rajesh, and Dr. S. R. M. Prasanna for their encouragement and help. I am also thankful to Prof. S. Nandi, Dept. of Computer Science IIT Guwahati for sanctioning full financial support for my travel to Bangkok to attend IEEE APCC 2007 conference.

I am thankful to the Institute of Electronics and Telecommunication Engineers (IETE), New Delhi, India, for supporting part of my research work.

I am also grateful to all the members of the Research and technical staff of the department, namely L. N. Sharma, Sanjib Das, and Utpal Kumar Sarma without whose help I could not have completed this assignment. I thank all my fellow research students and M. Tech students for their cooperation. My thanks also go out to all my friends, namely Dr. P. Vinod, A. Ali, Dakua, Katiyar, R. Subadar and Senthil who have made my stay at Guwahati a memorable period of my life.

I would like to thank my family for the support they provided me through my entire life and in particular, I must acknowledge my father Nirmalendu Paul, mother Sipra Paul, brother Satyakama Paul and aunt Manju Paul without whose love, encouragement and assistance, I would not have finished.

Finally, I must express my heart-felt gratitude to my wife Dipanwita Paul for her constant encouragement and support throughout my research work.

(Babu Sena Paul)

Abstract

Different issues related to modelling of multi-antenna wireless channels and relay based communication systems have been investigated in this thesis. The effects of array geometry and orientation of arrays in a MIMO system have been investigated in the frame work of geometrically based one ring scattering model for a macrocellular scenario. A technique based on scattering parameters has been developed to find the channel matrix for a MIMO system, modelled geometrically from a microwave perspective, employing suitably terminated antennas acting as scatterers. The performance of a 2×2 MIMO system has also been evaluated taking mutual coupling between the antenna elements into consideration. Using geometrical based single bounce modelling, characteristics of mobile-to-mobile communication channel has been studied and analytical expressions has been derived for probability density function of angle of arrival and time of arrival of signals in terms of model parameters. A virtual MIMO system in the form of two-hop relay channels constituting two diversity paths has been investigated for bit error rate performance with selection and maximal ratio combining techniques applied at the receiver.

The works reported in this thesis are expected to contribute towards the better understanding of certain issues related to modelling of multi-antenna wireless communication channels and relay based systems.

Contents

List of Figures

List of Tables

Nomenclature

AOA	Angle of Arrival
AOD	Angle of Departure
AWGN	Additive White Gaussian Noise
BER	Bit Error Rate
BS	Base Station
CDF	Cumulative Distribution Function
DOA	Direction of Arrival
EGC	Equal Gain Combining
GBSB	Geometrically Based Single Bounce
iid	Independent and Identically Distributed
ISI	Inter Symbol Interference
M2M	Mobile-to-Mobile
MHz	Mega Hertz
MIMO	Multiple Input Multiple Output
MISO	Multiple Input Single Output
MRC	Maximal Ratio Combining
MS	Mobile Station
pdf	Probability Density Function
QoS	Quality of Service
rms	Root Mean Square
RV	Random Variable
Rx.	Receiver
SC	Selection Combining
SIMO	Single Input Multiple Output
SIR	Signal to Interference Ratio
SISO	Single Input Single Output

***S*-matrix**	Scattering Matrix
***s*-parameter**	Scattering Parameter
SNR	Signal to Noise Ratio
TOA	Time of Arrival
Tx.	Transmitter
UCA	Uniform Circular Array
ULA	Uniform Linear Array

Mathematical Notations

α_{bs}	Angle between x-axis and the base station's antenna array.
α_{ms}	Angle between x-axis and the mobile station's antenna array.
α_v	Angle between x-axis and the direction of motion of the mobile station.
ϕ_{ms}^n	Angle between x-axis and the n^{th} incoming to the mobile station.
Φ_{max}^{BS}	Maximum angle subtended by the scattering circle at the base station.
λ	Wavelength.
BS_i	i^{th} antenna of the base station array
$\mathbf{C_{BS}}$	Coupling matrix at the base station.
$\mathbf{C_{MS}}$	Coupling matrix at the mobile station.
D	Distance between the transmitter and the receiver.
d_{bs}	Antenna spacings at the base station.
d_{ms}	Antenna spacing at the the mobile station.
f_{max}	Maximum doppler frequency.
f_n	Doppler frequency of the n^{th} wave.
$\mathbf{H}$	Channel matrix.
$\mathbf{H'}$	Channel matrix including coupling effects.
h_{ij}	Channel matrix element between the j^{th} transmit and i^{th} receive antennas.
$\mathbf{I}$	Identity matrix.

m	Nakagami parameter.
MS_i	i^{th} antenna of the mobile station array.
N	Number of scatterers.
N_R	Number antennas at the receiver.
N_T	Number of antennas at the transmitter.
$\mathbf{R_H}$	Correlation of the channel matrix.
S_n	n^{th} scatterer.
v	Velocity.
$\mathbf{w}$	Additive white Gaussian noise vector.
$\mathbf{x}$	Transmitted signal vector.
$\mathbf{y}$	Received signal vector.
$\mathbf{Z}$	The mutual impedance matrix.
Z_A	Antenna impedance.
Z_T	Terminating impedance at the antenna element.
$\langle a, b \rangle$	Correlation between a and b.
$\otimes$	Kronecker product.
$E[\cdot]$	Expectation operator.
$(\cdot)^H$	Hermetian.

List of Publications

Journals

Published:

1. B. S. Paul and R. Bhattacharjee, "Analysis of different combining schemes of two amplify-forward relay branches with individual links experiencing Nakagami fading," *International Journal of Information Technology*, vol. 4, no. 3, pp. 189–196, 2008.

2. H. Katiyar, B. S. Paul and R. Bhattacharjee, "User cooperation in TDMA wireless system," *IETE Technical Review*, vol. 25, no. 5, pp. Sep-Oct 270–276, 2008.

3. B. S. Paul and R. Bhattacharjee, "MIMO channel modeling: A Review," *IETE Technical Review*, vol. 25, no. 6, pp. 315–319, Nov-Dec 2008.

Accepted for publication:

1. B. S. Paul, A. Hassan, H.Medhasiya and R. Bhattacharjee, "Time and Angle of Arrival Statistics of Mobile-to-Mobile Communication Channel Employing Circular Scattering Model," *IETE Journal of Research*.

Under Review:

1. B. S. Paul and R. Bhattacharjee, "Time and Angle of Arrival Statistics of Mobile-to-Mobile Communication Channel Employing Dual Annular Strip Model," *IETE Journal of Research*.

Conferences

Published:

1. B. S. Paul and R. Bhattacharjee, "Effect of array geometry on the capacity of outdoor MIMO communication: A study," *In Proceedings of IEEE INDICON*, New Delhi, India, September, 2006.

2. B. S. Paul and R. Bhattacharjee, "Studies on the mutual coupling of one ring mimo channel simulation model," *In Proceedings of the International Conference on Computers and Devices for Communication (CODEC-06)*, Kolkata, India, pp. 100-103, December, 2006.

3. B. S. Paul and R. Bhattacharjee, "On different geometrically based channel models for MIMO communication," *In Proceedings of The 10th International Symposium on Wireless Personal Multimedia Communications (WPMC)*, India, pp. 824-827, December 2007.

4. B. S. Paul and R. Bhattacharjee, "Selection combining of two amplify-forward relay branches with individual links experiencing Nakagami fading," *In Proceedings of IEEE 2007 Asia Pacific Conference on Communication (APCC)*, Bangkok, pp. 449-452, October 2007.

5. B. S. Paul and R. Bhattacharjee, "Maximal ratio combining of two amplify-forward relay branches with individual links experiencing Nakagami fading," *In Proceedings of IEEE TENCON'07*, Taiwan, November 2007.

6. B. S. Paul and R. Bhattacharjee, "An S-parameter based modeling of a MIMO channel using half-wave dipole antennas," *In Proceedings of the Thirteenth National Conference on Communications (NCC)*, IIT Kanpur, India, January, 2007.

Chapter 1

Introduction

Wireless communication is one of the fastest growing segments of the communication industry. Since the mid 1990's wireless communication technology in general and cellular communication industry in particular has witnessed an explosive growth. In a brief span of time, wireless communication technology has already evolved through three generations, each generation being characterised by the access technology it used and the services it offered. The third generation technologies are currently in use and the fourth generation, also sometimes called as the next generation, are under development. Along with wireless cellular communication, wireless networks are also currently supplementing or in many cases replacing the wired network. The growth of wireless technology is not only in terms of the number of users but also in terms of technological developments and breakthroughs that have taken place over the last couple of decades [Gol05]. Wireless systems are also witnessing major changes in terms of the nature of traffic they require to deal with. Modern wireless systems process significantly large amount of multimedia content along with the usual voice traffic. Future wireless systems are envisaged to offer ubiquitous high data rate coverage over large areas. Such requirements pose fundamental challenges for a wireless system designer as well as for the wireless research community. The challenges mainly comes from the fact that the wireless systems are required to support growing demand for high data rate within the limited available spectrum and also require to overcome the effects of multipath fading and interference which are inherent with the wireless channel.

In recent times, multiple antenna systems has emerged as a promising technique for solving the capacity bottleneck in wireless systems. In literature, a wireless channel using multiple antennas at both the transmitter and receiver ends is referred to as a Multiple-input Multiple-output (MIMO)

channel. For a given transmit power and channel bandwidth, this new technology uses sophisticated techniques for boosting the channel capacity significantly higher than what is attainable by any known methods based on a Single-input Single-output (SISO) channel [GSS+03]. Such techniques are also called space-time techniques, where along with time, which is a natural dimension of any communication system, the spatial dimension of the channels are also exploited [GS05]. MIMO uses signal scattering in wireless channel to its advantage. Such scattering is otherwise considered as a pitfall for wireless communication. When wireless communication environment is endowed with rich scattering, MIMO channel capacity is shown to increase roughly proportional to spatial dimension of the channel, which is given by the minimum of the number of antennas used in the transmitter and the receiver. MIMO techniques have been well studied in the literature and a number of promises in these schemes are documented in a large number of research publications which have appeared over the last few years [FJ98, Tel99, GSS+03]. Use of multiple antennas in wireless communication systems started with the introduction of diversity antenna and beamforming systems. A diversity system uses an array with antenna elements separated enough to create multiple spatially uncorrelated signal paths. Such systems reduce signal outage and improves reliability by suitably combining the signals received from different antenna elements. A beamforming array, also called smart antennas, have closely spaced antenna elements and with the help of sophisticated adaptive signal processing techniques, can perform spatial filtering, extend the range of a communication system and also track mobile users. Depending on the location of the antenna array, i.e., whether at the transmitter or at the receiver, such multiple antenna systems are categorised as multiple-input single-output (MISO) or single-input multiple-output (MISO) system [PNG03]. As mentioned, a MIMO system uses multiple antennas at both the transmitter and the receiver. MIMO channel modelling constitutes an important component in the design, analysis and development of MIMO communication systems. A signal propagating over a wireless channel experiences fading due to its interaction with the propagation media. The mechanism behind electromagnetic wave propagation are diverse but can generally be attributed to reflection, diffraction and scattering, which occur due to the presence of various obstacles present in the propagation path. Wired channels are stationary and predictable whereas, wireless channels are random and do not offer easy analysis. Modelling of such radio channels are considered to be one of the most difficult part of mobile radio system design [Rap01].

Signal fading in a wireless channel are usually classified as large scale fading and small

scale fading. Large scale fading is also termed as path loss and depend upon signal attenuation in the propagation environment. Small scale fading or simply fading describes rapid fluctuations of signal amplitude and phases over a short period of time or small travel distances. Such fading results due to interference of multipath components and based on the delay spread of the resolvable multipath components. Fading can be further categorised as flat fading and frequency selective fading. Fading is also classified as slow or fast fading depending on the Doppler shift introduced in the signal due to mobility of communicating nodes. Channel modelling takes into account the effects of the propagation environment so that the same can be given due consideration during system design. A number of approaches have been developed for modelling of MIMO channels and analysing MIMO system performance based on such channel conditions [LR96, FMB98, SFGK00, KSP+02, AK02, PRR02, Jan02, OEP03, DM05, WHOB06, JT07], some of which are covered in greater detail in the later chapters of this thesis.

Along with the changing behaviour of communication traffic, nature of communication in wireless systems are also witnessing major changes. In a typical scenario, mobile devices communicate with each other via base stations which can handle larger power as well as have very high processing capabilities in comparison to the mobile devices. Recently, with the introduction of mobile adhoc networks, wireless sensor networks, and intelligent transport systems, direct communication between mobile transmitter and receiver over wireless medium has become a necessity. Such communication systems are commonly referred to as mobile-to-mobile (M2M) communication systems. Design of M2M systems require understanding and modelling of the channels and there has been a lot of research activities in recent times in this direction [AH86, Akk94, VF97, PHYK05a, PHYK05b, PSP05, ZS06]. An M2M system can have multiple antennas on one or both sides of the link.

Although from system design point of view MIMO has shown tremendous prospect, there are several implementation issues which are still considered to be major hindrances in harnessing the benefits of MIMO. Mobile devices have limited power and processing capabilities and often the physical size limitation does not permit placement of multiple antennas with proper placing as demanded from a MIMO system design consideration. The broadcast nature of the wireless channel makes it possible for the other nodes to overhear the transmission from a node [LV07]. Processing of these overheard information and relaying the same to the destination node can create spatial diversity and help in obtaining higher reliability and throughput for a network containing

single antenna nodes. Such communication in literature is referred to as cooperative relaying [SEA03a, SEA03b, HZF04, PSP06], which essentially creates a virtual MIMO system with single antenna devices.

This thesis has addressed certain issues related to modelling of multiple antenna wireless channels and relay based communication systems, which has been identified after a thorough study of the existing literatures. Next section gives an outline of the thesis, the issues addressed and highlights some of the contributions that have been made towards better understanding and modelling of multi-antenna channels and relay based wireless systems.

1.1 Outline of the Thesis and Contributions

As mentioned earlier, the thesis deals with channel modelling of multi-antenna wireless systems and also investigates relay based systems. This section provides an outline of the thesis discussing the issues addressed in the different chapters, and summarises the contributions.

Chapter 2 of the thesis starts with a brief review of some of the most popular MIMO channel modelling approaches. The effects of array geometry and change in orientation of the transmitting and the receiving arrays on MIMO system performance have been considered next. Details of an S-parameter based approach for determination of the channel matrix **H**, which has been developed in this thesis for the purpose of modelling MIMO channels from a microwave perspective has been addressed next. This has been followed by investigation on the effects of mutual coupling between the antennas on the capacity of a MIMO system, using geometry based channel modelling approach. The contributions made from the investigations reported in this chapter are summarised as follows:

- Evaluation of channel capacity variation for certain combination of array geometries.
- Development of a scattering matrix (S-matrix) based approach for determining the channel matrix **H** when the MIMO channel is modelled from a microwave perspective.
- Incorporation of the effect of mutual coupling in the geometrically based MIMO channel model for evaluation of the MIMO channel capacities.

Chapter 3 extends the geometrically based single bounce circular scattering model for macrocellular scenario to M2M communication scenario, where both the transmitting and the receiving

mobile stations are assumed to be surrounded by uniformly distributed local scatterers. As either the transmitter or the receiver or both may have multiple antennas, analytical expression for the angle of arrival statistics (AOA) are derived for such M2M channel. Knowledge of the AOA statistics aids in beam forming and beam steering applications. Analytical expressions for the time of arrival (TOA) statistics for M2M channels, has also been derived. The TOA statistics help in mobile device location applications and in determining the data rates at which the channel will behave as flat faded and hence the requirement of equalization at the receiver can be avoided. The analytical expressions for the AOA and the TOA are appropriately verified through computer simulations. Next, a dual annular strip model has been introduced and the analytical expressions for the AOA and the TOA has also been derived and verified through simulation studies. This model can handle uniform circular scattering and ring models as special cases. The model also can be easily extended to handle scatterer distributions that are uniform in the angular direction but nonuniform in the radial direction with reference to a polar coordinate system. The contributions made in this chapter can be summarised as follows:

- Extension of the geometry based single bounce macrocellular channel model to geometry based single bounce M2M channel model consisting of a disc of scatterers around the transmitting and the receiving mobiles and subsequently to dual annular strip model. The models have been used in obtaining the analytical expressions for the AOA and TOA in terms of the model parameters.

Chapter 4 of the thesis deals with relay based cooperative communication, which has gained considerable importance in the recent years. Expressions for the probability density functions of the signal envelope at the output of a selection combiner and a maximal ratio combiner at the destination node have been derived for a cooperative scheme having two diversity branches and each branch having a relay in it. The analytical formulations have been verified through computer simulation. The derived probability density functions have been used for evaluating the system performance in terms of bit error rates. The contributions made in this chapter are as follows:

- Analytical expression for the joint probability density function of two dual-hop amplify forward relay paths where the individual hops experiences Nakagami-m fading has been derived.

- Probability density function of the equivalent channel representing such system has been derived considering selection and maximal ratio combining.

- Bit error rate (BER) performances have been evaluated both for selection and maximal ratio combining. It has been found that maximal ratio combining does not provide significant improvement in the bit error rates over selection combing in the SNR range of 0 to 30 dB.

Chapter 5 concludes the thesis mentioning the major contributions that have been made. This chapter also gives some future directions to the present research work.

Chapter 2

Multi-antenna Channel Modelling

2.1 Introduction

Modern day wireless communication systems are required to support high data rates within a limited available bandwidth and offer high reliability. Multiple-Input Multiple-Output (MIMO) technology which exploits the spatial dimension of the channel has shown potential in providing enormous capacity gains and improvements in the quality of service (QoS) [Tel99, SFGK00, Kuh06, OC07, Tso06]. In any communication system, the capacity is dependent on the characteristics of the propagation channel which in turn are dependent on the environmental condition. In a MIMO system consisting of N_T transmit and N_R receive antennas, theoretical investigations have shown that for rich scattering environment the ergodic capacity of the system is the sum of the capacities of N [=$min(N_T, N_R)$, the spatial parameter defining the degrees of freedom] equivalent single-input single-output (SISO) channels. It has further been shown that for $N_T = N_R = N$ and N being very large, the ergodic capacity increases linearly with the increasing signal to noise ratio. Appropriate modelling of the MIMO channel behaviour help in efficient and proper designing of a MIMO system with reference to code design, power allocation at the transmitter antennas, modulation schemes etc. It also aids in evaluating the system performance before actual deployment. Channel modelling is an area of active research and several models have been developed to, simulate and design a high performance communication system.

Channel models can be classified into two broad categories, namely site specific physical models and analytical models as shown in Fig. 2.1 [ABB$^+$07].

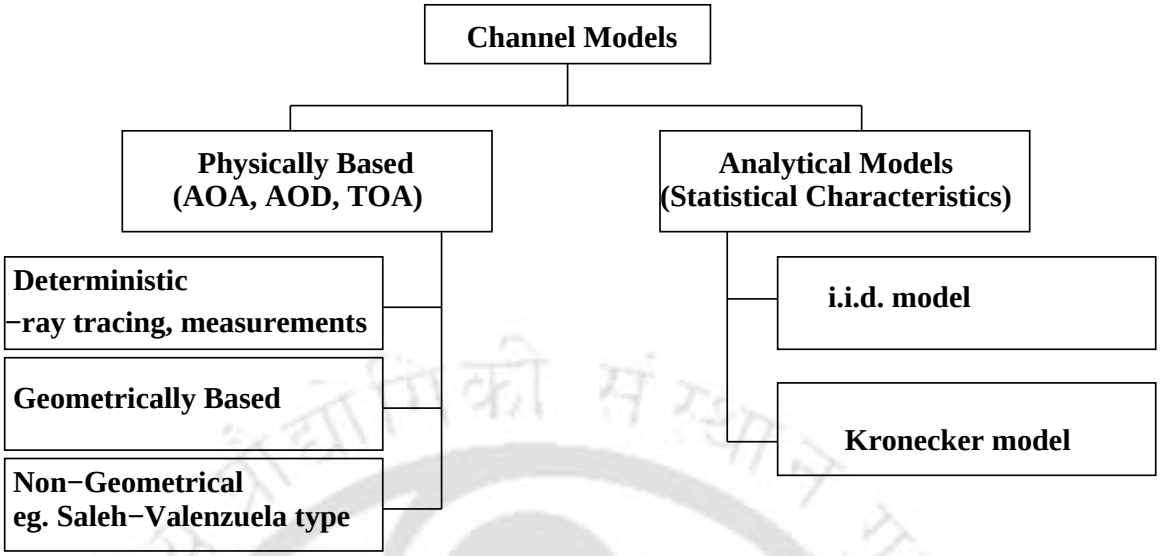

Figure 2.1: Channel model classification.

Site specific physical models help in network deployment and planning, while site independent models are mostly used for system design and testing. The physical models may be further classified into deterministic and stochastic models. A deterministic model tries to reproduce the actual physical radio propagation process for a given environment by taking into account the reflection, diffraction, shadowing by discrete obstacles, and the waveguiding in street canyons. Recorded impulse response and ray tracing techniques are some of the examples of deterministic channel modelling techniques. The stochastic models are based on the fact that although wireless propagation channels are unpredictable and time varying in nature, some of its parameters, like the angle of arrival (AOA), angle of departure (AOD), time delay profiles etc, can be modelled by statistical means. The stochastic channel models are generally computationally efficient. Most stochastic models have a geometrical basis, however a few non-geometric correlation based or parametric stochastic models can also be found in [ABB$^+$07] and references therein. In the realm of geometrically based stochastic modelling, several models have been proposed, but the basic philosophy remains the same. Usually, the models are validated by comparing the values or distributions of certain physical parameters like AOA, AOD, time of arrival (TOA), and power spectrum etc, obtained through the model with those acquired through measurements under specific conditions.

The rest of this chapter is organized as follows: Section 2.2 presents a brief review of the different MIMO channel models. Section 2.3 deals with the effects of arrays on macrocellular MIMO

system capacity estimated using geometry based modelling approach. Section 2.4 presents the details of methodologies developed for analysing MIMO channels from a microwave perspective. Section 2.5 deals with the effects of mutual coupling on MIMO system performance. Conclusions are drawn in section 2.6.

2.2 Review of MIMO Channel Models

A MIMO system consisting of N_T transmit and N_R receive antennas is shown in Fig. 2.2.

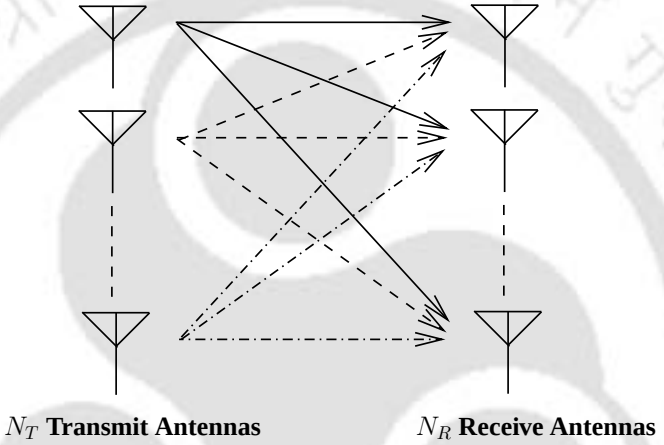

Figure 2.2: An $N_T \times N_R$ MIMO system.

The received signal $\mathbf{y}(n)$, at a discrete time index n, is related to the transmitted signal $\mathbf{x}(n)$ by

$$\mathbf{y}(n) = \mathbf{H}(n) * \mathbf{x}(n) + \mathbf{w}(n) \tag{2.2.1}$$

Here, $\mathbf{y}(n) = \left[y^1\ y^2\ \cdots\ y^{N_R}\right]^T$ is an $N_R \times 1$ vector, $\mathbf{x}(n) = \left[x^1\ x^2\ \cdots\ x^{N_T}\right]^T$ ia an $N_T \times 1$ vector. $\mathbf{w}(n) = \left[w^1\ w^2\ \cdots\ w^{N_R}\right]^T$ is an $N_R \times 1$ vector which represents additive white gaussian noise (AWGN) and $\mathbf{H}(n)$ is the channel matrix, giving the channel impulse response at any discrete time n. For a $N_T \times N_R$ MIMO system, $\mathbf{H}(n)$ is a $N_R \times N_T$ dimensional matrix. For a flat fading channel, the channel matrix may be considered to be constant over the frequency of operation for any particular time index n. Hence, equation 2.2.1 can be written as,

$$\mathbf{y} = \mathbf{H}\mathbf{x} + \mathbf{w} \tag{2.2.2}$$

where the time index n has been suppressed to simplify the notation. The channel matrix $\mathbf{H}$ is

given by,

$$\mathbf{H} = \begin{bmatrix} h_{1,1} & \cdots & h_{1,N_T} \\ \vdots & \ddots & \vdots \\ h_{N_R,1} & \cdots & h_{N_R,N_T} \end{bmatrix} \tag{2.2.3}$$

where, h_{ij} represents the channel coefficient between the i^{th} receiver antenna and j^{th} transmit antenna. For a frequency flat channel, the individual elements of the channel matrix are of the form,

$$h_{mn} = \alpha_{mn} e^{j\phi_{mn}} \tag{2.2.4}$$

where, h_{mn} refers to the channel between the m^{th} transmit antenna and the n^{th} receive antenna. α_{mn} and ϕ_{mn} are the corresponding channel gains and phase shifts, respectively. The distribution of α_{mn} depends on the environment. For a macrocellular environment, having no line of sight between the transmitter and the receiver, the transmitted signal reaches the receiver after being scattered by different scatterers (e.g. buildings, trees etc.) surrounding the receiver. Thus, multiple copies of the transmitted signal are received from different directions with different delays and phase shifts. The resultant baseband signal at the receiver can be modelled by a complex gaussian random process. The amplitude distribution for such a process is given by Rayleigh distribution. Hence, for a macrocellular environment, with no line of sight path between the transmitter and the receiver, α_{mn} is taken to be Rayleigh distributed. If a line of sight path exists between the transmitter and the receiver then the amplitude distribution becomes Rician. For a more generalized representation, channel gains can be assumed to be Nakagami-m distributed as it can represent both Rayleigh and Rician distributions depending on the value of the m parameter. The phase is generally assumed to be uniformly distributed between 0 and 2π.

One of the objectives of any MIMO channel modelling techniques is to model the channel matrix $\mathbf{H}$ efficiently. The elements of the channel matrix are often assumed to be independent and identically distributed, thus having very little or no correlation between them and thereby exhibiting maximum capacity gains. But in practice, the elements of the channel matrix have finite correlations due to the limited spacing between the antennas. The correlation is inversely proportional to the distance of separation between the antenna elements. The coherence distance gives a measure of the separation between the antennas below which the correlation between the channel elements is significant. The rule of thumb is to take the coherence distance to be $\lambda/4$, where λ is the operating wavelength.

2.2.1 Deterministic models

The deterministic channel modelling techniques try to replicate the physical scenario between the transmit and receive arrays. Often the antenna parameters like the antenna patterns, array size and geometry, the effects of mutual coupling between the array elements, polarisation are not accounted for [ABB+07]. Ray tracing softwares, and techniques are popular ways for modelling the channel deterministically. In ray tracing softwares, the geometry and the electromagnetic characteristics of any particular scenario are stored in files. These files are later used for simulating the electromagnetic propagation process between the transmitter and the receiver. These models are fairly accurate and may be used as an alternative of measurement campaigns when time is at premium. In ray tracing techniques, flat top polygons of different sizes and shapes are generally used to represent buildings. The ray tracing softwares are basically based on the phenomenons of geometrical optics, like reflection, refraction, diffraction. For urban scenarios geometrical optics can be aptly applied as the wavelength of operation is much smaller than the dimension of the obstacles.

2.2.2 Geometrically based channel models

Geometry based channel models may be thought of as a simplification of the deterministic channel models (e.g. ray tracing). Deterministic channel models require to handle a huge data base of the environment and its propagation conditions. In geometry based channel models the scatter locations are considered to be random and governed by some well defined probability distribution functions depending on the scenario. The channel impulse response in these models are obtained based on phenomenons of geometrical optics, after positioning of the scatterers.

In Fig. 2.3 a typical geometrically based channel model for a macrocellular scenario has been shown. In a macrocellular scenario, the base station (BS) is generally placed on an elevated platform or on top of a hill and hence is devoid of scatterers, whereas the mobile station (MS) is surrounded by scatterers from all sides. The scenario has been modelled in Fig. 2.3 by placing a ring of scatterers around the MS. The model parameters are

1. The distance of separation between the BS and the MS (D).

2. Radius of the scattering circle at the MS (R).

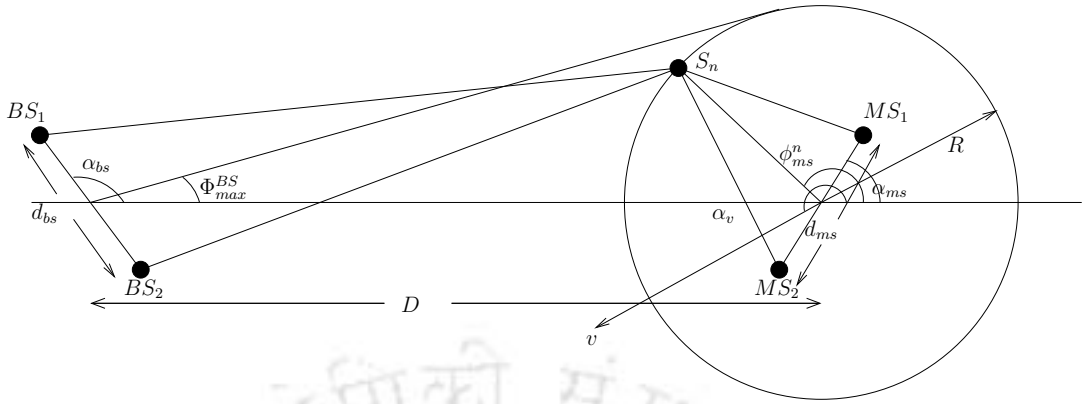

Figure 2.3: Geometry based one ring model.

3. Distribution of the scatterers around the MS ($p(\phi_{ms})$).

4. Inter-element separation of the BS and MS antenna arrays (d_{bs},d_{ms}).

5. Orientation of the transmit and receive arrays (α_{bs},α_{ms}).

6. Direction of movement of the MS w.r.t a reference plane (e.g. the line joining the BS & MS) (α_v).

In geometry based single bounce modelling it is assumed that a wave from the BS(MS) reaches the MS(BS) after being scattered by a single scatterer. Multiple scattering is generally neglected as the energy contributed by a multiple scattered wave is marginal. Based on the assumption, $D \gg R \gg \max\{d_{bs}, d_{ms}\}$, each incoming wave may be considered as a plane wave. With reference to Fig. 2.3 the TOA and AOA statistics depend grossly on the distance of separation between the BS and the MS, the radius of the scattering circle at the MS and the distribution of the scatterers.

It has been shown that the diffused component of the $BS_1 - MS_1$ link can be approximated as [PH04],

$$h_{11}(t) = \lim_{N\to\infty} \frac{1}{\sqrt{N}} \sum_{n=1}^{N} a_n b_n e^{j(2\pi f_n t + \theta_n)} \tag{2.2.5}$$

where,

$$a_n = e^{j\pi \frac{d_{bs}}{\lambda}\left[\cos(\alpha_{bs}) + \Phi^{BS}_{\max} \sin(\alpha_{bs}) \sin(\phi^n_{ms})\right]} \tag{2.2.6}$$

$$b_n = e^{j\pi \frac{d_{ms}}{\lambda} \cos(\phi^n_{ms} - \alpha_{ms})} \tag{2.2.7}$$

where, N denotes the total number of scatterers present around the MS. f_n denotes the doppler shift of the n^{th} plane wave reaching the MS after being scattered by the scatterer S_n and f_{max} gives the maximum doppler shift. The phases θ_n are independent, identically distributed random variables with uniform distribution over [0, 2π). The mean value and the power of the diffused component $h_{11}(t)$ are equal to $E\{h_{11}(t)\}$ = 0 and $E\{|h_{11}(t)|^2\}$ = 1, with $E\{\cdot\}$ as the expectation operator. The diffused components $h_{12}(t)$ ($BS_2 - MS_1$ link) and $h_{21}(t)$ ($BS_1 - MS_2$ link) can be obtained by replacing a_n by its complex conjugate a_n^* and b_n by b_n^* respectively. $h_{22}(t)$ ($BS_2 - MS_2$ link) is obtained by replacing both a_n by a_n^* and b_n by b_n^*. The diffused components thus obtained are used to form the channel matrix **H**.

Geometrical based models depicting other scenarios, e.g. M2M communication, indoor channels, have been reported in literature. [PHYK05a, PHYK05b] deals with the reference and simulation model for a M2M communication scenario. [LR96] deals with the geometric model for indoor channels. In this model, the transmitter and the receiver are positioned at the foci of an ellipse. The scatterers are assumed to be distributed inside the ellipse.

A geometrical based approach where scatterers are represented by antenna elements with appropriate load conditions was proposed in [BDBU05]. Further investigation on such models have been reported in [PB07c]. Mutual coupling among the antenna elements affect the MIMO system capacity. Incorporation of mutual coupling effects in MIMO channel models have been addressed in [SR01, PB06b].

2.2.3 Non-geometrical physical models

In a non-geometrical physical model there is no reference to the geometry of the scenario it depicts. Saleh Valenzuela model and its extensions [WJ01] makes a typical example for the non-geometrical physical model. In this model, the multipath components are assumed to arrive in clusters. The rate of decay of the multipath components, within a cluster and among the clusters, are governed by well defined statistical distributions. In this model, the discrete channel impulse representation is employed. The channel impulse response is given as,

$$h(t) = \sum_k \beta_k e^{j\theta_k} \delta(t - \tau_k) \tag{2.2.8}$$

where,

k = number of multipath, ideally k extends from 0 to ∞.

β_k = real positive gain of the k^{th} multipath.

τ_k = propagation delay of the k^{th} multipath.

θ_k = phase shift associated with the k^{th} multipath, and is assumed to be uniformly distributed and statistically independent over [0,2π).

$\delta(\cdot)$ = Dirac delta function.

2.2.4 Independent and identically distributed *(iid)* model

The independent and identically distributed channel model [Tel99] is the simplest of all the analytical channel models. The correlation matrix between the channel elements is defined as,

$$\mathbf{R_H} = \mathbf{E}\left[\mathbf{h}\mathbf{h}^H\right] \tag{2.2.9}$$

where, $\mathbf{h} = \mathbf{vec}\{\mathbf{H}\}$. For an *iid* channel the correlation matrix is given as $\mathbf{R_H} = \rho^2\mathbf{I}$, where $\mathbf{I}$ is the unity matrix. Thus for an *iid* channel the correlation matrix is a diagonal matrix, with each element equal to ρ^2. The non diagonal elements of the correlation matrix gives the cross correlation between the channel elements and are all equal to zero. This represents a scenario with rich scattering where all the channel matrix elements are mutually independent. ρ^2 gives the variance of the MIMO channel elements $\mathbf{H}$ and also the channel power. Early works for capacity evaluation for MIMO systems used *iid* channel models.

2.2.5 Kronecker model

The Kronecker model [SFGK00] was developed on the basic assumption that the transmitter and the receiver correlations are separable. Thus the channel correlation matrix $\mathbf{R_H}$ may be written as the Kronecker product of the transmitter correlation matrix ($\mathbf{R_{Tx}}$) and the receiver correlation matrix ($\mathbf{R_{Rx}}$).

$$\mathbf{R_H} = \mathbf{R_{Tx}} \otimes \mathbf{R_{Rx}} \tag{2.2.10}$$

where, $\otimes$ denotes the Kronecker product. The transmitter and the receiver correlation matrices are given as,

$$\mathbf{R_{Tx}} = \mathbf{E}\left[\mathbf{H}^H\mathbf{H}\right] \quad \text{and} \quad \mathbf{R_{Rx}} = \mathbf{E}\left[\mathbf{H}\mathbf{H}^H\right]$$

where, $E[\cdot]$ and $(\cdot)^H$ denote expectation and conjugate transposition, respectively. It has been shown that the channel matrix $\mathbf{H}$ is given as,

$$\mathbf{H} = \mathbf{R}_{\mathbf{RX}}^{\mathbf{1/2}} \mathbf{G} \mathbf{R}_{\mathbf{TX}}^{\mathbf{1/2}} \tag{2.2.11}$$

where, $\mathbf{G} = \mathbf{unvec}(\mathbf{g})$ and $\mathbf{g}$ is a $nm \times 1$ vector (for a $n \times m$ channel) with *iid* gaussian elements having zero mean and unity variance. The equation 2.2.11 is widely used for theoretical analysis and MIMO channel simulation.

2.3 Array effects on macrocellular MIMO system capacity

This section investigates the effect of different array configurations on the capacity of a MIMO channel, in the framework of geometrically based single bounce (GBSB) modelling [AK02, HP04, PH04]. Most theoretical investigations in literature consider 2×2 MIMO systems. A 2×2 MIMO system is limited to linear arrays. To study the effect of different array geometries, a 4×4 MIMO system has been considered. The variation of the ergodic capacity for different array geometries at the BS and MS has been evaluated through computer simulation, as a function of (a) SNR and (b) change in orientation of MS. The transmitting and the receiving array elements have been assumed to be ideal point sources having an omnidirectional radiation pattern. The array geometries considered for the study are, uniform circular array (UCA), uniform linear array (ULA), Rhombic array and star array as shown in Fig. 2.4. A macrocellular scenario as shown in Fig. 2.3 has been considered with scatterers assumed to be uniformly distributed on a ring having the MS at its center.

The capacity of an $N \times N$ matrix channel corrupted with AWGN and involving fixed received power (or fixed signal-to-noise ratio), can be written as (Appendix B),

$$C = \log_2 \det \left[\mathbf{I} + \tfrac{\mathrm{SNR}}{\mathrm{N}} \mathbf{H}\mathbf{H}^{\dagger} \right] \tag{2.3.1}$$

where, N is the number of transmit antennas, SNR is the average received signal-to-noise ratio and $\mathbf{I}$ is the identity matrix with dimension $N \times N$. $\mathbf{H}$ is the channel matrix and $\mathbf{H}^{\dagger}$ is the Hermitian transpose of $\mathbf{H}$. The assumption of fixed SNR requires suitable normalisation of the channel matrix $\mathbf{H}$ to make comparisons with the iid channel. The channel matrix is normalised such that its Frobenius norm is equal to the product of the number of receive and transmit antennas [BUBD06].

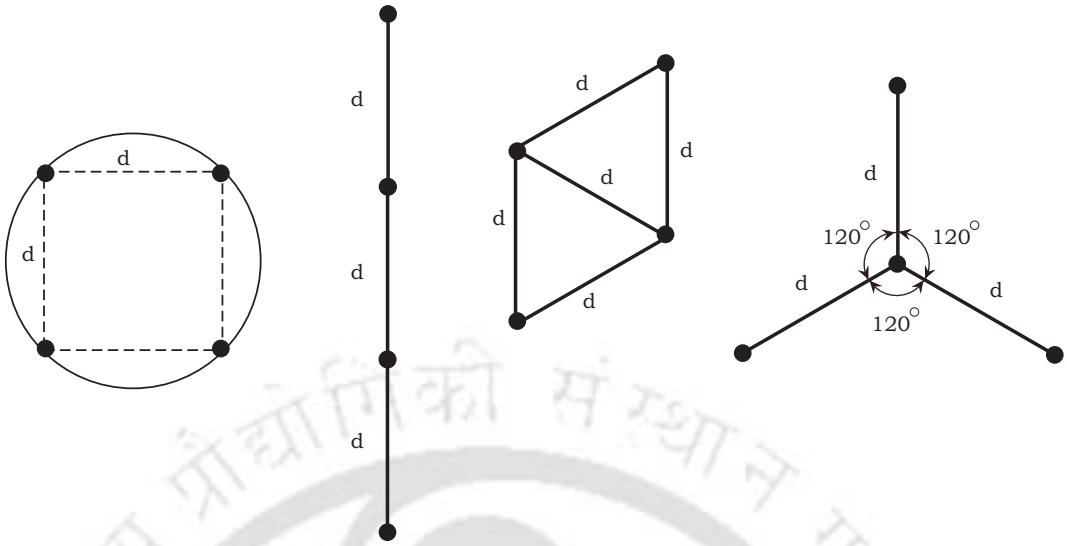

Figure 2.4: Different array geometries.

If the elements of the channel matrix **H** are known, the capacity is calculated from equation 2.3.1. The elements of the channel matrix have been generated using methods outlined in subsection 2.2.2. With four different array configurations, two arrays taken at a time, one for BS and the other for MS, sixteen different combinations are possible. Each of these configurations has been investigated. In the simulation it has been assumed that the distance between the BS and the MS is much greater than the radius of the circle containing the scatterers, which in turn is much greater than the inter-element spacing of the antenna arrays.

For simulation, the distance between the BS and the MS has been taken to be 200λ. Twenty-five scatterers have been considered which are uniformly distributed on a ring of radius 53.5λ. The ring subtends an angle of 15^o at the BS as in [SFGK00]. The MS has been placed at the center of the scattering circle. The BS has been assumed to be placed at the origin of the XY coordinate system and the MS on the X axis at a distance of 200λ. The frequency of operation has been taken to be 900 MHz. The SNR has been varied form 0 to 35 db and the variation of the capacity, over this SNR range, for different antenna configurations have been found out and plotted in Fig. 2.5. The minimum separation between any two adjacent antennas (d in Fig. 2.4) in the array has been kept at λ, the operating wavelength.

It has been observed that a fixed MIMO link with properly aligned linear arrays at both the transmitter and the receiver end, gives the best performance with regards to the maximum achievable capacity. The AOA has been taken to be uniformly distributed between 0 to 360^o at the MS.

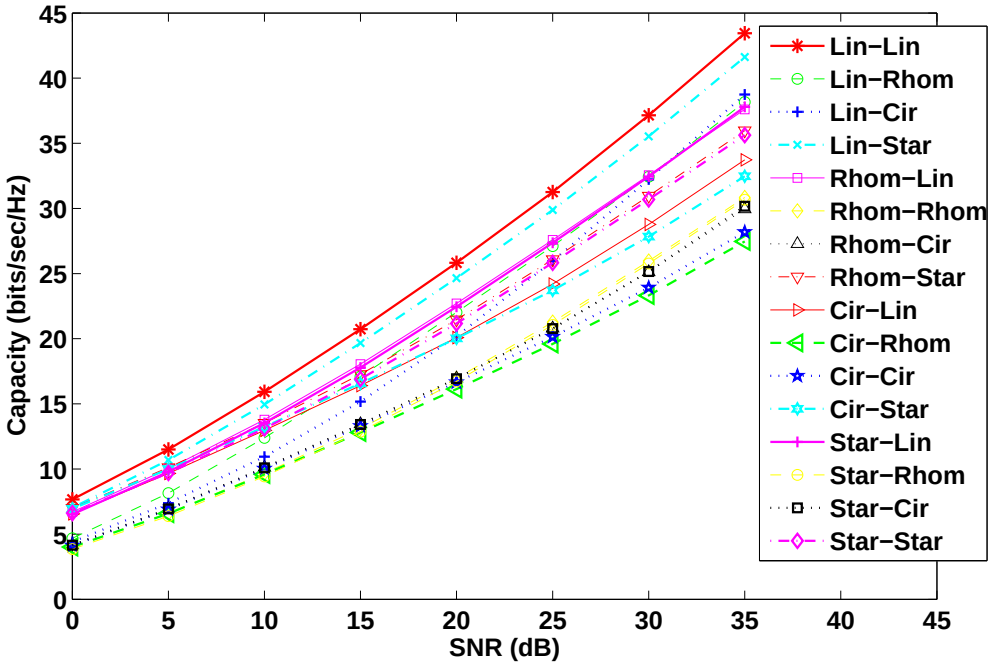

Figure 2.5: Plot of SNR Vs Capacity for combination of different array geometries at the base and mobile station.

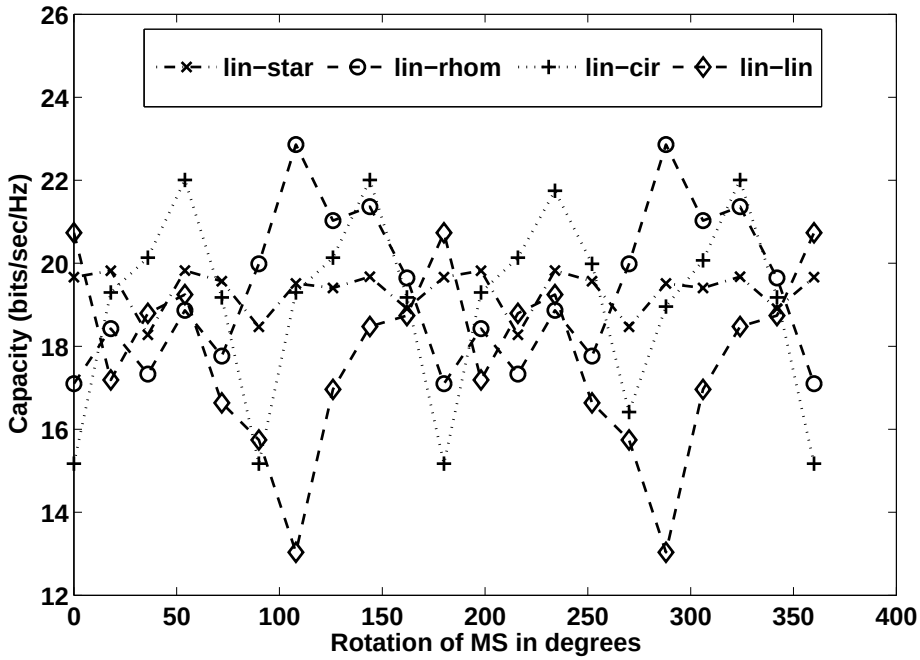

Figure 2.6: Plot of the ergodic capacity at different angles of rotation of the mobile station for different array configuration combinations at the base station and the mobile station.

Table 2.1: Mean and standard deviation of the channel capacity for different antenna configurations at the base station and the mobile station.

Antenna Configuration (Base station - Mobile station)	**Mean capacity**	**Standard deviation of capacity**
Linear - Star	19.329	0.5385
Linear - Rhombic	19.3252	1.8706
Linear - Circular	19.0339	2.3052
Linear - Linear	17.7068	2.1586
Rhombic - Linear	18.1234	2.1508
Rhombic - Rhombic	15.8692	2.0647
Rhombic - Circular	16.0031	1.8878
Rhombic - Star	16.8327	0.6509
Circular - Linear	13.7701	1.9131
Circular - Rhombic	14.4071	1.5555
Circular - Circular	14.7101	1.118
Circular - Star	15.9099	0.8794
Star - Linear	14.8893	1.8601
Star - Rhombic	15.7319	2.0896
Star - Circular	15.8679	1.8361
Star - Star	16.7008	0.5816

However, when there is a misalignment of orientation between the arrays due to mobility, combination of other array geometries have been found to perform better than combination of linear arrays at the BS and the MS. The variation of the capacity have been simulated for all the sixteen array combinations, but only four of them have been plotted for better legibility. The array at the MS has been rotated in steps of 18^o. It has been observed that the combination of linear and star shaped antenna arrays at the BS and the MS, respectively, performs better than other combinations. The mean capacity is maximum with minimum standard deviation for the said array combination. The variation of the system capacity with the array rotation has been shown in Fig. 2.6. Table 2.1 gives the mean and standard deviation of the capacity for different antenna array configurations at the BS and the MS. The simulation parameters have been kept same as the earlier case and the simulations have been carried out at an SNR of 15 dB. From the above investigations and results, it can be concluded that for MIMO links where relative rotational displacement between transmit and receive arrays are expected, choice of antenna array configuration has to be given due

consideration [PB06a].

2.4 MIMO channel modelling from microwave perspective

In recent times, understanding of MIMO channel behaviour and its modelling from electromagnetic perspective has found attention from several researchers [Loy02, BDBU05, WSW04]. Such modelling can take into account the effect of coupling between antenna elements. An antenna, depending upon its termination, can produce different degrees of scattering. Replacing physical scatterers by suitably terminated antennas in developing MIMO channel model was proposed in [BDBU05] and a MIMO channel model purely from microwave perspective by using half wave dipoles representing the transmitters, the receivers as well as the scatterers was presented. The model provides an assessment of the channel capacity in the strict mathematical sense and allows investigation of issues such as antenna array spacing and orientation in different wireless scenarios. In this modelling approach, the impedance matrix $\mathbf{Z}$ for the MIMO system (comprising of transmitter and receiver antennas as well as scatterers) are computed. Once $\mathbf{Z}$ is computed the channel matrix is determined by computing the voltage ratio between a pair of transmitter and receiver antennas with proper load condition applied to the unexcited transmitter and receiver antennas and the scatterers. When the dipoles representing the scatterers are short circuited, they act as perfect reflectors. The unexcited transmitter and receiver antennas are kept matched terminated. By changing the termination of the dipole antennas representing scatterers different scattering coefficients can be generated to model appropriate scenarios.

While $\mathbf{Z}$-matrix based approach works well, scattering parameter (S-parameter) (Appendix A) matrices is a more natural representation of the scattering environment for capacity formulation as stated in [WSW04, WJ04]. In the next subsection, methodologies have been developed for determining the channel matrix using S-parameter based approach. The model has been extended further to take into account dual polarised systems as polarisation diversity is also considered to be a viable option for increasing system capacity [PNG03, OEP04].

2.4.1 Geometry based MIMO channel modelling from microwave perspective using scattering matrix

As discussed, for the MIMO model under consideration, the entire system is modelled using half-wave dipole antennas. Each dipole antenna corresponds to a port of a microwave system. If there are N_T transmit, N_R receive and N scattering antennas, then the scattering matrix $\mathbf{S}$ is a $(N_T + N_R + N)X(N_T + N_R + N)$ matrix and the same is first determined. $(N_T + N_R + N)X(N_T + N_R + N)$ scattering matrix thus obtained is then reduced to $(N_T + N_R)X(N_T + N_R)$ matrix by applying appropriate loading condition at the N dipoles acting as scatterers. Method of moment based approach can be used to generate the $\mathbf{S}$-matrix taking into account the mutual coupling among the elements.

In this work, a software package, WIREMOM [Wir] has been used to compute the $\mathbf{S}$-matrix. The parameters like the distance between the BS and the MS, the radius of the ring, the inter-element separation at the BS and the MS, number of scatterers, number of BS and MS antennas, frequency of operation, dipole length are first set. The co-ordinates of the tips (ends) of the BS, MS and the scattering antennas are found out. These coordinates are supplied to WIREMOM package to generate the wire structure of the model and the $\mathbf{S}$-matrix is then computed. Once the S-matrix is so obtained, the terminating condition for the scatterer dipoles are applied to reduce the scattering matrix to a $(N_T + N_R)X(N_T + N_R)$ matrix. For scenarios reported in this thesis, the scatterers are considered to be perfect reflector, therefore the dipoles are terminated to short circuits. The reduced scattering matrix obtained can be written of the form

$$\begin{bmatrix} \mathbf{b_{TX}} \\ \mathbf{b_{RX}} \end{bmatrix} = \begin{bmatrix} \mathbf{S_{TX}} & \mathbf{S_{TX,RX}} \\ \mathbf{S_{RX,TX}} & \mathbf{S_{RX}} \end{bmatrix} \begin{bmatrix} \mathbf{a_{TX}} \\ \mathbf{a_{RX}} \end{bmatrix} \tag{2.4.1}$$

where, the vectors $\mathbf{a_{TX}}$ and $\mathbf{b_{TX}}$ respectively represent the incoming and outgoing waves at the transmitting antennas. Similarly, the vectors $\mathbf{a_{RX}}$ and $\mathbf{b_{RX}}$ represent the incoming and outgoing waves at the receiver antennas, respectively. Assuming proper matching of the transmitter and the receiver antennas, the $(N_R \times N_T)$ channel matrix $\mathbf{H}$ can be computed from equation 2.4.1, in particular, from the sub-matrix $\mathbf{S_{RX,TX}}$. The channel matrix thus obtained can be used to find the system capacity using equation 2.3.1 and the same has been repeated here for ready reference,

$$C = \log_2 \det \left[\mathbf{I} + \tfrac{SNR}{N_T}\mathbf{H}\mathbf{H}^\dagger\right] \quad bits/\sec/Hz \tag{2.4.2}$$

Table 2.2: Model parameters for Case I.

Model parameters	**Parameter values**
Frequency of operation	1 GHz
MIMO configuration	2×2
Interelement separation at Tx. (d_{bs})	λ (= 0.3m)
Inter-element separation at Rx. (d_{ms})	λ (= 0.3m)
Distance between Tx. and Rx. (D)	50λ (= 15m)
Radius of the scattering circle around Tx. (R_1)	16λ (= 4.8m)
Radius of the scattering circle around Rx. (R_2)	16λ (= 4.8m)
No. of scatterers around the Tx. (S_{bm})	20
No. of scatterers around the Rx. (S_n)	20

Two different cases have been considered to validate the S-parameter based microwave modelling approach. First, a two ring model has been considered followed by a macrocellular scenario having dual polarised antennas at the transmitter and the receiver.

2.4.2 Case I: Two-ring model of MIMO system

A 2×2 MIMO system modelled using two-ring model with half wavelength dipole antennas representing scatterers around the transmitting and receiving antenna pairs has been shown in Fig. 2.7. The transmitting and receiving antennas themselves are half wave dipoles. The two ring model under consideration is used to represent various indoor and outdoor scenarios depending on the proper choice of the model parameters. The same model was considered in [BDBU05]. For validating the proposed S-parameter based approach for evaluation of channel matrix $\mathbf{H}$ and system capacity, the same set of model parameters as in [BDBU05] have been used. The various model parameters used are shown in Table 2.2. Figure 2.8 plots the ergodic capacity for the two ring model for different values of the SNR. It can be seen that the results are in agreement with those reported in [BDBU05]. Small differences in capacity as observed in Fig. 2.8 (particularly at higher SNR) may be due to the approaches involved in evaluating the impedance matrix $\mathbf{Z}$ and $\mathbf{S}$ parameters. As mentioned, $\mathbf{S}$ parameters have been calculated using a method-of-moment (MoM) based package WireMoM, whereas in [BDBU05], $\mathbf{Z}$ parameters have been computed using an induced field approach.

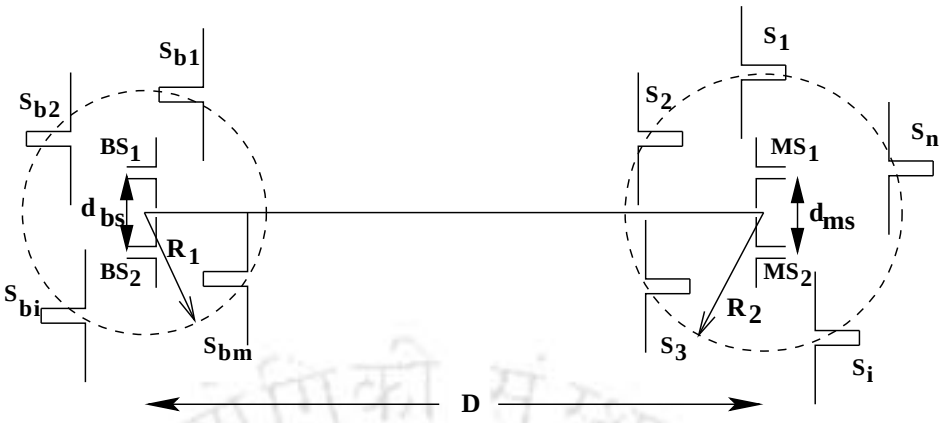

Figure 2.7: Two ring model with half wave length dipole antenna as scatterers.

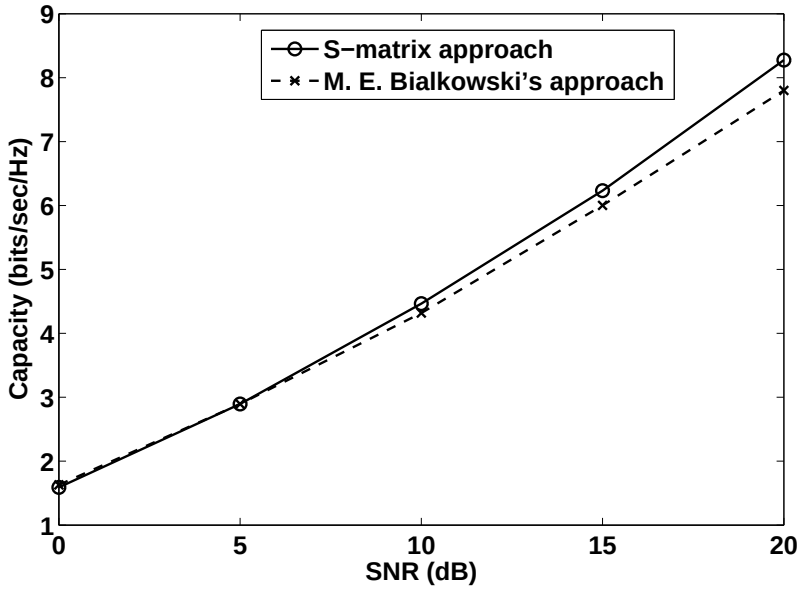

Figure 2.8: Plot of the capacity at different SNR using S-matrix approach and M. E. Bialkowski's [BDBU05] approach.

2.4.3 Case II: Macrocellular scenario with dual polarised transmitting and receiving antennas

A macrocellular scenario modelled by the the one ring scattering model has been shown in Fig. 2.9. For such scenario, the BS being elevated can be considered to be devoid of scatterers, whereas the MS is surrounded by scatterers. In order to study the performance of dual polarised antenna system, the BS and the MS have been assumed to include two collocated half wavelength

dipole antennas perpendicular to each other. The antennas BS_1 and MS_1 lie in the same plane and perpendicular to the plane containing the antennas BS_2 and MS_2. The simulation parameters have been shown in Table 2.3. Fig. 2.10 plots the ergodic capacity of the dual polarised system and compares the same with the capacity achieved by two parallel SISO channels. It can be observed that the capacity achieved for such dual polarised system is the same as that of two parallel SISO channels.

Table 2.3: Model parameters for Case II.

Model Parameters	**Values**
Frequency of operation	1 GHz
MIMO configuration	2×2 collocated dual polarised
Inter-element separation at Tx.	collocated
Inter-element separation at Rx.	collocated
Distance between Tx. and Rx. (D)	1000λ (= 300m)
Radius of the scattering circle around Rx. (R)	35λ (= 10.5m)
No. of scatterers around the Rx.	25

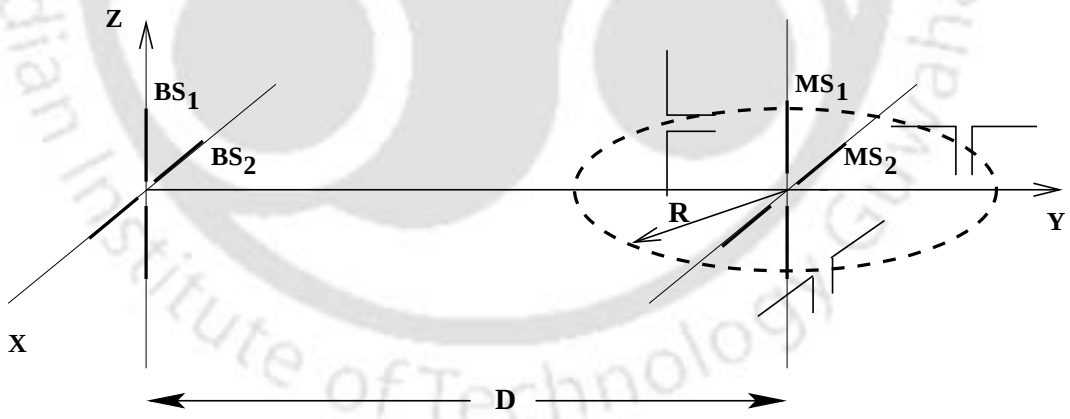

Figure 2.9: Dual polarised dipole antennas at the transmitter and the receiver with the receiver surrounded by scatterers.

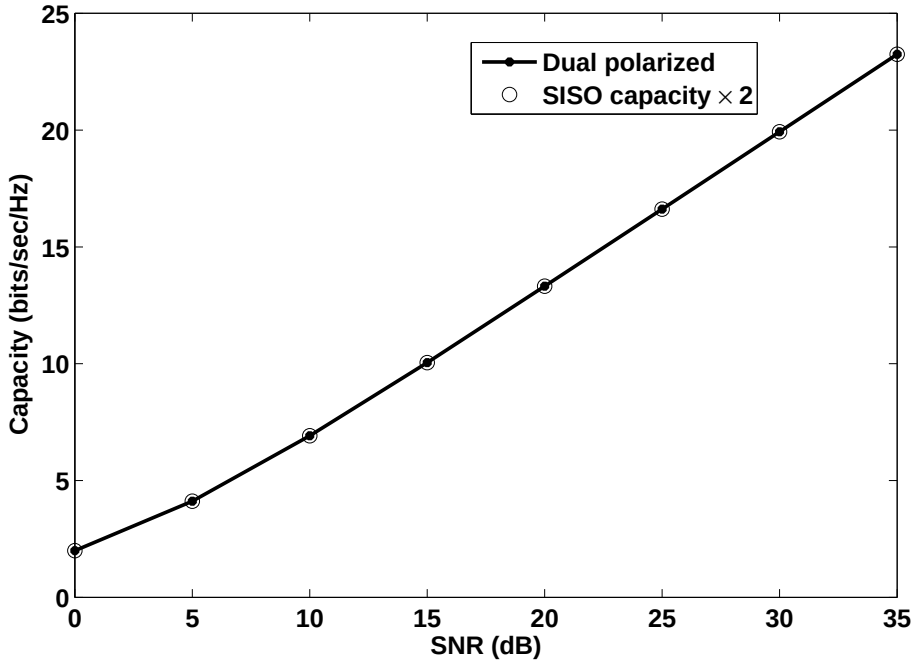

Figure 2.10: Plot of channel capacity variation with SNR when both the transmitter and the receiver have dual polarised dipole antennas.

2.5 Mutual coupling and its effect on MIMO system capacity

The capacity of MIMO system depend on the SNR and correlation properties among the channel transfer functions of different pairs of transmit and receive antennas. The correlations between the channel elements depend not only on the channel conditions but also on the proximity between the antennas which results into mutual coupling between them. To find the channel matrix $\mathbf{H}$ (without the mutual coupling effect) and its spatial fading correlation, many models have been reported in literature [SV87, SFGK00, ECS$^+$01, PH04]. One ring channel model [SFGK00, PH04, HP04] is a widely used model for studying outdoor MIMO communication. In practical MIMO system, the antennas in the MS cannot be placed far apart because of the space constraint. Therefore, mutual coupling effects also need to be considered while using the simulation model for evaluating system performance.

2.5.1 Coupling matrix for two dipole antennas

In order to account for mutual coupling effects, a $N_T \times N_R$ MIMO system as described in section 2.2 has been considered. The channel coefficients h_{ij} of the channel matrix $\mathbf{H}$ are determined employing the geometrically based single bounce one-ring model as described earlier. When mutual coupling at both transmit and receive antennas are taken into consideration, the channel matrix can be modified as [SR01]

$$\mathbf{H}^{'} = \mathbf{C_{BS}}\mathbf{H}\mathbf{C_{MS}} \tag{2.5.1}$$

where $\mathbf{C_{BS}}$ and $\mathbf{C_{MS}}$ respectively represent the coupling matrices for the BS and MS arrays. $\mathbf{C_{BS}}$ and $\mathbf{C_{MS}}$ are related to the impedance matrices of the corresponding arrays using the relation [GK83]

$$\mathbf{C} = (Z_A + Z_T)(\mathbf{Z} + Z_T\mathbf{I})^{-1} \tag{2.5.2}$$

where, Z_A is the self impedance of the antennas. A half wave dipole antenna under resonant condition has self impedance of 73.13 Ω. Z_T is the terminating impedance of the measuring equipment, and for maximum power transfer it is considered to be the conjugate of Z_A. $\mathbf{Z}$ is the mutual impedance matrix. For an array having K elements dimension of $\mathbf{Z}$ is $K \times K$. The mutual impedance matrix for an array of K elements can be written as,

$$\mathbf{Z} = \begin{bmatrix} Z_{11} & Z_{12} & \cdots & Z_{1K} \\ Z_{21} & Z_{22} & \cdots & Z_{2K} \\ \vdots & \vdots & \ddots & \vdots \\ Z_{K1} & Z_{K2} & \cdots & Z_{KK} \end{bmatrix} \tag{2.5.3}$$

where, Z_{ij} represents the mutual impedance at the i^{th} antenna element due to current flowing in the j^{th} antenna element of the array and Z_{ii} represent the self impedance of the i^{th} antenna element.

In general, evaluation of self impedance and mutual impedances are quite involved for many practical antennas. However, in the case of linear dipole antenna arrays which are widely used, self and mutual impedances can be computed easily. Considering the transmitter and receiver array elements as dipole antennas, for a 2×2 MIMO system, the matrix elements can be written as follows [SR01]:

Z_{11} = Z_{22} = input impedance of the antenna elements which also represents the self impedance

of the elements. Z_{12} and Z_{21} give the mutual impedances and by reciprocity Z_{12} = Z_{21} where,

$$Z_{12} = C_0 \int_{-l_2}^{l_2} \left(\frac{e^{-jk_0R_1}}{R_1} + \frac{e^{-jk_0R_2}}{R_2} - 2\cos k_0 l_1 \frac{e^{-jk_0R_0}}{R_0} \right) \sin k_0(l_2 - |z_2|)\, dz_2 \tag{2.5.4}$$

where,

$$C_0 = \frac{jZ_0}{4\pi \sin k_0 l_1 \sin k_0 l_2} \tag{2.5.5}$$

$$R_1 = \left\lfloor (l_1 - z_2)^2 + d^2 \right\rfloor^{1/2} \tag{2.5.6}$$

$$R_2 = \left\lfloor (l_1 + z_2)^2 + d^2 \right\rfloor^{1/2} \tag{2.5.7}$$

$$R_0 = \left\lfloor z_2^2 + d^2 \right\rfloor^{1/2} \tag{2.5.8}$$

d = perpendicular distance between the two antenna elements.

k_0 =free space wave number.

Z_0 =377 Ω.

$2l_i$ =length of the i^{th} antenna element.

Z_{ii} =input impedance of the i^{th} antenna element.

2.5.2 Performance of macrocellular MIMO system with the inclusion of mutual coupling

A 2×2 MIMO system consisting of dipole antennas have been investigated in this section. The scattering environment has been represented by the geometrically based one ring model, described earlier. The dipole antennas have an omnidirectional radiation pattern in the azimuth plane and such antennas are used in many practical communication system. Therefore, evaluation of mutual impedance effect for a MIMO system consisting of dipole antennas would provide some insight about the performance of actual systems. The variation of the correlation, with and without coupling, between different channel paths has been studied. The variation of the ergodic capacity with MS element separation taking mutual coupling into account, can be studied at any particular SNR. Here the system SNR has been considered to be 20 dB and 5 dB, representing the high and low SNR regions. The ergodic capacity is computed according to the equation 2.3.1.

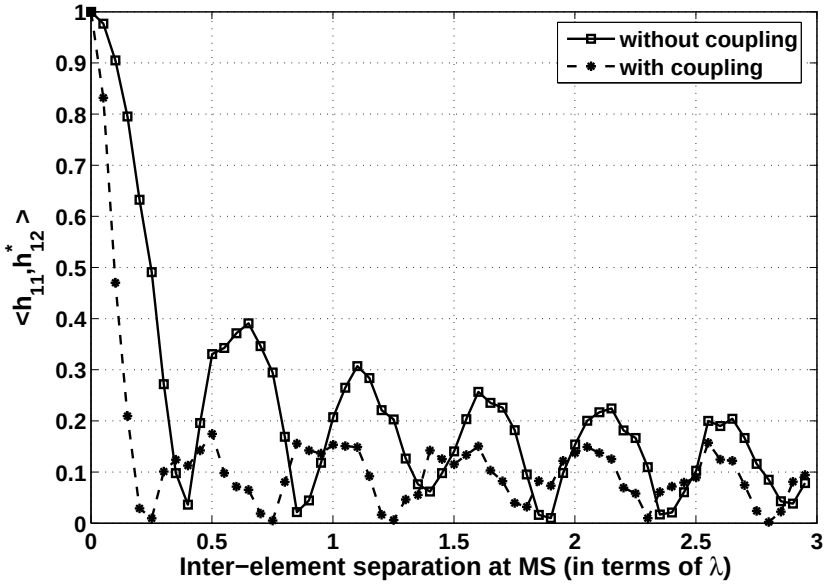

Figure 2.11: Correlation between h_{11} and h_{12}, for different inter-element separations at the mobile station, both with and without taking mutual coupling taken into consideration.

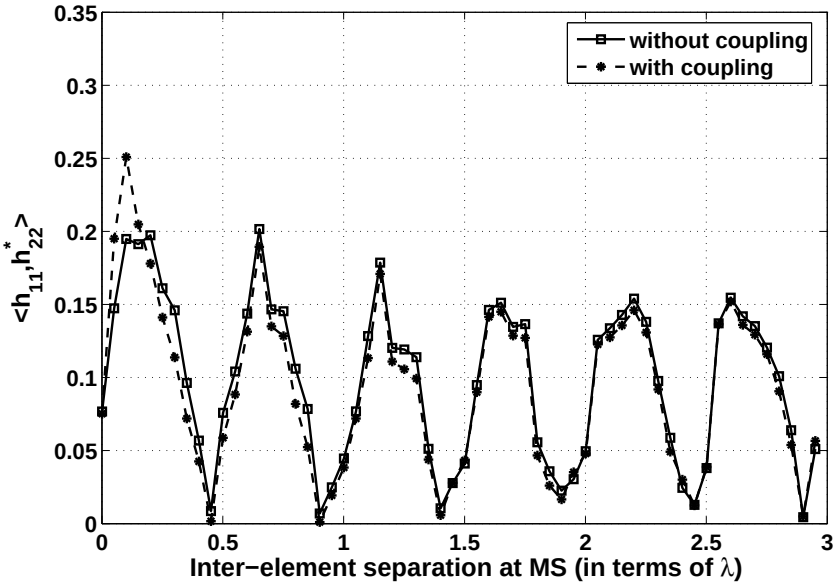

Figure 2.12: Correlation between h_{11} and h_{22}, for different inter-element separations at the mobile station, both with and without mutual coupling taken into consideration.

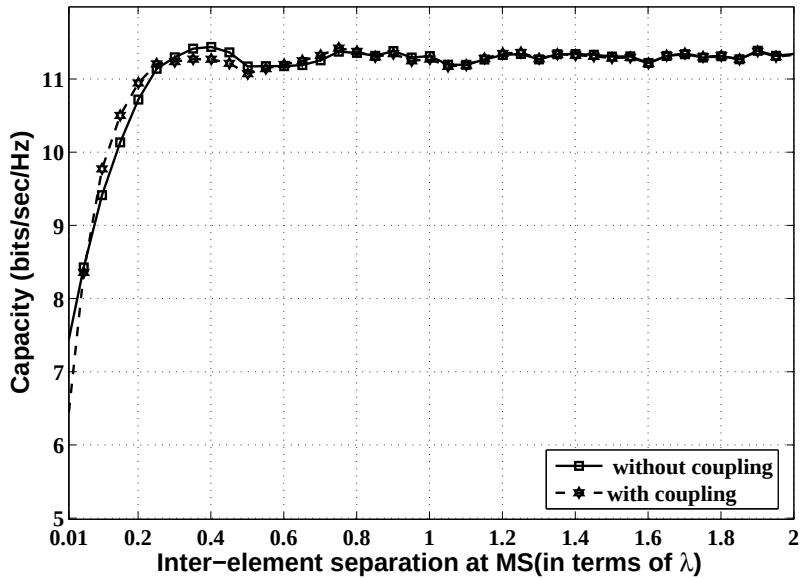

Figure 2.13: Plots of channel capacity, with and without mutual coupling taken into consideration, for different inter-element separations at the mobile station at 20 dB SNR.

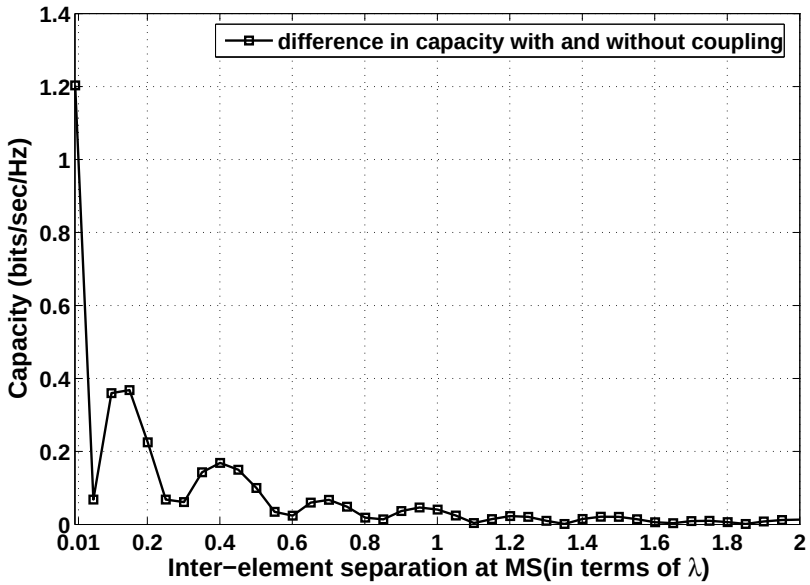

Figure 2.14: Plot of the difference between channel capacity, with and without mutual coupling taken into consideration, for different inter-element separations at the mobile station at 20 dB SNR.

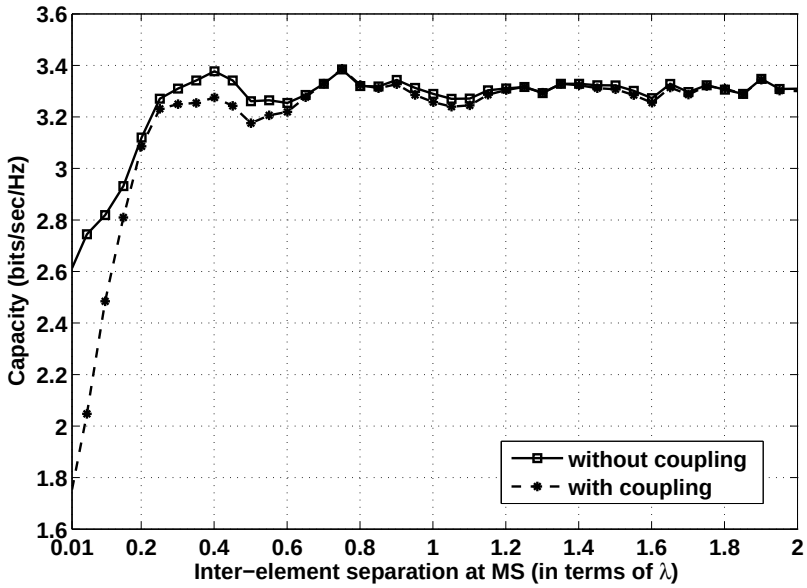

Figure 2.15: Plots of channel capacity, with and without mutual coupling taken into consideration, for different inter-element separations at the mobile station at 5 dB SNR.

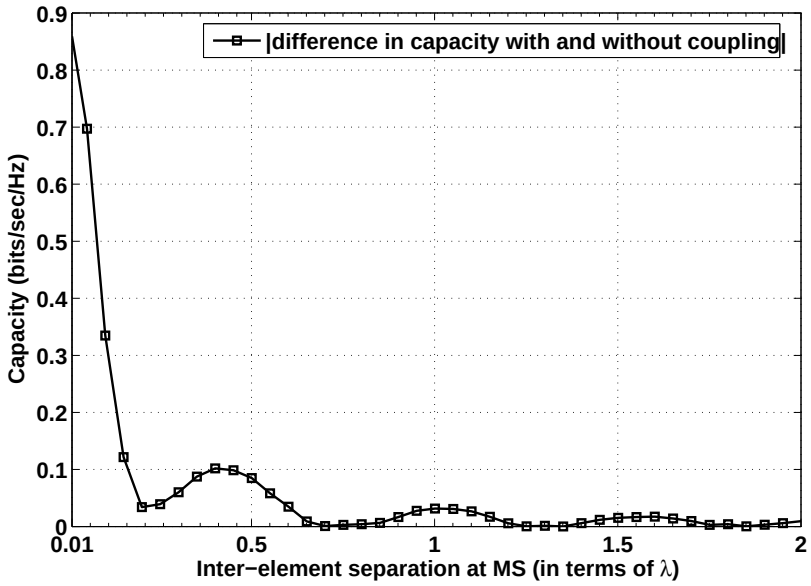

Figure 2.16: Plot of the difference between channel capacity, with and without mutual coupling taken into consideration, for different inter-element separations at the mobile station at 5 dB SNR.

Simulation studies have been performed to evaluate the effect of mutual coupling. The individual elements of the channel matrix without taking mutual coupling into consideration have been

evaluated using equation 2.2.5 or modifying it as detailed in section 2.2.2. The channel elements for the case when mutual coupling is taken into consideration have been obtained from equation 2.5.1. The space-time cross correlation function between the major diagonal elements (h_{11} and h_{22}) of the channel matrix is defined as

$$\rho_{11,22}\left(d_{bs}, d_{ms}, \tau\right) = \left\langle h_{11}\left(t\right), h_{22}^{*}\left(t+\tau\right)\right\rangle \tag{2.5.9}$$

The space cross correlation function may be written as

$$\rho_{11,22}\left(d_{bs}, d_{ms}\right) = \left\langle h_{11}, h_{22}^{*}\right\rangle \tag{2.5.10}$$

Combining equations 2.2.5 and 2.5.10, the space cross correlation function can be given as

$$\rho_{11,22}\left(d_{bs}, d_{ms}\right) = \frac{1}{N}\sum_{n=1}^{N} a_n^2\left(d_{bs}\right)\cdot b_n^2\left(d_{ms}\right) \tag{2.5.11}$$

$$\begin{aligned} &= \tfrac{1}{N}\sum_{n=1}^{N} e^{j2\pi\left(\frac{d_{bs}}{\lambda}\right)\left[\cos(\alpha_{bs})+\Phi_{\max}^{BS}\sin(\alpha_{bs})\sin(\phi_{ms}^{n})\right]} \\ &\quad \cdot e^{j2\pi\left(\frac{d_{ms}}{\lambda}\right)\cos(\phi_{ms}^{n}-\alpha_{ms})} \end{aligned} \tag{2.5.12}$$

The space correlation between any other element pairs of the channel matrix can be obtained in the same manner.

Fig. 2.11 and Fig. 2.12 gives the plot of the correlation between different paths. It may be observed from Fig. 2.11, that the mutual coupling decreases the correlation between the channel paths. The knowledge of the correlation between the different channel paths for different inter-element separation help in designing MIMO systems with spatial multiplexing or beamforming capabilities. Fig. 2.13 and Fig. 2.15 plot the capacity with and without coupling for 20 dB and 5 dB SNR, respectively, using equation 2.3.1. Fig. 2.14 and Fig. 2.16 respectively plots the absolute value of the difference in capacity, with and without coupling, as a function of the MS inter-element separation for 20 dB and 5 dB SNR. In simulation the inter-element separation at the BS has been taken as 5λ so that coupling in the BS is practically negligible and the frequency of operation was has been set at 1 GHz. The inter-element spacing at the MS has been varied up to 2λ . The angular spread subtended at the BS has been taken to be 30^{o}. It has been observed that for small antenna separations at the MS, inclusion of mutual impedance produces considerable difference in the estimated capacity as compared to the capacity estimated by the one ring model

without considering mutual coupling. Due to space constraint, antenna separation at the MS is expected to be small. Mutual coupling should be considered while modelling MIMO channels. However, if the antenna spacings at the MS is reasonably large, mutual coupling effect becomes negligible. From the simulation results it has been observed that for element separation greater than 1.5λ at the MS the effect of mutual coupling can be neglected while computing the capacity.

2.6 Conclusion

In this chapter, first an overview of the different multi-antenna channel modelling techniques has been presented, which has been followed by the details of the investigations carried out on certain aspects of MIMO channel modelling. The effect of array geometry on the capacity of a MIMO system has been investigated in the framework of geometry based single bounce modelling technique. Four different arrays namely, ULA, UCA, rhombic array and star array each having four elements have been considered for this purpose. Among the different $BS-MS$ array combinations, the combination of linear arrays has been found to provide best performances with regards to maximum achievable capacity. Moreover, it has been found that the combination of linear array at the BS and star shaped array at the MS performs best among all the combinations studied, if the rotational effects resulting due to movement of MS are taken into account. For the array combinations under consideration, the mean capacity is maximum and its standard deviation is minimum for the said array combination. MIMO channel modelling from microwave perspective has been considered next and a scattering matrix based approach has been developed for obtaining channel matrix $\mathbf{H}$ for such modelling approach. The chapter concludes by presenting the studies performed on the effect of mutual coupling on MIMO channels. It has been observed that for small inter-element separations (typically less than 1.5λ), mutual coupling effects the capacity of a MIMO system to a considerable extent.

Chapter 3

Modelling of Channel Characteristics for Mobile-to-Mobile Communication

3.1 Introduction

Recently, with the advent and popularity of wireless adhoc networks, advanced cellular networks and wireless sensor networks, studies on mobile-to-mobile (M2M) communication and relay based communication has attracted significant attention of the scientific community [PHYK05a, PHYK05b, PSP05, ZS06]. In an M2M channel, both the transmitter and the receiver are surrounded by local scatterers thus making the channel different from a conventional macrocellular channel. The presence of scatterers around the transmitter modifies the statistics of the physical channel parameters. As stated earlier, in a wireless channel, multipath restricts the performance by introducing fading in narrow band channels and inter symbol interference (ISI) in wideband systems. The use of antenna arrays and/or directional antennas helps in mitigating multipath interference. Spatial channel models that describe the angle of arrival and time of arrival of the multipath components are useful in evaluating the performance of wireless communication system using antenna arrays [Jan01]. The process of beam steering and beam shaping by antenna arrays require prior knowledge of the angle of arrival (AOA) of the desired signal so that the main lobe of the beam can be steered to the direction of the desired signal and beam nulls can be formed in the direction of the interfering signals. The AOA, also known as direction of arrival (DOA), statistics can be obtained from the measured data or from site specific channel models. In multi-element antenna systems, spatial correlation is a measure of relationship between two antennas' signals. The ideal

huge capacity anticipated by a MlMO system is realizable under the assumption of no spatial correlation [OAH04]. The Kronecker model discussed in chapter 2 of the thesis was developed to account for spatial correlation between antenna elements in a realistic way under the assumption that the spatial correlation at the transmitter and receiver ends are independent [AESVH06]. It is worth mentioning here that correlation and AOA statistics are strongly coupled [OHA04]. The nonuniform distribution of the AOA can significantly affect the performance of array based techniques, as the AOA statistics determine the cross correlation among the array elements [AK02]. Knowledge of AOA statistics is therefore very important and the AOA distribution reflects the scattering environment characteristics. The information of the time of arrival (TOA) statistics helps in determining the data rates and symbol periods so as to avoid ISI. Hence, there is a need to develop a statistical model which can characterize the distribution of the TOA and AOA of an M2M channel.

For macrocellular scenario it is generally assumed that the AOA at the MS is uniformly distributed in [0, 2π] as the scatterers are likely to surround the mobile from all directions. Moreover, in a macrocellular scenario BSs are generally positioned on an elevated plane, e.g., hill tops, roof tops etc., which are devoid of scatterers. In the next section, the geometry based single bounce one ring channel model representing the macrocellular scenario has been extended so as to model the M2M channels. The proposed model also takes into account the scatterers surrounding the transmitter. Analytical expression for TOA and AOA probability density functions for the single bounce geometrical model have been derived and the same is verified through simulation studies.

3.2 Model Description

The M2M channel model under consideration may be considered as a geometry based single bounce model as shown in Fig. 3.1. M_1 and M_2 denotes the transmitting and receiving mobile communicating devices respectively, separated by a distance D. In this model, scatterers are assumed to be distributed in two circular regions around M_1 and M_2. In general, the distribution of scatterers may be arbitrary, and it will affect the TOA and AOA pdfs evaluated using the model. The analysis presented here have been carried out assuming uniform distribution of scatterers. R_1 and R_2 respectively denotes the radii of the scattering regions around M_1 and M_2. N_1 & N_2 represents the number of scatterers at the transmitting and receiving ends. It has been assumed that

a ray emanating from the transmitter reaches the receiver only after being scattered by a single scatterer either at the transmitter or at the receiver end. It has also been assumed that all scattered rays that reach the receiver have the same power. The rays reaching the receiver after multiple scattering have been assumed to have very little power compared to the rays reaching the receiver after single scattering. Hence multiple scattering has not been taken into account. The separation between the transmitter and the receiver has been assumed to be large in comparison with the radii of the scattering regions. This assumption permits the application of geometrical optics and the waves can be represented as rays.

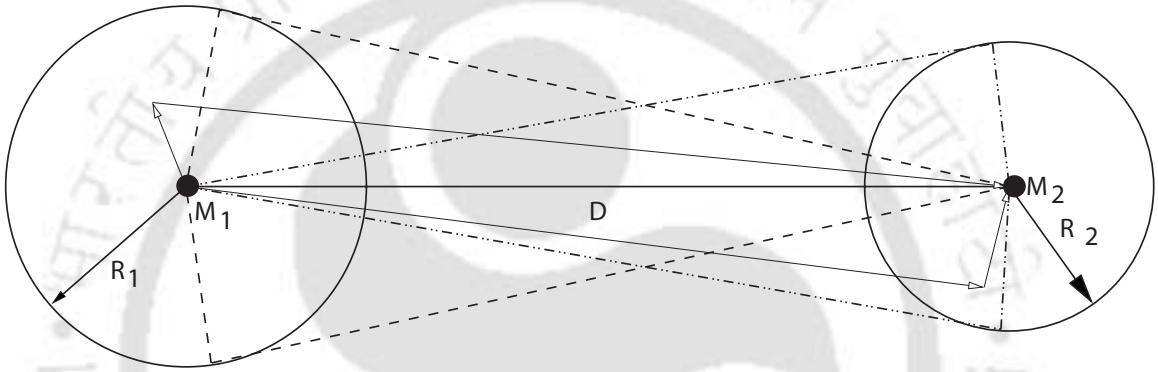

Figure 3.1: Uniformly distributed circular scattering regions surrounding the mobile nodes modelling M2M propagation environment.

3.3 Derivation of Time of Arrival Probability Density Function

In this section expression for the TOA pdf for the geometrical model described in section 3.2 has been derived. For the model under consideration, a transmitted signal after being scattered by the scatterers, reaches the receiver through multipath components having different time delays, depending on the path lengths. The difference in the time delays of the different multipath components introduces delay spread in the channel, which in turn may introduce ISI, depending on the data rates of the system. The maximum data rate that can be supported by a channel without introducing ISI and the requirement for equalization is determined by the time dispersive nature of the channel. It also helps in determining the navigational services like locating of a device. Moreover, as there is a strong relation between the signal bandwidth and the delay spread (which are inversely related), thus making characterization of the TOA statistics essential.

In deriving TOA pdf expression analytically for the model described in section 3.2, joint

TOA/AOA pdf can be derived from which marginal TOA pdf can be found. In [PRR96, ER99], it has been observed that the particular approach becomes intractable even for uniformly distributed scatterers. An alternative approach for obtaining analytical expression for the TOA pdf for macro-cellular scenario through computation of cumulative distribution function (CDF) of the TOA using a geometrical basis was presented in [ER99]. In deriving TOA pdf for M2M channel model the same methodology have been adopted.

In order to obtain the TOA CDF for a M2M communication channel, represented through geometrical model, containing finite number of scatterers, the first step is to determine the scatterers responsible for contributing towards a certain TOA, say τ. If the scatterers are assumed to reside on an ellipse having M_1 and M_2 at its foci, the rays from M_1 to M_2 (or from M_2 to M_1) involving such scatterers will have equal path delays. An ellipse corresponding to a given path delay τ, intersecting with the circular scattering regions is shown in Fig. 3.2. The scatterers with in the ellipse produces delay less than τ. The scatterers present in the shaded regions shown in Fig. 3.2 contribute towards determining the CDF, $F_\tau(\tau)$. Hence the CDF for the TOA for any particular τ, may be written as,

$$\begin{aligned} F_\tau(\tau) &= Pr\{t_{TOA} \leq \tau\} \\ &= \lim_{N\to\infty} \frac{n(\tau)}{N} \end{aligned} \tag{3.3.1}$$

where,

$F_\tau(\tau)$ is the CDF of the TOA.

Pr represents the probability.

$n(\tau)$ gives the total number of scatterers present inside the ellipse having constant delay τ and hence contributing towards the CDF.

N gives the total number of scatterers present in the system which is assumed to be very large.

If $n_1(\tau)$ and $n_2(\tau)$ represent the total number of scatterers around M_1 and M_2 respectively, and contributing to the CDF and N_1 and N_2 are the total number of scatterers around M_1 and M_2 respectively, then equation 3.3.1 can be written as,

$$F_\tau(\tau) = \lim_{N_1,N_2\to\infty} \frac{n_1(\tau) + n_2(\tau)}{N_1 + N_2} \tag{3.3.2}$$

The TOA pdf is obtained from the TOA CDF, $F_\tau(\tau)$, on differentiating it with respect to time delay τ. Hence the TOA pdf, $f_\tau(\tau)$, can be written as,

$$f_\tau(\tau) = \lim_{N_1,N_2\to\infty} \frac{1}{N_1+N_2} \frac{d}{d\tau} \left(n_1(\tau) + n_2(\tau)\right) \tag{3.3.3}$$

Let, ρ_1 and ρ_2 be the scatterer densities around M_1 and M_2 respectively, and assuming uniform distribution of the scatterers, the number of scatterers $n_1(\tau)$, $n_2(\tau)$, N_1 and N_2 can be written as follows,

$$n_1(\tau) = \rho_1 \Delta A_1(\tau) \tag{3.3.4}$$

$$n_2(\tau) = \rho_2 \Delta A_2(\tau) \tag{3.3.5}$$

$$N_1 = \rho_1 \pi R_1^2 \tag{3.3.6}$$

$$N_2 = \rho_2 \pi R_2^2 \tag{3.3.7}$$

The areas ΔA_1 and ΔA_2 are as shown in Fig. 3.2.

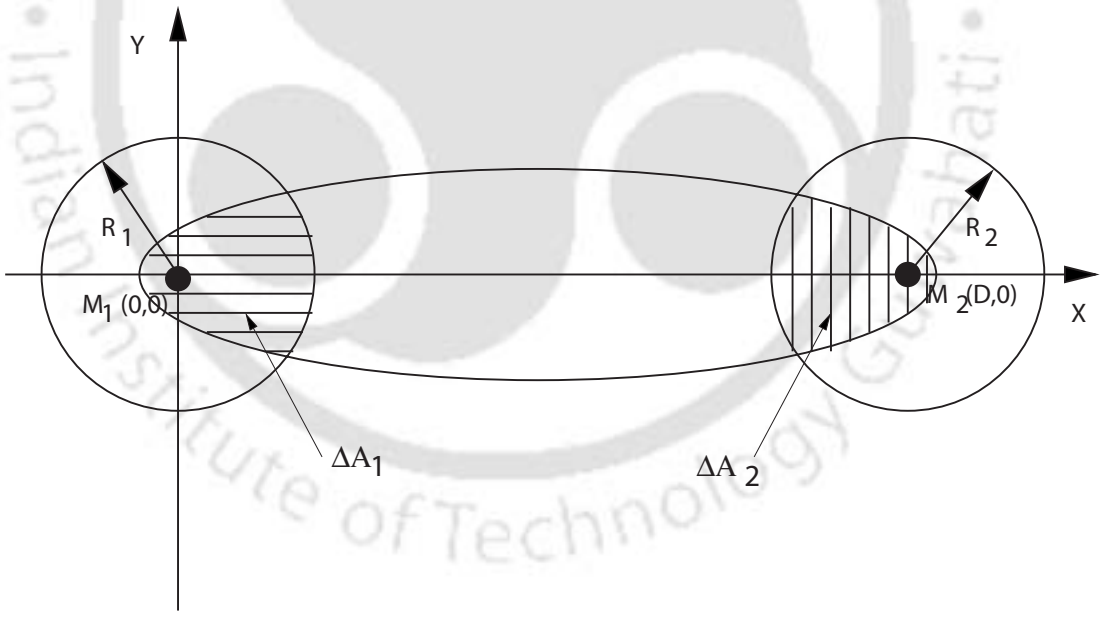

Figure 3.2: Shaded regions of scatterers for evaluating TOA CDF.

Combining equation 3.3.3 to 3.3.7, the pdf of the TOA may be written as,

$$f_\tau(\tau) = \frac{\rho_1}{\rho_1\pi R_1^2 + \rho_2\pi R_2^2} \frac{d\Delta A_1(\tau)}{d\tau} + \frac{\rho_2}{\rho_1\pi R_1^2 + \rho_2\pi R_2^2} \frac{d\Delta A_2(\tau)}{d\tau} \tag{3.3.8}$$

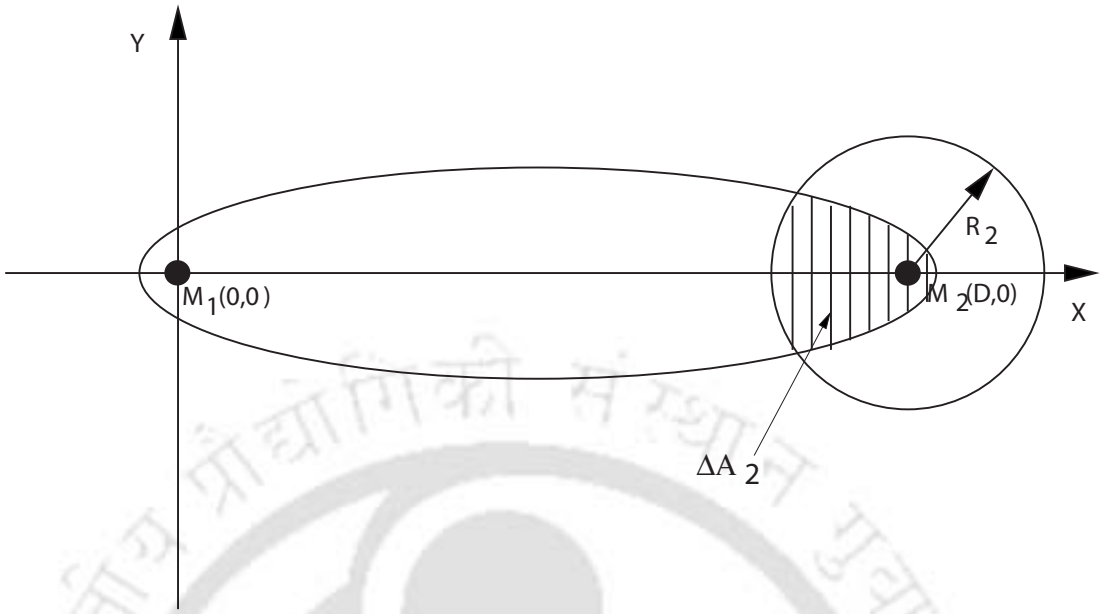

Figure 3.3: Area contributing to the TOA pdf, with M_1 as the transmitter and M_2 as the receiver.

Equation 3.3.8 can be written as,

$$f_\tau(\tau) = \frac{\rho_1}{\rho_1\pi R_1^2 + \rho_2\pi R_2^2}\cdot\pi R_1^2\cdot\left(\frac{1}{\pi R_1^2}\cdot\frac{d\Delta A_1(\tau)}{d\tau}\right) + \frac{\rho_2}{\rho_1\pi R_1^2 + \rho_2\pi R_2^2}\cdot\pi R_2^2\cdot\left(\frac{1}{\pi R_2^2}\cdot\frac{d\Delta A_2(\tau)}{d\tau}\right) \tag{3.3.9}$$

With reference to Fig. 3.3 and 3.4, it may be observed that the terms inside the parentheses of equation 3.3.9 corresponds to the TOA pdf for a macrocellular scenario. The term inside the first parenthesis of equation 3.3.9 gives the TOA pdf for a macrocellular scenario depicted in Fig. 3.4, whereas the term within the second parenthesis gives the TOA pdf for the scenario shown in Fig. 3.3. Thus, it may be observed that the TOA pdf for a M2M channel can be written in terms of the TOA pdf of two macrocellular channels combined with suitable weighting factors. For the sake of brevity and better readability, the terms within the parenthesis of equation 3.3.9 are denoted as,

$$f_{1\tau}(\tau) = \left(\frac{1}{\pi R_1^2}\cdot\frac{d\Delta A_1(\tau)}{d\tau}\right) \tag{3.3.10}$$

$$f_{2\tau}(\tau) = \left(\frac{1}{\pi R_2^2}\cdot\frac{d\Delta A_2(\tau)}{d\tau}\right) \tag{3.3.11}$$

Hence equation 3.3.9 can be written as,

$$f_\tau(\tau) = \frac{\rho_1 R_1^2}{\rho_1 R_1^2 + \rho_2 R_2^2}\cdot f_{1\tau}(\tau) + \frac{\rho_2 R_2^2}{\rho_1 R_1^2 + \rho_2 R_2^2}\cdot f_{2\tau}(\tau) \tag{3.3.12}$$

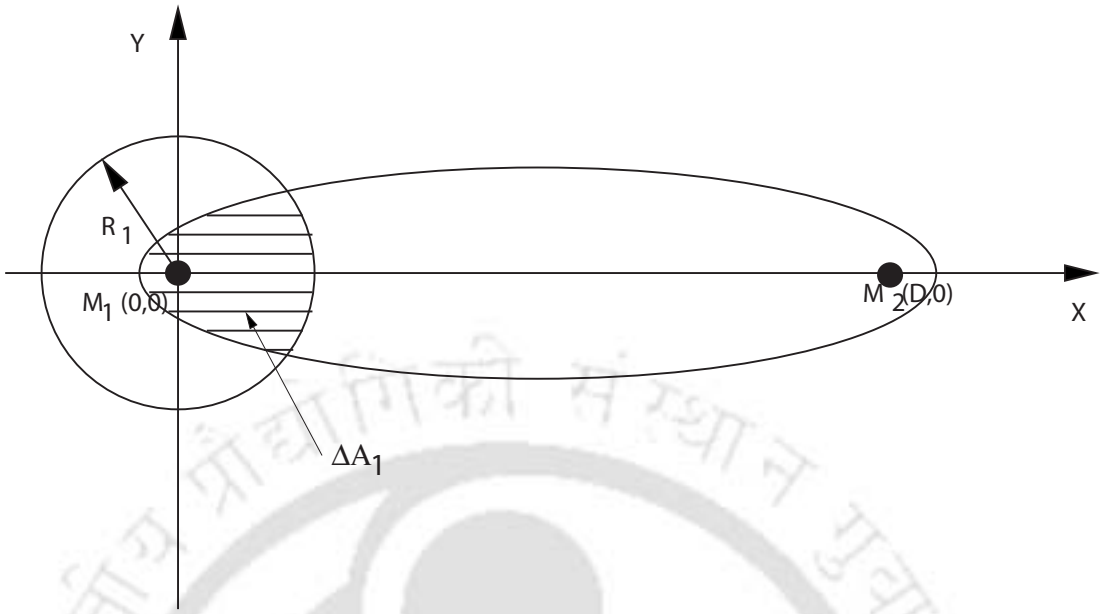

Figure 3.4: Area contributing to the TOA pdf, with M_2 as the transmitter and M_1 as the receiver.

or else,

$$f_\tau(\tau) = \frac{\rho_1 R_1^2/\rho_2 R_2^2}{1+\rho_1 R_1^2/\rho_2 R_2^2} \cdot f_{1\tau}(\tau) + \frac{1}{1+\rho_1 R_1^2/\rho_2 R_2^2} \cdot f_{2\tau}(\tau) \tag{3.3.13}$$

$$f_\tau(\tau) = \frac{\rho}{1+\rho} \cdot f_{1\tau}(\tau) + \frac{1}{1+\rho} \cdot f_{2\tau}(\tau) \tag{3.3.14}$$

$$\rho = \frac{\rho_1 R_1^2}{\rho_2 R_2^2} \tag{3.3.15}$$

where, ρ gives the relative scatterer density at M_1 with reference to scatterer density at M_2. $f_{i\tau}(\tau)$, for i = 1 and 2 respectively represent the TOA pdf's for a macrocellular communication system, where the scatterers are present only around the MS (M_2 for Fig. 3.3 and M_1 for Fig. 3.4), whereas the BS (M_1 for Fig. 3.3 and M_2 for Fig. 3.4) is devoid of scatterers. Expressions for TOA pdf for a circular scattering model having uniform distribution of scatterers representing macrocellular environment can be found in [ER99], which has been reproduced in equation 3.3.16 for the sake

of completeness,

$$\begin{aligned} f_\tau(\tau) &= \frac{1}{\pi R^2}\frac{d\Delta A(\tau)}{d\tau} \\ &= \frac{c}{\pi R^2} \\ &\quad \times \left[\frac{\pi\tau^2c^2k_2 - \tau ck_2^2 + \pi k_2k_1^2 + \tau ck_1^2 - 2Rk_1^2}{4k_1k_2}\right. \\ &\quad + \frac{\tau^2c^2k_0k_4 + \tau ck_0k_1^2}{2k_4^2 + 2k_0^2k_1^2} + \frac{\tau^2c^2 + k_1^2}{2k_1} \\ &\quad \times \arctan\left(\frac{k_0k_1}{k_4}\right) - \frac{R - \tau c}{\left(4R^2D^2 - k_3^2\right)^{1/2}} \\ &\quad \left.\times \left(2R^2 + \frac{\tau ck_1^2k_4\left(1 + k_0^2\right)}{\left(2k_4^2 + 2k_0^2k_1^2\right)^{1/2}}\right)\right] \end{aligned} \tag{3.3.16}$$

where,

$$\begin{aligned} k_0 &= \tan\left(\frac{1}{2}\arccos\left(\frac{-\tau^2c^2 + D^2 + 2R\tau c}{2RD}\right)\right) \\ k_1 &= \sqrt{\tau^2c^2 - D^2} \\ k_2 &= \sqrt{D^2 - 4R^2 - \tau^2c^2 + 4R\tau c} \\ k_3 &= -\tau^2c^2 + D^2 + 2R\tau c \\ k_4 &= D - \tau c \\ c &= velocity\,of\,light. \\ R &= radius\,of\,the\,circle\,containing\,scatterers\,around\,the\,mobile\,station. \\ D &= distance\,between\,the\,base\,station\,and\,the\,mobile\,station. \end{aligned}$$

Equation 3.3.16 is valid only for $(D/c) < \tau \leq (D + 2R/c)$. When $\tau = (D/c)$, the values of k_0, k_1, and k_4 becomes equal to zero and a few of the terms result in an indeterminate $\frac{0}{0}$ condition. Although it may be possible to apply L' Hospital's rule and find the limit as $\tau \to (D/c)$, the value of τ has been restricted to be strictly greater than D/c to avoid any singularity.

The above formulation of the TOA pdf for a M2M channel, depicted by two discs of scatterers around the transmitting and the receiving mobile stations, has been verified through computer simulations. Uniform distribution of scatterer positions have been obtained by generating ordered

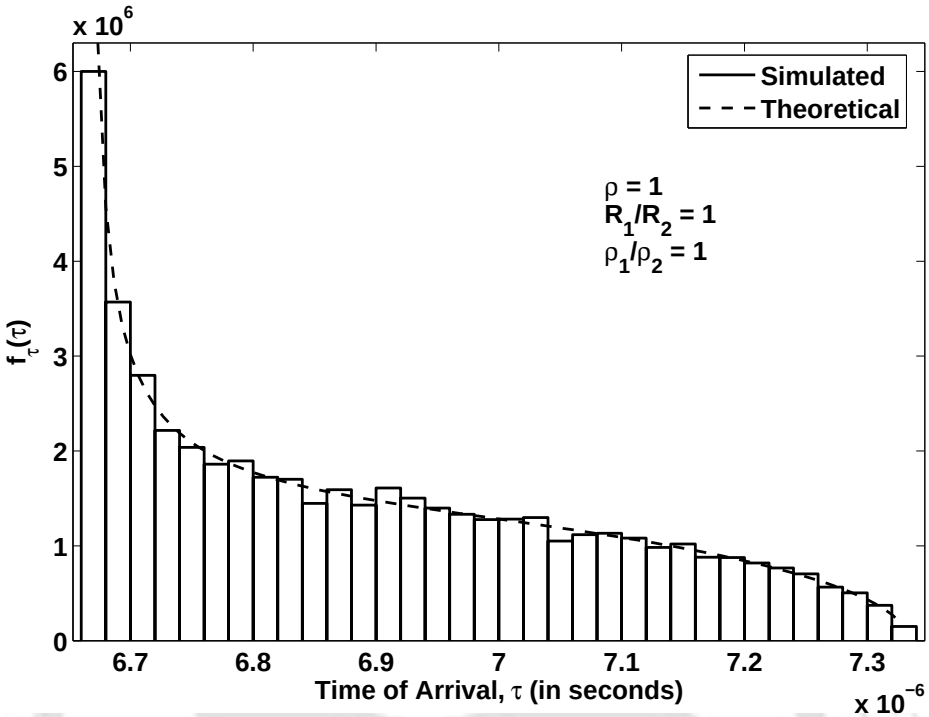

Figure 3.5: Theoretical and simulated density function of TOA for $D = 2000m, R_1 = 100m, R_2 = 100m, \frac{N_1}{N_2} = 1$.

pairs of random variables giving the angular positions and the radial distances from the mobile devices. The angular positions have been chosen to be uniformly distributed in [0,2π). The radial distances have been obtained from the product of the square root of uniformly distributed numbers between 0 and 1, multiplied with the radius of the scattering circles (R_1 for scatterers around mobile station M_1 and R_2 for scatterers around mobile station M_2). The simulations have been run for ten iterations each having different number of scatterers distributed uniformly with all the other model parameters remaining the same. The distribution of the scatterers remain the same but the actual scatterer position changes in different runs. The final results have been obtained by averaging the results of different iterations. Some representative results for different model parameters, as given in the legends and captions of the respective figures, have been shown in Fig. 3.5 to Fig. 3.7. For the results shown in these figures, D, the separation between the two mobile stations M_1 and M_2 has been taken as 2000 m. For R_1/R_2 = 1, the radii R_1 and R_2 have been taken as 100 m each. For different simulation trials, changes have been made in the values of R_2 and N_2. Theoretical and simulated results for various values of ρ and R_1/R_2 have been plotted. From the plots, it can be seen that theoretical and simulation results are in close agreement. The

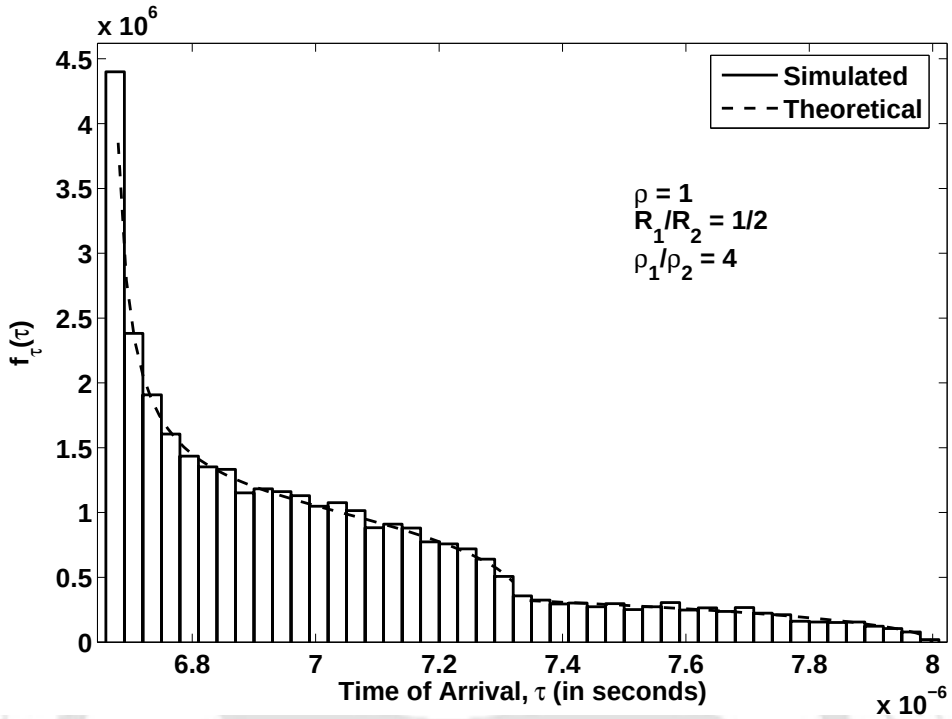

Figure 3.6: Theoretical and simulated density function of TOA for $D = 2000m, R_1 = 100m, R_2 = 200m, \frac{N_1}{N_2} = 1$.

validity of equation 3.3.14 is thus verified.

3.4 Derivation of AOA Probability Density Function for M2M channel

Multiple antenna elements are often used either at the transmitter and/or at the receiving end of a communication system. The multiple antennas may be used for spatial multiplexing or beamforming purposes. In beamforming applications, the knowledge of the AOA helps in steering the main lobe to the desired direction. Beam steering reduces the effect of interference and maximises the desired signal by forming beam nulls at the direction of the interfering signals and directing the main lobe to the direction of the desired signal.

For a M2M channel, since the scatterers are present both at the transmitter and the receiver ends, as discussed earlier, the AOA statistics will differ from those for macrocellular scenario. The AOA statistics for macrocellular scenario represented by circular scattering model have been

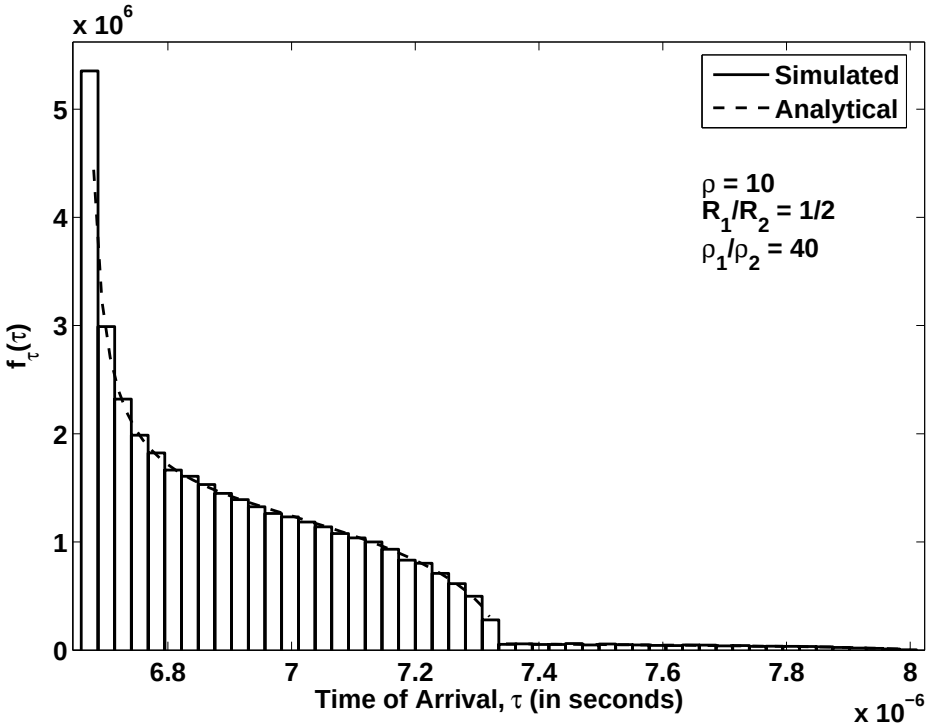

Figure 3.7: Theoretical and simulated density function of TOA for $D = 2000m, R_1 = 100m, R_2 = 200m, \frac{N_1}{N_2} = 10$.

dealt with and reported in detail in the literature [ER99, Jan01]. In an M2M channel, the scatterers around both the mobile units M_1 and M_2 and their distributions along with the model parameters viz. the distance between the mobile terminals, radii of the circular scattering region, relative scatterer density, determines the AOA statistics at the receiving mobile station. As in the previous section, the pdf of the AOA at the mobile station can be obtained by differentiating the CDF of the AOA at the receiving mobile station with respect to the angle of arrival θ.

The pdf of the AOA, $f_\theta(\theta)$, at the mobile station, M_1, spans the range $[-\pi, \pi]$. The probability of a scatterer being placed inside the shaded regions corresponding to an AOA less than or equal to θ, as shown in Fig. 3.8 and Fig. 3.9, gives the AOA CDF for that particular angle θ. As symmetry exists in the system model around the x-axis, the AOA pdf is symmetrical about θ = 0.

The AOA CDF is given by the ratio of the number of scatterers lying inside the shaded regions

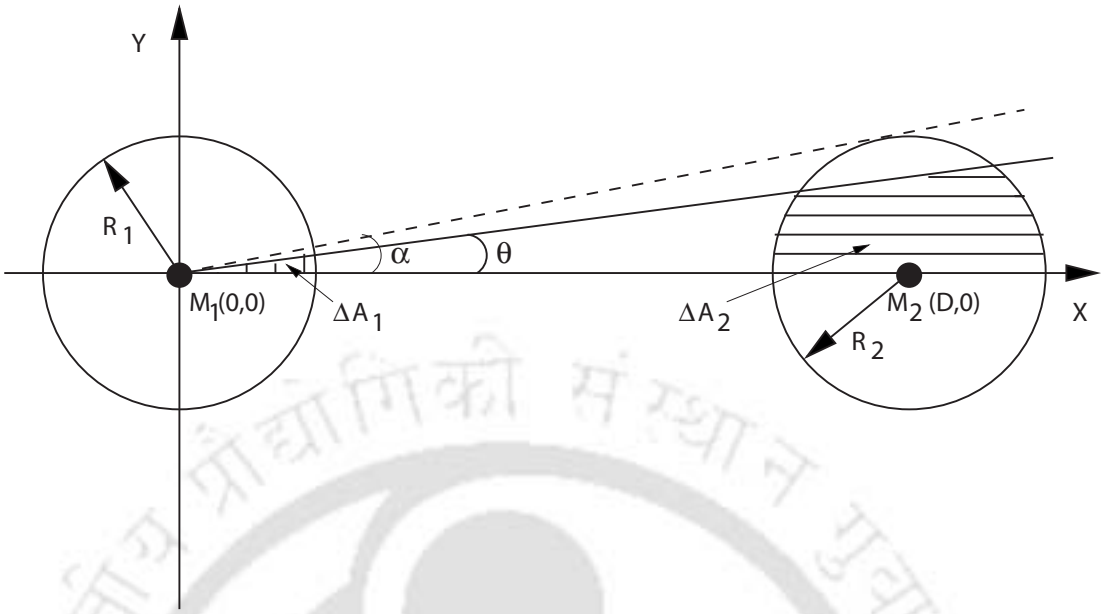

Figure 3.8: Shaded regions for evaluating AOA CDF, for $\theta \leq \alpha$, where, $\alpha = \sin^{-1}(R_2/D)$.

to the total number of scatterers in the system. The AOA CDF can be written as,

$$\begin{aligned} F_\theta(\theta) &= Pr\{\phi_{AOA} \leq \theta\} \\ &= \lim_{N\to\infty} \frac{n_\theta(\theta)}{N} \\ &= \lim_{N_1,N_2\to\infty} \frac{n_1(\theta)+n_2(\theta)}{N_1+N_2} \end{aligned} \tag{3.4.1}$$

where, $n_\theta(\theta)$ gives the number of scatterers contributing towards the CDF for an AOA, θ. Similarly, $n_1(\theta)$ and $n_2(\theta)$ respectively, corresponds to the number of scatterers around M_1 and M_2 which contributes towards the CDF for an AOA, θ. N denotes the total number of scatterers in the system, while N_1 and N_2 gives the total number of scatterers around M_1 and M_2 respectively and $N = N_1 + N_2$.

The AOA pdf is obtained upon differentiating equation 3.4.1 with respect to θ. Hence,

$$f_\theta(\theta) = \lim_{N_1,N_2\to\infty} \frac{1}{N_1+N_2} \frac{d}{d\theta} \left(n_1(\theta)+n_2(\theta)\right) \tag{3.4.2}$$

With reference to Fig. 3.8 and Fig. 3.9, as the scatterers are uniformly distributed, the number of scatterers occupying different regions may be written in terms of the scatterer densities and the

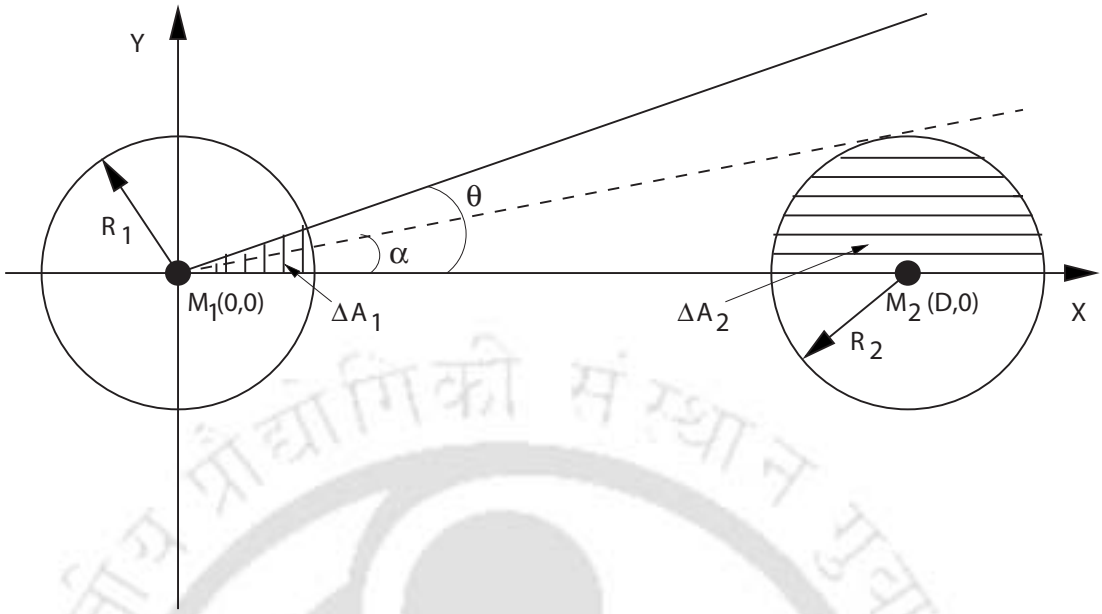

Figure 3.9: Shaded regions for evaluating AOA CDF, for $\theta \geq \alpha$, where, $\alpha = \sin^{-1}(R_2/D)$.

areas covered. Hence,

$$n_1(\theta) = \rho_1 \Delta A_1(\theta) \quad (3.4.3)$$

$$n_2(\theta) = \rho_2 \Delta A_2(\theta) \quad (3.4.4)$$

$$N_1 = \rho_1 \pi R_1^2 \quad (3.4.5)$$

$$N_2 = \rho_2 \pi R_2^2 \quad (3.4.6)$$

where, ρ_1 and ρ_2 are the scatterer densities around the mobile stations M_1 and M_2 respectively. The areas $\Delta A_1(\theta)$ and $\Delta A_2(\theta)$ are as shown in Fig. 3.8 and Fig. 3.9.

The sectorial area $\Delta A_1(\theta)$ is given by,

$$\Delta A_1(\theta) = \frac{\theta R_1^2}{2} \quad (3.4.7)$$

Combining equation 3.4.2 to equation 3.4.7 gives,

$$\begin{aligned}
f_\theta(\theta) &= \frac{1}{\rho_1\pi R_1^2+\rho_2\pi R_2^2}\frac{d}{d\theta}\left(\rho_1\Delta A_1(\theta)+\rho_2\Delta A_2(\theta)\right)\\
&= \frac{\rho_1}{\rho_1\pi R_1^2+\rho_2\pi R_2^2}\frac{d\Delta A_1(\theta)}{d\theta}\\
&\quad+\frac{\rho_2}{\rho_1\pi R_1^2+\rho_2\pi R_2^2}\frac{d\Delta A_2(\theta)}{d\theta}\\
&= \frac{\rho_1}{\rho_1\pi R_1^2+\rho_2\pi R_2^2}\frac{d(\frac{\theta R_1^2}{2})}{d\theta}\\
&\quad+\frac{\rho_2}{\rho_1\pi R_1^2+\rho_2\pi R_2^2}\frac{d\Delta A_2(\theta)}{d\theta}\\
&= \frac{\rho_1 R_1^2}{\rho_1 R_1^2+\rho_2 R_2^2}\frac{1}{2\pi}\\
&\quad+\frac{\rho_2\pi R_2^2}{\rho_1\pi R_1^2+\rho_2\pi R_2^2}\frac{1}{\pi R_2^2}\frac{d\Delta A_2(\theta)}{d\theta}\\
&= \frac{\rho_1 R_1^2/\rho_2 R_2^2}{1+\rho_1 R_1^2/\rho_2 R_2^2}\frac{1}{2\pi}\\
&\quad+\frac{1}{1+\rho_1 R_1^2/\rho_2 R_2^2}\frac{1}{\pi R_2^2}\frac{d\Delta A_2(\theta)}{d\theta}\\
&= \frac{\rho}{1+\rho}\frac{1}{2\pi}+\frac{1}{1+\rho}\frac{1}{\pi R_2^2}\frac{d\Delta A_2(\theta)}{d\theta}
\end{aligned} \tag{3.4.8}$$

where,

$$\rho = \frac{\rho_1 R_1^2}{\rho_2 R_2^2} \tag{3.4.9}$$

The term $\frac{1}{\pi R_2^2}\frac{d}{d\theta}\left(\Delta A_2(\theta)\right)$ denoted as $f_{2\theta}(\theta)$ gives the pdf of the AOA for a macrocellular scenario, which has been derived in [ER99]. The pdf of the AOA for a macrocellular scenario, having D as the separation between the transmitter and the receiver and R_2 as the radius of the scattering circle, is given as,

$$f_{2\theta}\left(\theta\right) = \begin{cases} \frac{2D\cos(\theta)\sqrt{D^2\cos^2(\theta)-D^2+R_2^2}}{\pi R_2^2} & for,\ -\sin^{-1}\left(\frac{R_2}{D}\right)\le\theta\le\sin^{-1}\left(\frac{R_2}{D}\right) \\ 0 & elsewhere \end{cases} \tag{3.4.10}$$

Combining equation 3.4.8 and equation 3.4.10, the pdf of the AOA at the mobile station M_1, for a M2M channel can be written as,

$$f_\theta\left(\theta\right) = \begin{cases} \frac{\rho}{1+\rho}\cdot\frac{1}{2\pi}+\frac{1}{1+\rho}\cdot\frac{2D\cos(\theta)\sqrt{D^2\cos^2(\theta)-D^2+R_2^2}}{\pi R_2^2} & for,\ -\sin^{-1}\left(\frac{R_2}{D}\right)\le\theta\le\sin^{-1}\left(\frac{R_2}{D}\right) \\ \frac{\rho}{1+\rho}\frac{1}{2\pi} & elsewhere \end{cases} \tag{3.4.11}$$

The above formulation for the pdf of the AOA has been verified through computer simulation. Uniformly distributed scatterers have been generated by the method described in section 3.3. Some of the representative results have been plotted in Fig. 3.10 to Fig. 3.13. Theoretical and simulated results for various values of ρ and R_1/R_2 have been plotted for $D = 500m$. The agreement of the theoretical and the simulation results verifies the validity of equation 3.4.11.

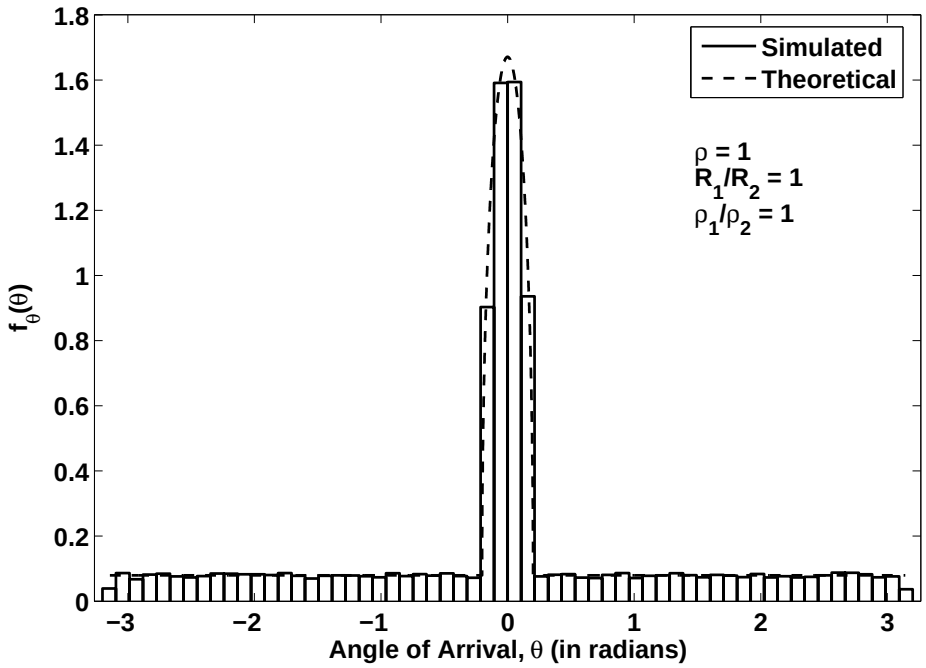

Figure 3.10: Theoretical and simulated density function of AOA for $D = 500m, R_1 = 100m, R_2 = 100m, \frac{N_1}{N_2} = 1$.

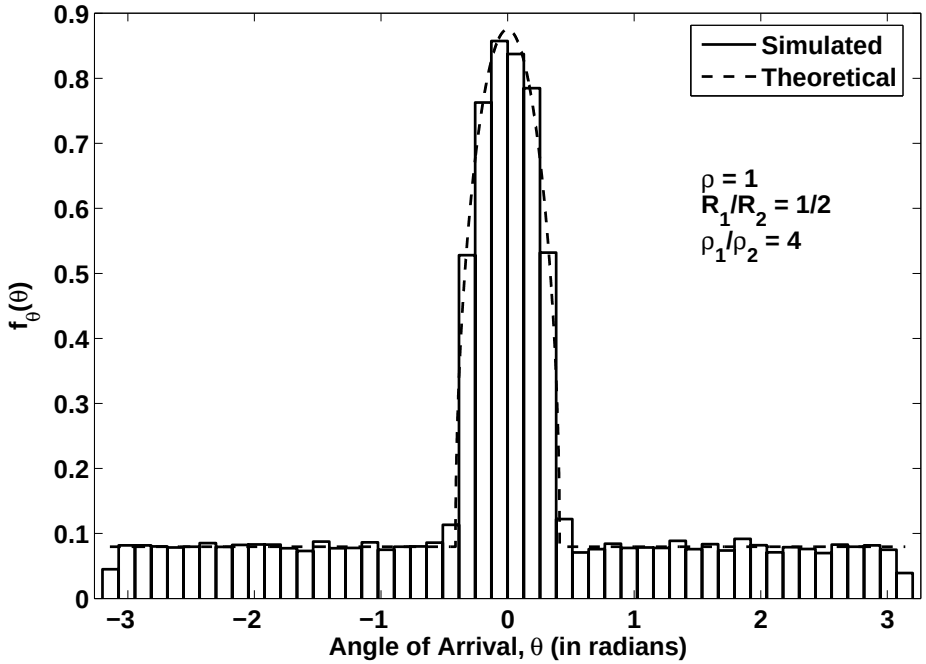

Figure 3.11: Theoretical and simulated density function of AOA for $D = 500m, R_1 = 100m, R_2 = 200m, \frac{N_1}{N_2} = 1$.

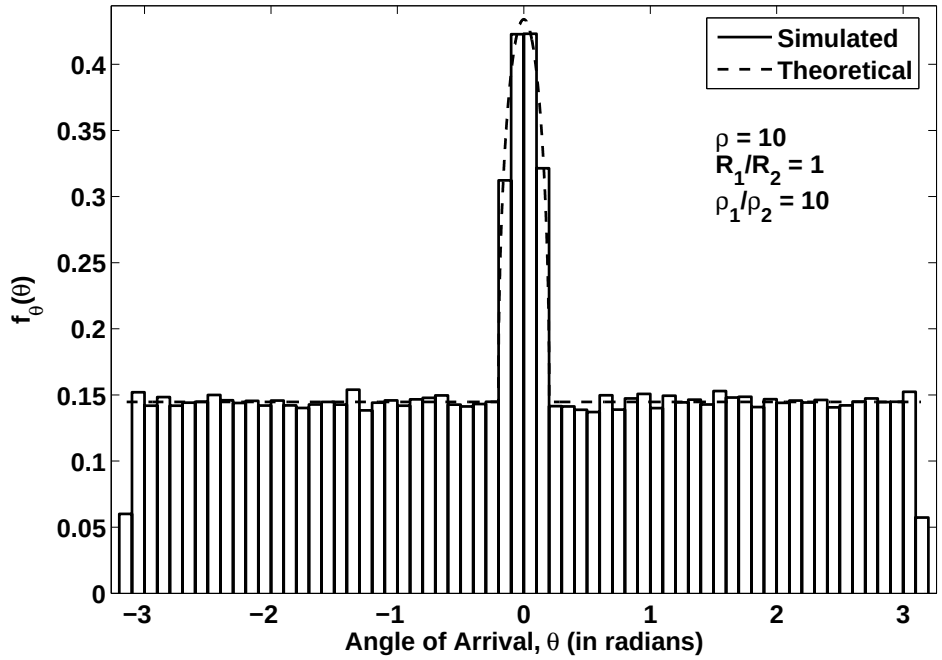

Figure 3.12: Theoretical and simulated density function of AOA for $D = 500m, R_1 = 100m, R_2 = 100m, \frac{N_1}{N_2} = 10$.

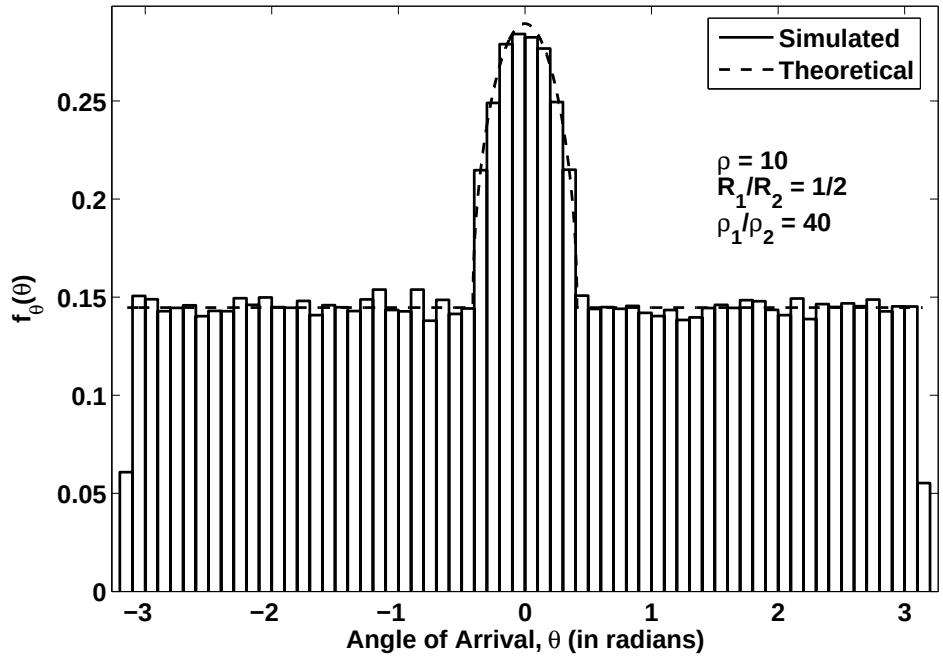

Figure 3.13: Theoretical and simulated density function of AOA for $D = 500m, R_1 = 100m, R_2 = 200m, \frac{N_1}{N_2} = 10$.

3.5 Dual Annular Strip Model (DASM) for M2M communication

In this section M2M geometry based channel model considered in section 3.2 has been generalised further. Here, the M2M channel model has been developed by considering annular ring of scatterers surrounding the transmitting and the receiving mobile stations. Such modelling approach provides the flexibility to study models represented by circular rings of scatterers, annular rings of scatterers and discs of scatterers by simply varying the radial dimensions. Further, this model can be useful in the study of different channel statistics when the scatterers are uniformly distributed along the angular dimension but not so in the radial dimension with reference to a polar coordinate system. The TOA analysis has been done in line with section 3.3. As shown in Fig. 3.14, any scatterer lying inside or on the constant delay ellipse results in TOA less than or equal to some time delay, say τ. With reference to Fig. 3.14, the hashed areas ΔA_1 and ΔA_2 contributes to

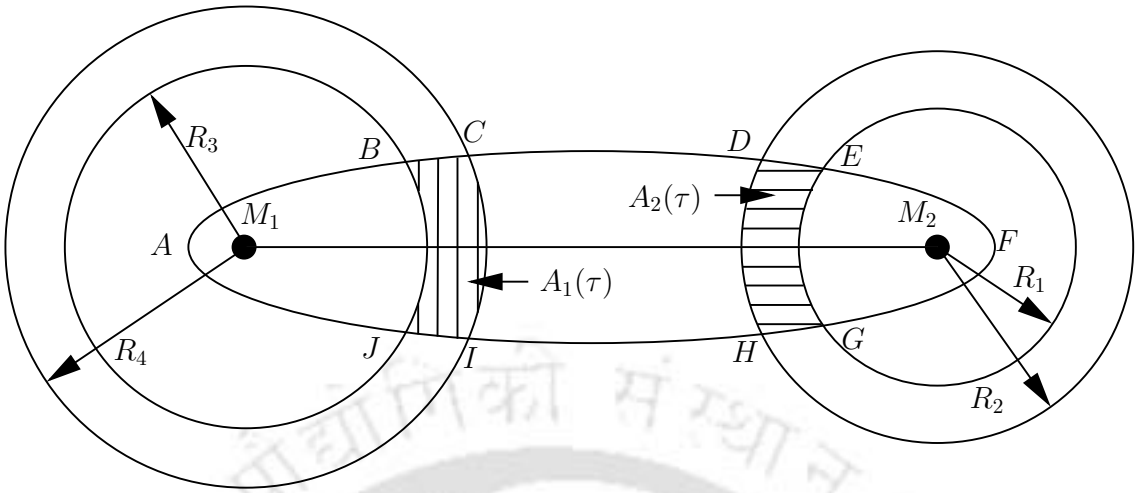

Figure 3.14: Shaded regions of scatterers for evaluating the TOA CDF for dual annular strip model.

the TOA CDF. The TOA CDF may be written as

$$F_\tau(\tau) = \frac{Number\,of\,scatterers\,contributing\,to\,the\,time\,delay\,less\,than\,or\,equal\,to\,'\tau'}{Total\,number\,of\,scatterers\,in\,the\,system} \tag{3.5.1}$$

As the scatterers are assumed to be uniformly distributed the number of scatterers is proportional to the area in which they are present. Hence equation 3.5.1 can be written as

$$F_\tau(\tau) = \frac{Area\,contributing\,to\,the\,time\,delay\,less\,than\,or\,equal\,to\,'\tau'}{Total\,area\,over\,which\,the\,scatterers\,are\,present} \tag{3.5.2}$$

With reference to Fig. 3.14, equation 3.5.2 can be written as

$$F_\tau(\tau) = \frac{A_1(\tau) + A_(\tau)}{\pi(R_2^2 - R_1^2) + \pi(R_4^2 - R_3^2)} \tag{3.5.3}$$

The TOA pdf can be obtained on differentiating the TOA CDF (equation 3.5.3) with respect to τ

$$f_\tau(\tau) = \frac{1}{\pi(R_2^2 - R_1^2) + \pi(R_4^2 - R_3^2)} \frac{d}{d\tau}\left(A_1(\tau) + A_2(\tau)\right) \tag{3.5.4}$$

$$\begin{aligned} f_\tau(\tau) &= \frac{1}{\pi(R_2^2 - R_1^2) + \pi(R_4^2 - R_3^2)} \\ &\quad \times \frac{d}{d\tau}\left[Area\,enclosed\,in\,(ACIA - ABJA + DFHD - EFGE)\right] \end{aligned} \tag{3.5.5}$$

$$\begin{aligned} f_\tau(\tau) &= \frac{1}{\pi\left(R_2^2+R_4^2-R_1^2-R_3^2\right)}\cdot\Bigg[\pi R_4^2\cdot\left(\frac{1}{\pi R_4^2}\cdot\frac{d}{d\tau}\left(Area\ \ in\ \ ACIA\right)\right) \\ &\quad -\pi R_3^2\cdot\left(\frac{1}{\pi R_3^2}\cdot\frac{d}{d\tau}\left(Area\,in\,ABJA\right)\right) \\ &\quad +\pi R_2^2\cdot\left(\frac{1}{\pi R_2^2}\cdot\frac{d}{d\tau}\left(Area\,in\,DFHD\right)\right) \\ &\quad -\pi R_1^2\cdot\left(\frac{1}{\pi R_1^2}\cdot\frac{d}{d\tau}\left(Area\,in\,EFGE\right)\right)\Bigg] \end{aligned} \tag{3.5.6}$$

$$f_\tau(\tau)=\frac{1}{\pi\left(R_2^2+R_4^2-R_1^2-R_3^2\right)}\cdot\left[\pi R_4^2\cdot f_{4\tau}(\tau)-\pi R_3^2\cdot f_{3\tau}(\tau)+\pi R_2^2\cdot f_{2\tau}(\tau)-\pi R_1^2\cdot f_{1\tau}(\tau)\right] \tag{3.5.7}$$

where, $f_{i\tau}(\tau)$ represents the pdf of the TOA for the macrocellular scenario having R_i as the radius of the scattering circle and i can take any of integer values from 1 to 4. $f_{i\tau}(\tau)$ is given by equation 3.3.16, hence equation 3.5.7 can be written as,

$$f_\tau(\tau)=\frac{c}{\pi\left(R_2^2+R_4^2-R_1^2-R_3^2\right)}\cdot\left[Z_2+Z_4-Z_1-Z_3\right] \tag{3.5.8}$$

where, i = 1,2,3,4 and Z_i is given as,

$$\begin{aligned} Z_i=\Bigg[&\frac{\pi\tau^2c^2k_{2i}-\tau ck_{2i}^2+\pi k_{2i}k_{1i}^2+\tau ck_{1i}^2-2R_ik_{1i}^2}{4k_{1i}k_{2i}} \\ &\times\frac{\tau^2c^2k_{0i}k_{4i}+\tau ck_{0i}k_{1i}^2}{2k_{4i}^2+2k_{0i}^2k_{1i}^2}+\frac{\tau^2c^2+k_{1i}^2}{2k_{1i}} \\ &\times a\tan\left(\frac{k_{0i}k_{1i}}{k_{4i}}\right)-\frac{R_i-\tau c}{\left(4R_i^2D^2-k_{3i}^2\right)^{1/2}} \\ &\times\left(2R_i^2+\frac{\tau ck_{1i}^2k_{4i}\left(1+k_{0i}^2\right)}{2k_{4i}^2+2k_{0i}^2k_{1i}^2}\right)\Bigg] \end{aligned} \tag{3.5.9}$$

and

$$\begin{aligned} k_{0i}&=\tan\left(\tfrac{1}{2}a\cos\left(\tfrac{-\tau^2c^2+D^2+2R_i\tau c}{2R_iD_i}\right)\right) \\ k_{1i}&=\sqrt{\tau^2c^2-D^2} \\ k_{2i}&=\sqrt{D^2-4R_i^2-\tau^2c^2+4R_i\tau c} \\ k_{3i}&=-\tau^2c^2+D^2+2R_i\tau c \\ k_{4i}&=D-\tau c \end{aligned} \tag{3.5.10}$$

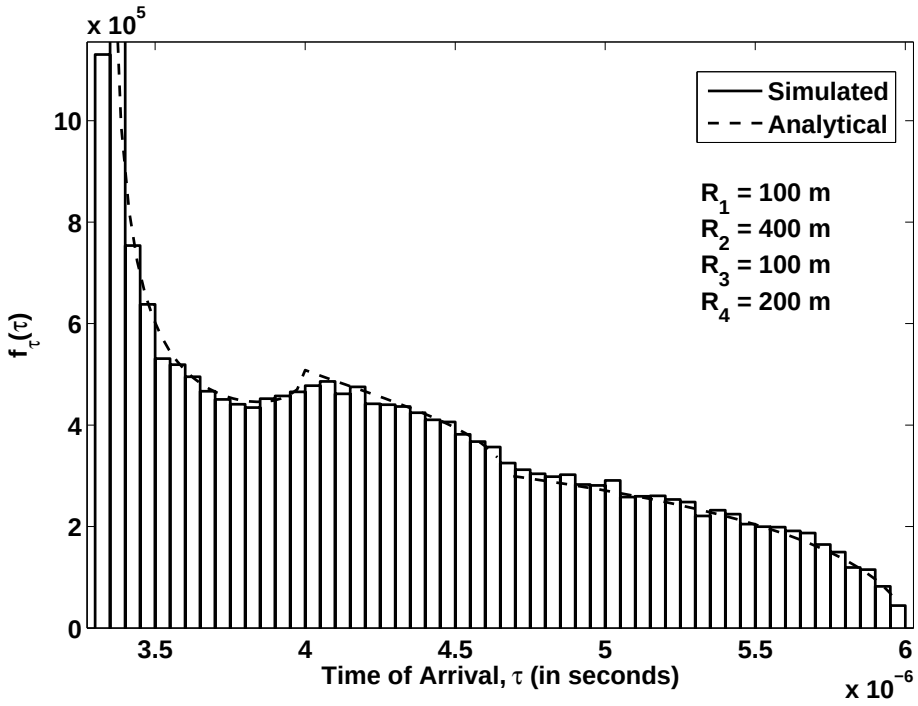

Figure 3.15: Plots of the theoretical and simulated probability density function of TOA having annular ring of scatterers around the transmitter and the receiver.

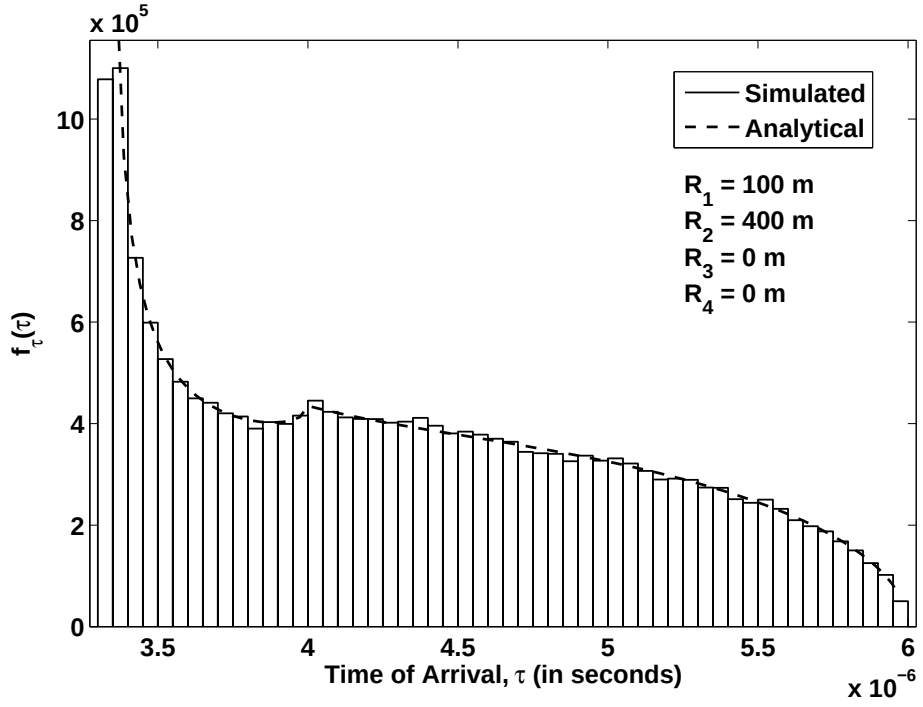

Figure 3.16: Plots of the theoretical and simulated probability density function of TOA having an annular ring of scatterers around the receiver.

Simulations have been performed for different values of R_1, R_2, R_3 and R_4. D, the distance between the transmitting and the receiving mobile stations have been kept fixed at 1000 m. Fig. 3.15 and 3.16 shows the plot of the simulated results and those obtained from equation 3.5.8. It can be seen that the results are in close agreement, thus verifying the validity of equation 3.5.8.

The analysis of the AOA for the dual annular ring model for M2M channel has been done in line with section 3.4. The hashed region in Fig. 3.17 gives the area responsible for contributing to the AOA pdf in the range θ and $\theta + d\theta$. The AOA ranges between $[-\pi, \pi]$ and is symmetrical about $\theta = 0$. For the ease in analysis the angular range is divided into different sections. The ranges are $\alpha_2 \leq \theta \leq \pi$, $\alpha_1 \leq \theta \leq \alpha_2$, $-\alpha_1 \leq \theta \leq \alpha_1$, $-\alpha_2 \leq \theta \leq -\alpha_1$ and $-\pi \leq \theta \leq -\alpha_2$.

The elementary area dA contributing to the elementary AOA $d\theta$ having $\alpha_2 \leq \theta \leq \pi$ is given in equation 3.5.11. The contribution to the AOA is due to the scatterers around the mobile station M_1.

$$dA = \frac{1}{2}\left(R_4^2 - R_3^2\right) d\theta \tag{3.5.11}$$

Similarly for the ranges $\alpha_1 \leq \theta \leq \alpha_2$, $-\alpha_1 \leq \theta \leq \alpha_1$, $-\alpha_2 \leq \theta \leq -\alpha_1$ and $-\pi \leq \theta \leq -\alpha_2$, the incremental area dA contributing to the AOA in the range θ and θ + dθ can be written as,

$$dA = 2D\cos(\theta)\sqrt{R_2^2 - D^2\sin^2(\theta)}d\theta + \frac{1}{2}\left(R_4^2 - R_3^2\right) d\theta \qquad \alpha_1 \leq \theta \leq \alpha_2 \tag{3.5.12}$$

$$dA = \left[2D\cos(\theta)\sqrt{R_2^2 - D^2\sin^2(\theta)} - 2D\cos(\theta)\sqrt{R_1^2 - D^2\sin^2(\theta)}\right] d\theta + \frac{1}{2}\left(R_4^2 - R_3^2\right) d\theta \qquad -\alpha_1 \leq \theta \leq \alpha_1 \tag{3.5.13}$$

$$dA = 2D\cos(\theta)\sqrt{R_2^2 - D^2\sin^2(\theta)}d\theta + \frac{1}{2}\left(R_4^2 - R_3^2\right) d\theta \qquad -\alpha_2 \leq \theta \leq -\alpha_1 \tag{3.5.14}$$

$$dA = \frac{1}{2}\left(R_4^2 - R_3^2\right) d\theta \qquad -\pi \leq \theta \leq -\alpha_2 \tag{3.5.15}$$

where, the first term in equation 3.5.12 to equation 3.5.14 is due to contributions from scatterers surrounding the mobile station M_2. The term in equation 3.5.15 and the second term of 3.5.12 to equation 3.5.14 is contributed by scatterers surrounding M_1.

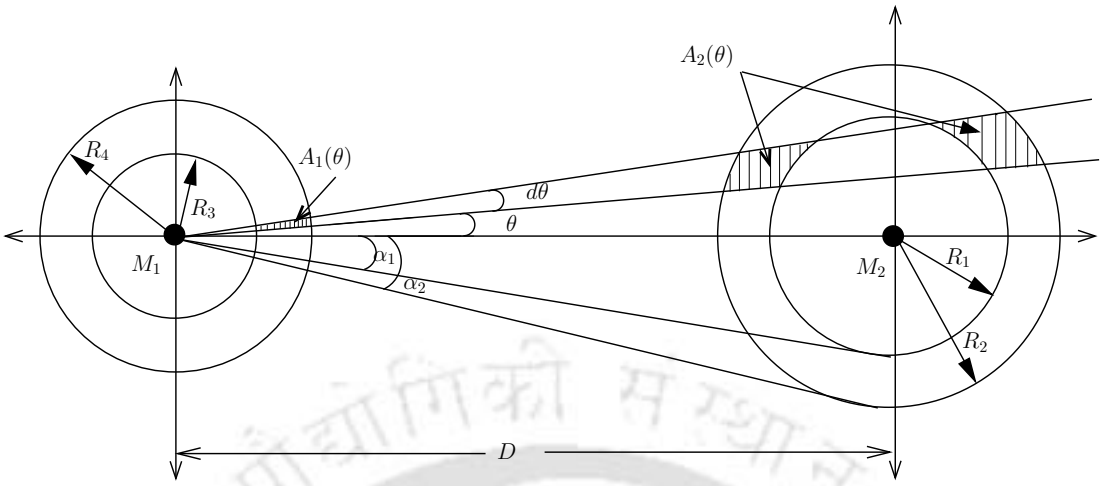

Figure 3.17: Dual annular strip model for determining the AOA pdf for a mobile-to-mobile channel.

The AOA pdf can be written as,

$$f_\theta(\theta) = \frac{1}{A} \cdot \frac{d}{d\theta}\left(A_1(\theta) + A_2(\theta)\right) \tag{3.5.16}$$

Substituting the values of $\frac{dA}{d\theta}$ in equation 3.5.16 from equation 3.5.11 to 3.5.15 for different ranges of θ, the pdf of AOA can be obtained and is given in equation 3.5.17. In equation 3.5.16, A is the total area over which the scatterers are uniformly distributed. Thus $A = \pi(R_4^2 + R_2^2 - R_3^2 - R_1^2)$.

$$f_\theta(\theta) = \begin{cases} \frac{0.5\left(R_4^2 - R_3^2\right)}{\pi\left(R_4^2 + R_2^2 - R_3^2 - R_1^2\right)} & \alpha_2 \le \theta \le \pi \\ \frac{2D\cos(\theta)\sqrt{R_2^2 - D^2\sin^2(\theta)} + 0.5\left(R_4^2 - R_3^2\right)}{\pi\left(R_4^2 + R_2^2 - R_3^2 - R_1^2\right)} & \alpha_1 \le \theta \le \alpha_2 \\ \frac{2D\cos(\theta)\sqrt{R_2^2 - D^2\sin^2(\theta)} - 2D\cos(\theta)\sqrt{R_1^2 - D^2\sin^2(\theta)} + 0.5\left(R_4^2 - R_3^2\right)}{\pi\left(R_4^2 + R_2^2 - R_3^2 - R_1^2\right)} & -\alpha_1 \le \theta \le \alpha_1 \\ \frac{2D\cos(\theta)\sqrt{R_2^2 - D^2\sin^2(\theta)} + 0.5\left(R_4^2 - R_3^2\right)}{\pi\left(R_4^2 + R_2^2 - R_3^2 - R_1^2\right)} & -\alpha_2 \le \theta \le -\alpha_1 \\ \frac{0.5\left(R_4^2 - R_3^2\right)}{\pi\left(R_4^2 + R_2^2 - R_3^2 - R_1^2\right)} & -\pi \le \theta \le -\alpha_2 \end{cases} \tag{3.5.17}$$

For simulation purposes uniformly distributed scatterers have been generated using the method described in section 3.3. Plot of the results obtained theoretically from equation 3.5.17 and those obtained through simulation have been shown in Fig. 3.18 to Fig. 3.21 for different values of

model parameters given in the legends of the respective figures. Four different cases have been considered. In the first case, both the transmitter and the receiver are assumed to be surrounded by scatterers distributed uniformly in annular rings of equal width. In the second case, the scatterers have been assumed to be uniformly distributed over annular rings of unequal width. Thirdly, scatterers have been considered to be uniformly distributed on discs of unequal radii with transmitter and receiver at the centres of the discs. Uniformly distributed in discs (of unequal dimension) around the transmitter and the receiver were considered. Finally, the AOA for a model having an annular ring of uniformly distributed scatterers only around the receiver has been studied. The shape of the AOA pdf is similar for all the four cases. It consists of two parts, one dome-shaped part and a flat portion. Moreover, in all the cases the pdfs are symmetric around $\theta = 0$. The width of the dome-shaped portion is determined by the outer radius of the annular ring around the receiver and the distance between the transmitter and the receiver. The flat portion of the AOA pdf is contributed due to the scatterers around the transmitter those which do not contribute to the dome-shaped portion. The agreement of the theoretical and the simulated results verify the validity of equation 3.5.17.

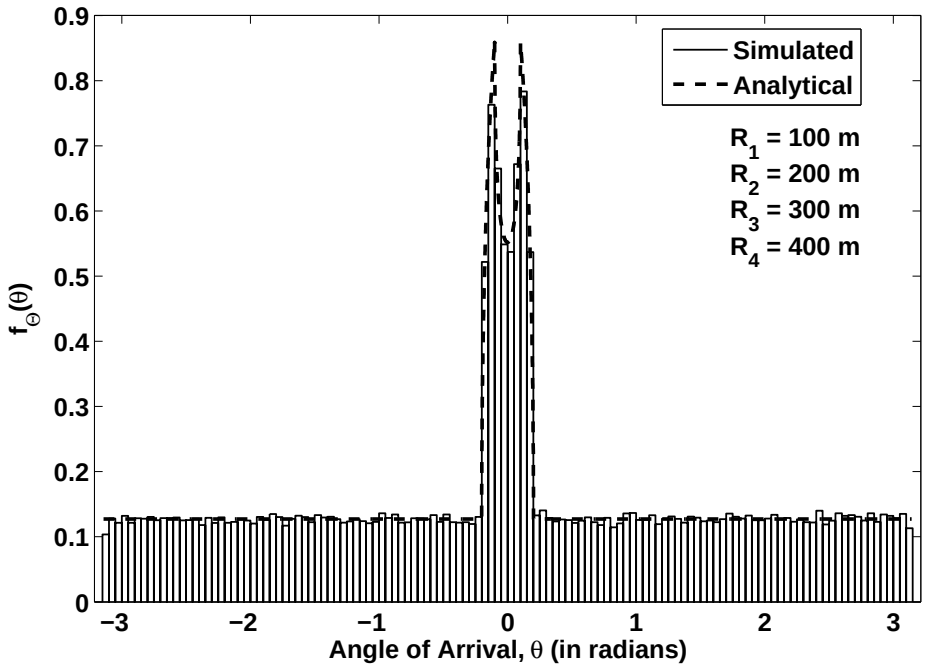

Figure 3.18: Plots of the theoretical and simulated probability density function of AOA having annular ring of scatterers of equal width around the transmitter and the receiver.

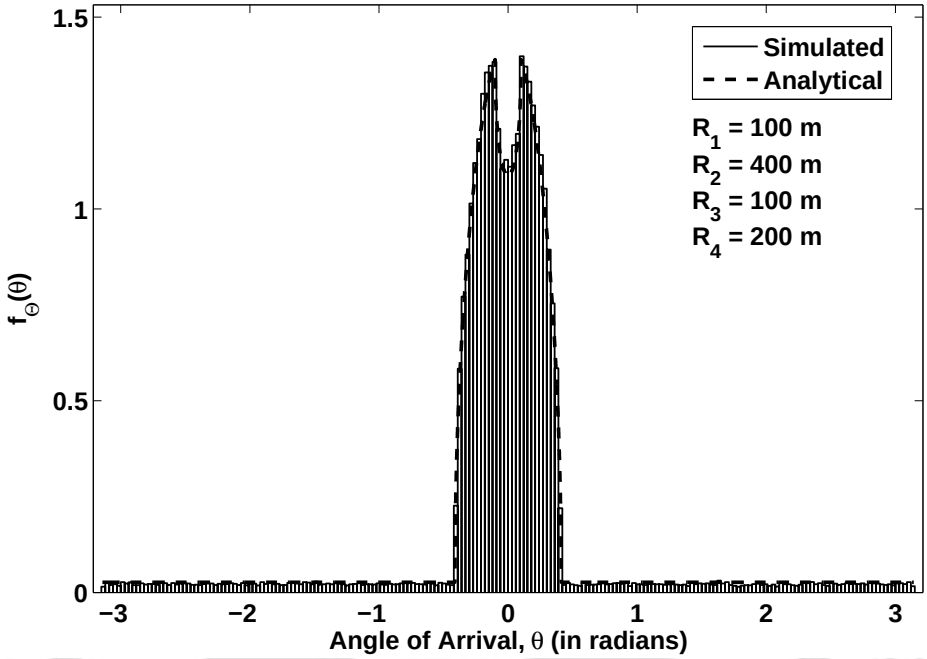

Figure 3.19: Plots of the theoretical and simulated probability density function of AOA having annular ring of scatterers of different width around the transmitter and the receiver.

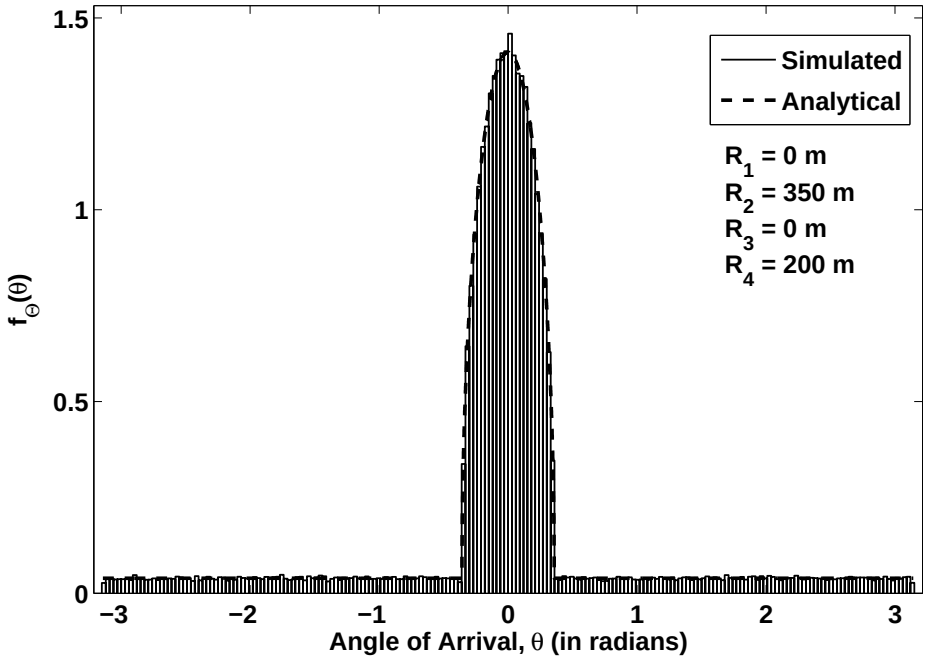

Figure 3.20: Plots of the theoretical and simulated probability density function of AOA having a disc of scatterers around the transmitter and the receiver.

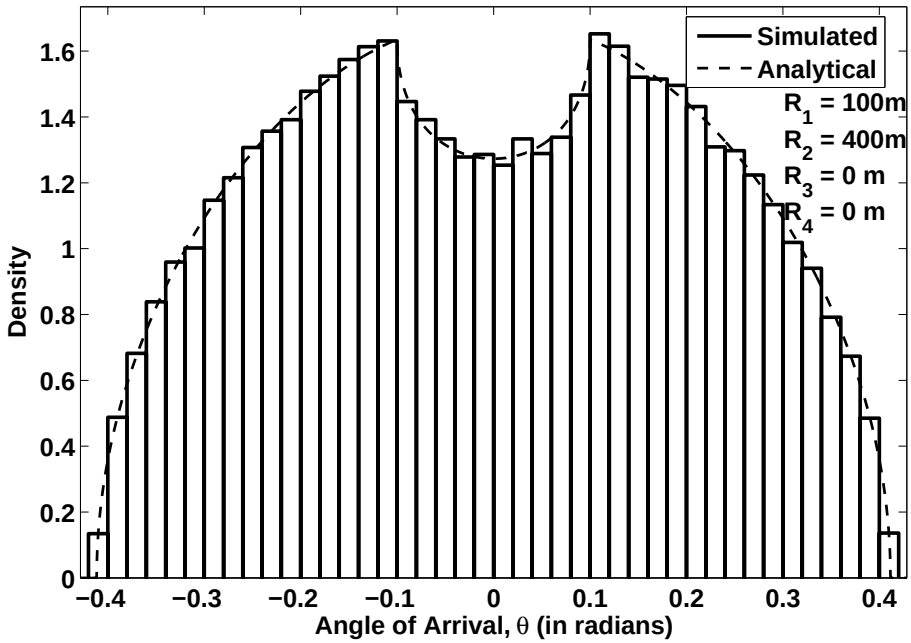

Figure 3.21: Plots of the theoretical and simulated probability density function of AOA having an annular ring of scatterers around the receiver.

3.6 Conclusion

In this chapter, geometrically based single bounce channel models for a M2M channel have been discussed. The scatterers have been assumed to be uniformly distributed in circular discs having the transmitter and the receiver located at their centres. The probability density functions for the TOA and the AOA for such M2M channel model have been derived. The derived density functions have been verified through computer simulations. The analytical expressions are useful for the design of M2M communication systems. The analysis has been further extended to a more generalized dual annular strip model (DASM). The uniform circular scattering model can be considered to be a special case of DASM . DASM can also be used for circular scattering model with non uniform distribution of scatterers, for scenarios where scatterers are uniformly distributed along the angular dimension but have non uniform distribution in the radial dimension, with reference to a polar coordinate system. For this case, the circular scattering region can be segmented into smaller annular strips and a circle of small radius over which the scatterer distribution can be assumed to be uniform.

Chapter 4

Relay Based Virtual MIMO System

4.1 Introduction

In the previous chapters, discussions have been kept restricted to geometrical based modelling and their analysis. In this chapter a virtual MIMO system, which is realized using user cooperation and relaying has been considered. In the subsequent analysis, the fading statistics of the individual links has been modelled using well defined statistical distributions.

Communication through cooperative relaying is emerging as an important technique in modern wireless systems. Wireless relaying allows mobile terminals to participate in the transmission of information, themselves not being the initial source or the final destination [SEA03a, SEA03b, HZF04, PSP06]. Diversity is used to mitigate the effects of fading and it increases the reliability of radio links in wireless networks. The main idea of cooperative diversity schemes is to use relay nodes as virtual antennas to facilitate the communication of a source-destination pair by introducing diversity in the system [LTW04]. Potential application areas of cooperation diversity include advanced cellular architectures, mobile wireless ad-hoc networks, and other hybrid networks in order to increase coverage, throughput, and capacity to transmit to the actual destination or next relay [PWS$^+$04].

The relays in a cooperative diversity system can broadly be classified into two different categories depending on their functionalities. The relays are classified as either non-regenerative or regenerative type. The non-regenerative relays simply amplify and forward (A & F) the received signal to the next participating relay and/or to the destination node. The complexity and latency of these type of relays are less as compared to the regenerative type. A regenerative relay decodes,

encodes and then forwards the received signal to the next participating relay and/or the destination node. As the received signal requires to be decoded and encoded at the relay, such relaying process proves to be computationally complex and time intensive. The non-regenerative relays are generally preferred when complexity and/or latency issues are important, as these relays are usually battery powered and have limited processing capabilities [PSP06]. Non-regenerative type relays have been considered in this thesis. However, in a non-regenerative relaying system, because of the presence of intermediate relay nodes, the statistics of the signal received at the destination depends on the channel conditions of all the individual links. For properly utilizing the characteristics of relay links in the system design, it is required to understand the statistical behaviour of such channels. Analysis of statistical behaviour of relay channel has been a research area of considerable interest and recently some papers dealing with the methods of determining the fading statistics of such relay channels have appeared in the literature [KSM05, PSP06]. Mostly, the individual relay links are assumed to be independent Rayleigh faded channels. In this thesis two-hop relay links have been considered where individual links are assumed to be independent but not necessarily identical Nakagami-m distributed. The Nakagami fading model has been considered because of the flexibility it offers in changing the fading statistics of the individual links by changing the parameter m, which is known as the Nakagami parameter [Nak60].

The rest of the chapter is organized as follows: Section 4.2 discusses the two hop relay system. Section 4.3 deals with the diversity combining of such relay paths employing selection and maximal ratio combining in a relay based system. Finally, conclusions are drawn in section 4.4.

4.2 Two hop relay based system

The simplest form of relay based communication is a two-hop communication link as shown in Fig. 4.1. The first hop is from the source node denoted by ‘S’ to the relay node denoted by ‘R’ and the second hop is from the relay node to the destination node denoted by ‘D’. The source node may be a base station in case of an advanced cellular system or a mobile station in an adhoc network.

In the rest of the thesis, relay is assumed to be an ideal noise free repeater of non-regenerative type [HA04a]. Relays of non-regenerative types may be further classified into two different groups based on the type of amplification. A relay with constant amplification factor is said to be a fixed

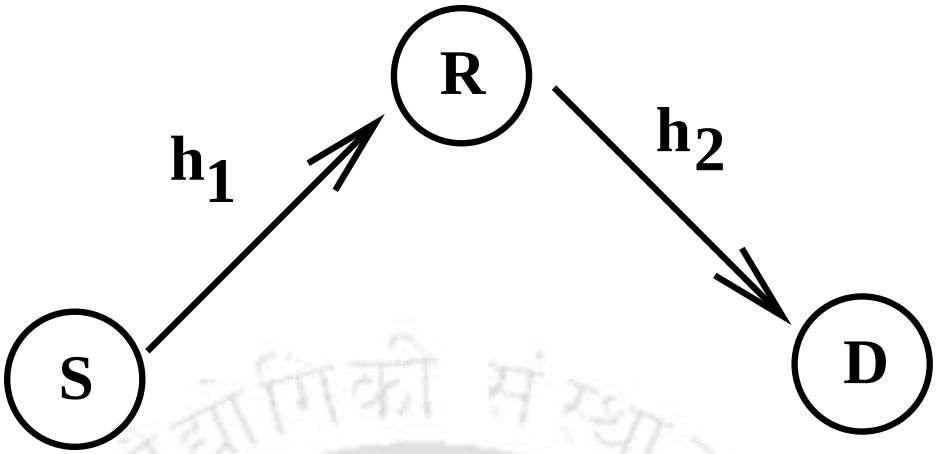

Figure 4.1: A typical two hop relay based system.

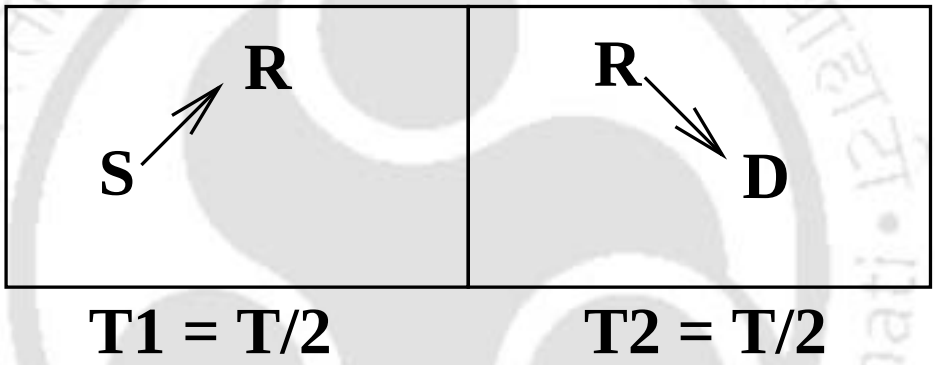

Figure 4.2: The transmission schedule for a typical two hop relay based system shown in Fig. 4.1.

gain relay. For a variable gain relay, the amplification factor varies with time [KTM03]. For most cases, the gain variation depends on the variation of the channel. The relays under consideration are assumed to be of fixed gain type. The gain has been assumed to be unity without any loss of generality [HA04b] and the assumption of noise free repeater simplifies analytical modelling. However, from practical consideration it is important to determine the degradation produced in the BER performance due to finite SNR at the relay node. The effect of the presence of noise at the relay on the BER performance of a two hop relay has been determined through simulation studies over practical ranges of SNR at the relay and the destination.

In Fig. 4.1, the signal reaches the destination (D) from the source (S) via a relay node (R). h_1(t) and h_2(t) represent the channel between the S-R and R-D link, respectively. As mentioned, h_1(t) and h_2(t) are modelled as Nakagami-m distributed so that various fading scenarios can be generated as particular cases of the generalized model. The probability density function (pdf) of

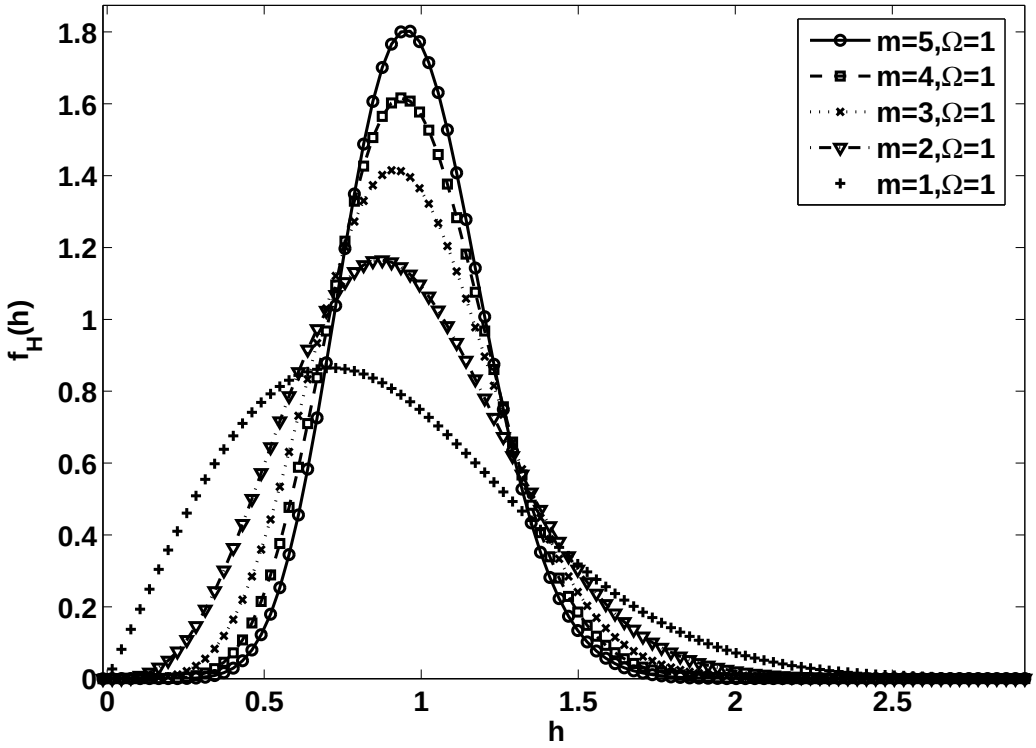

Figure 4.3: The plot of Nakagami-m distribution for different values of m.

the amplitudes of h_1(t) and h_2(t) can be written as [Nak60],

$$f_{H_i}(h_i) = 2\left(\frac{m_i}{\Omega_i}\right)^{m_i} \frac{h_i^{2m_i-1}}{\Gamma(m_i)} \exp\left(-\frac{m_i}{\Omega_i} h_i^2\right) \tag{4.2.1}$$

where, h_i>1 and i=1,2. Γ(.)represents the Gamma function. m_i denotes the m parameter of Nakagami-m distribution for the i^{th} hop. m=1, corresponds to the conventional Rayleigh fading model while for m>1, the channel behaves more like a Rician channel. The plot of Nakagami distribution for different values of m is shown in Fig. 4.3.

Let, H_1 and H_2 be the random variables (RVs') representing the amplitudes of the S-R and R-D links respectively, m_1 and m_2 are the corresponding Nakagami-m parameters. In a typical two-hop cooperative relaying environment, the source transmits the information in a time slot $\frac{T}{2}$ and the relay amplifies and retransmits the same information to the destination node in the next $\frac{T}{2}$ time slot as shown in Fig. 4.2. For the flat fading case the received signal at the destination node

can be written as,

$$y(t) = A(t)\, h_1(t)\, h_2(t)\, x(t) + A(t)\, h_2(t)\, n_1(t) + n_2(t) \tag{4.2.2}$$

for,

$$\frac{T}{2} \leq t \leq T$$

where,

$x(t)$ is the transmitted signal.

$A(t)$ is the gain of the relay.

$n_1(t)$ and $n_2(t)$ are the additive noise at the relay and the destination respectively.

As mentioned, for the sake of simplicity but without any loss of generality the relay has been assumed to be a constant gain relay having an unity gain, i.e. $A(t)$=1. Moreover, the relay has also been assumed to behave like a noise free repeater, thus $n_1(t)$=0. So equation 4.2.2 may be rewritten as,

$$y(t) = h_1(t)\, h_2(t)\, x(t) + n_2(t) \tag{4.2.3}$$

With the above assumptions, the effective channel between the source and the destination is basically the product of two Nakagami-m distributed RVs' and can be written as $Z = H_1 H_2$. The density function of the RV Z gives the channel statistics between the source and the destination via a relay. The density function of any RV obtained from the product of two independent RVs' is given in [RS00, Pap91].

Hence,

$$f_Z(z) = \int_{-\infty}^{\infty} f_{H_1}(h_1) f_{H_2}\left(\frac{z}{h_1}\right) \frac{1}{|h_1|} dh_1 \tag{4.2.4}$$

where, f_{H_1} and f_{H_2} are the probability density functions of the independent random variables H_1 and H_2 respectively. As f_{H_1} and f_{H_2} are zero for $h_1 < 0$ and $h_2 < 0$, the lower limit of equation 4.2.4 may be set to zero. Using equation 4.2.1 to 4.2.4, the probability density function $f_Z(z)$ can

be written as,

$$f_Z(z) = \frac{4}{z\Gamma(m_1)\Gamma(m_2)} \left(\frac{z^2 m_1 m_2}{\Omega_1 \Omega_2}\right)^{\frac{m_1+m_2}{2}} \times K_{(m_1-m_2)}\left(2\sqrt{\frac{z^2 m_1 m_2}{\Omega_1 \Omega_2}}\right) \tag{4.2.5}$$

where, m_1 and m_2 are the respective Nakagami parameters of the S-R and R-D link, $K_\nu(.)$ denotes the modified Bessel Function of second kind with order ν [GR94].

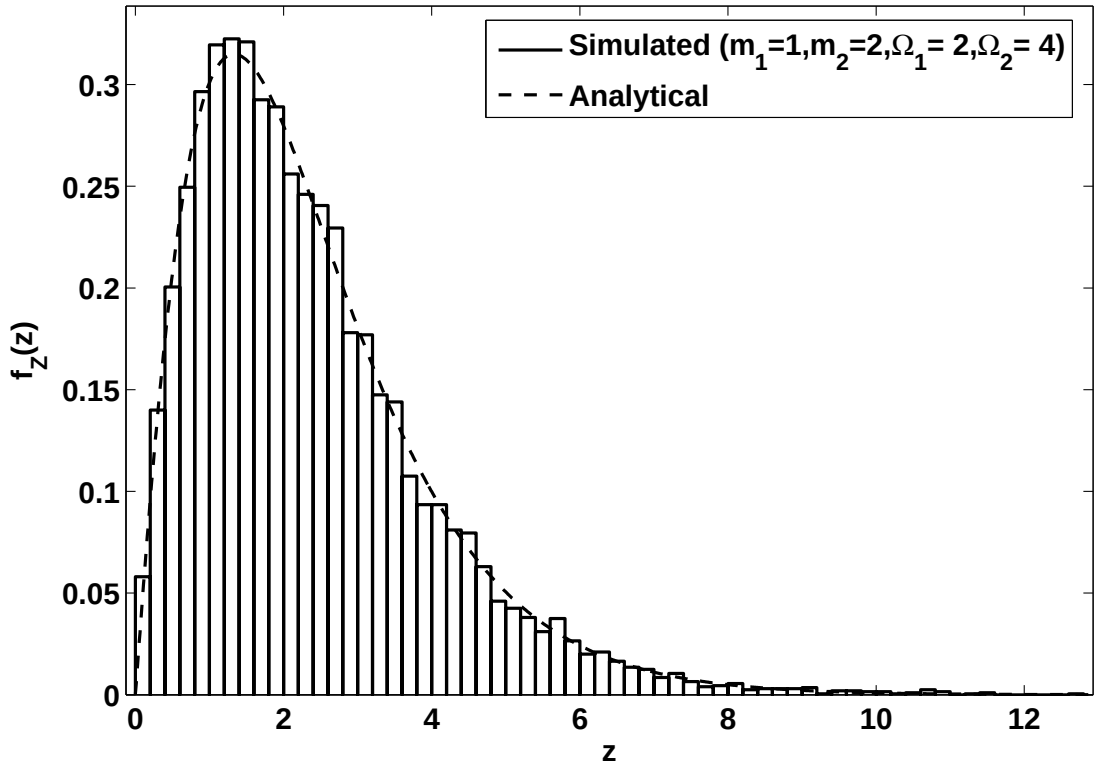

Figure 4.4: The S-D channel statistics of a two hop relay system.

A comparison between the density functions obtained analytically from equation 4.2.5 with the density function obtained through simulations has been shown in Fig. 4.4. For the purpose of simulating the S-D channel statistics, the Nakagami-m channels of the individual links were generated by employing techniques reported in literature [BC05]. In this technique, samples of Nakagami distributed numbers with parameter m and Ω are generated from $2m$ number of independent and identically distributed (*iid*) Gaussian random variables. Ω for the Nakagami distributed random numbers thus generated is $2m\sigma_x^2$, where σ_x^2 gives the variance of the Gaussian distributed RVs.

4.3 Diversity combining of relay paths

With the probability density function of fading derived for relay paths, the diversity combining has been considered next. Diversity combining is a very efficient receiver end technique for performance improvement of a wireless communication link. There are different methods of combining the received signals obtained by different diversity branches. These methods have a trade-off between complexity and performance. The most commonly used combining schemes are a) selection combining (SC), b) maximal ratio combining (MRC), and c) equal gain combining (EGC). In this work the first two combining techniques have been considered. EGC can be considered as a special case of MRC.

In SC, signal from one of the L-diversity branches is selected for further processing. The diversity branch having the highest SNR or in an interference limited system, having the highest signal to co-channel interference ratio (SIR) is generally chosen. Measurement of SNR or SIR at the receiver end is difficult, so the path having the highest total power is chosen assuming that all the diversity branches are affected by the same noise power [Rap01].

In MRC, the signals obtained at the receiver from different diversity branches are co-phased and the gain on each branch is set equal to the signal amplitude to the mean noise power ratio [Jak74]. Thus the branch weights are given by,

$$w_i = a_i e^{j\theta_i} \quad i = 1, 2, ...L \tag{4.3.1}$$

where,

$$a_i = r_i/N_i \tag{4.3.2}$$

N_i is the mean noise power at the i^{th} branch.
r_i is the received signal at the i^{th} branch.

In Fig. 4.5, a scenario has been considered where it is assumed that direct communication between the source and the destination is blocked. This type of scenario can generally be observed in urban locations where the link between the source and the destination is blocked by high rise buildings and constructions. In such a scenario, communication between the source and the destination can be established through relay nodes. Diversity in the form of cooperative diversity can be achieved by properly scheduling the transmission between the nodes. For the system model under consideration, the transmission is scheduled in three orthogonal time slots. As shown in Fig.

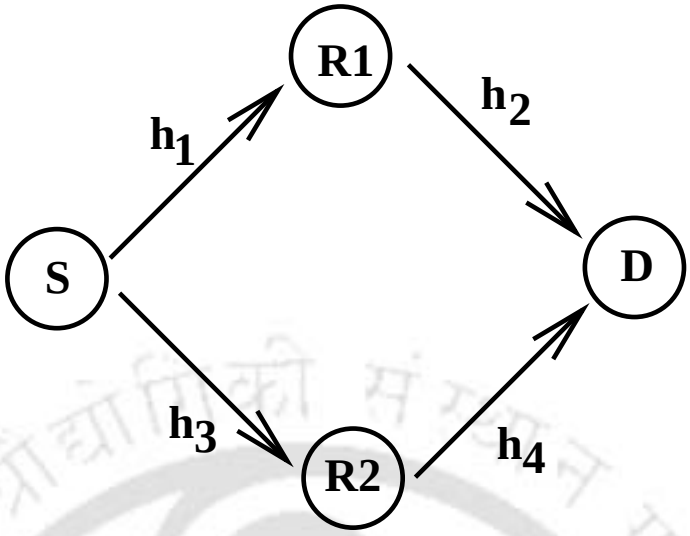

Figure 4.5: Two branch dual hop relay diversity links.

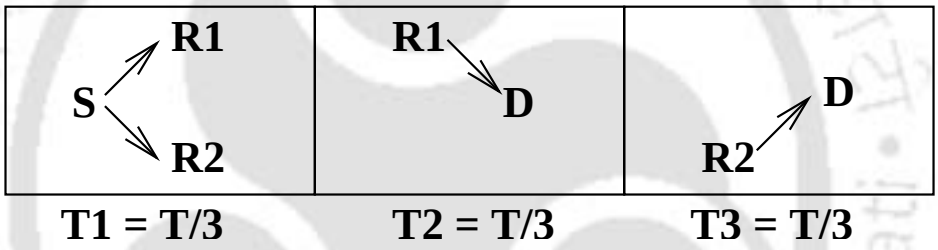

Figure 4.6: The transmission schedule for a two branch dual hop relay system shown in Fig. 4.5.

4.6, the source node S transmits the message to both the relay nodes R1 and R2 in the first time slot T1. In the second time slot T2, the relay node R1 forwards the message (received in the first time slot T1) to destination node D, where it is buffered for later processing. In the third time slot T3, the relay node R2 transmits the message (received in the first time slot T1) to the destination node D, and is combined with the buffered copy of the message from relay node R1. This procedure increases the reliability of the transmission at the cost of reduced data rates and spectral efficiency. The S-D link via relay R1 and that via relay R2 are assumed to be independent. $f_{Z_1}(z_1)$ and $f_{Z_2}(z_2)$ representing the pdf of the S-D channel via relay R1 and R2 respectively, are therefore independent.

The joint probability density function, $f_{Z_1Z_2}(z_1z_2)$, of the two independent relay channels, enclosed by the dashed box in Fig. 4.7 may be written as,

$$f_{Z_1Z_2}(z_1z_2) = f_{Z_1}(z_1)\, f_{Z_2}(z_2) \tag{4.3.3}$$

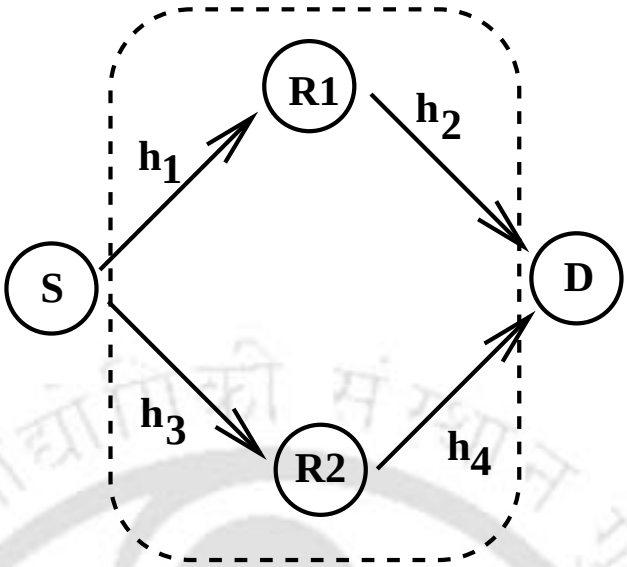

Figure 4.7: The channel between the source and the destination.

Combining equation 4.2.5 and equation 4.3.3,

$$\begin{aligned} f_{Z_1Z_2}(z_1z_2) = & \frac{16}{z_1z_2\prod_{i=1}^{4}\Gamma(m_i)} \\ & \times\left(\frac{z_1^2m_1m_2}{\Omega_1\Omega_2}\right)^{\frac{m_1+m_2}{2}}\left(\frac{z_2^2m_3m_4}{\Omega_3\Omega_4}\right)^{\frac{m_3+m_4}{2}} \\ & \times K_{(m_1-m_2)}\left(2\sqrt{\frac{z_1^2m_1m_2}{\Omega_1\Omega_2}}\right) \\ & \times K_{(m_3-m_4)}\left(2\sqrt{\frac{z_2^2m_3m_4}{\Omega_3\Omega_4}}\right) \end{aligned} \tag{4.3.4}$$

where, m_1, Ω_1 and m_2, Ω_2 represents the Nakagami distribution parameters of the wireless links S-R1 and R1-D respectively. Similarly, m_3, Ω_3 and m_4, Ω_4 represents the same for the S-R2 and R2-D links respectively.

4.3.1 Selection combining

A two branch selection diversity system has been shown in Fig. 4.8. The instantaneous SNR in terms of voltage, denoted as SNR_V, may be written as,

$$SNR_{V_{sel}} = \frac{1}{\sqrt{N}}\max(z_1, z_2) \tag{4.3.5}$$

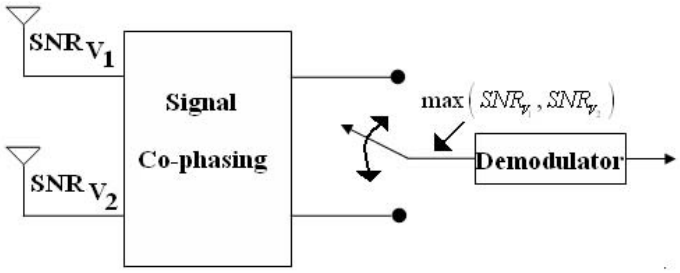

Figure 4.8: The block diagram of a selection combiner.

where, z_1 and z_2 represents the instantaneous signal voltages at the receiver from two independent diversity branches. For the sake of simplicity and in order to reduce the number of variables the noise power N is assumed to be unity. Therefore equation 4.3.5 may be written as,

$$SNR_{V_{sel}}|_{N=1} = \max(z_1, z_2) \tag{4.3.6}$$

The pdf of voltage signal to noise ratio or power signal to noise ratio at the output of the selection combiner are required to evaluate the system performances. In this regard the pdf of the voltage signal to noise ratio is first evaluated by setting the noise power to unity. The other pdf's can be eventually obtained from the said pdf by simple transformation of variables.

The voltage signal to noise ratio at the output of the selection combiner is same as that of the voltage signal to noise ratio of the strongest diversity branch at its input. For a two branch relay diversity system the output voltage signal to noise ratio is equal to that of branch 1 when the voltage signal to noise ratio of branch 2 is less than or equal to that of branch 1 and vice versa. So if the voltage signal to noise ratio at the output of the selection combiner is denoted by s, it may be concluded that at least one of the diversity branches have the voltage signal to noise ratio equal to s while the others are less than or equal to s.

For the two branch diversity system under consideration, if $z_1 = s$ then $z_2 \leq s$. The line labeled I_1 in Fig. 4.9 corresponds to this event. The line I_2 corresponds to the situation when $z_1 \leq s$ and $z_2 = s$. The event that the envelope at the output of the selection combiner is s, is the sum of all the events over I_1 and I_2 that produce s as its output. This can be obtained by integrating

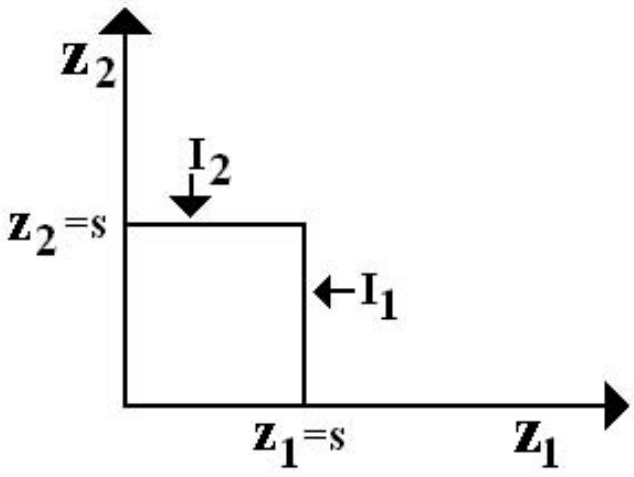

Figure 4.9: Combination of values of z_1 and z_2 that forms an envelope s at the output of the selection combiner.

$f_{Z_1Z_2}(z_1z_2)$ along the lines described in Fig. 4.9. So, the envelope at the output of the selection combiner may be written as,

$$f_S(s) = \int_0^s f_{Z_1Z_2}(z_1z_2)|_{z_1=s} dz_2 + \int_0^s f_{Z_1Z_2}(z_1z_2)|_{z_2=s} dz_1 \tag{4.3.7}$$

$$f_S(s) = I_1 + I_2 \tag{4.3.8}$$

From equation 4.3.4,

$$I_1 = \frac{4}{s\Gamma(m_1)\Gamma(m_2)}\left(\frac{s^2 m_1 m_2}{\Omega_1\Omega_2}\right)^{\frac{m_1+m_2}{2}} \times K_{(m_1-m_2)}\left(2\sqrt{\frac{s^2 m_1 m_2}{\Omega_1\Omega_2}}\right) \times \frac{4}{\Gamma(m_3)\Gamma(m_4)}\left(\frac{m_3 m_4}{\Omega_3\Omega_4}\right)^{\frac{m_3+m_4}{2}} \times \int_0^s z_2^{m_3+m_4-1} K_{(m_3-m_4)}\left(2\sqrt{\frac{z_2^2 m_3 m_4}{\Omega_3\Omega_4}}\right) dz_2 \tag{4.3.9}$$

Similarly,

$$I_2 = \frac{4}{s\Gamma(m_3)\Gamma(m_4)}\left(\frac{s^2 m_3 m_4}{\Omega_3\Omega_4}\right)^{\frac{m_3+m_4}{2}} \times K_{(m_3-m_4)}\left(2\sqrt{\frac{s^2 m_3 m_4}{\Omega_3\Omega_4}}\right) \times \frac{4}{\Gamma(m_1)\Gamma(m_2)}\left(\frac{m_1 m_2}{\Omega_1\Omega_2}\right)^{\frac{m_1+m_2}{2}} \times \int_0^s z_1^{m_1+m_2-1} K_{(m_1-m_2)}\left(2\sqrt{\frac{z_1^2 m_1 m_2}{\Omega_1\Omega_2}}\right) dz_1 \tag{4.3.10}$$

In a more compact form, the density function at the output of the selection combiner may be written as [PB07b],

$$f_S(s) = C\left\{ s^{m_1+m_2-1} K_{(m_1-m_2)}\left(2\sqrt{\frac{s^2 m_1 m_2}{\Omega_1\Omega_2}}\right) \times \left(\frac{1}{\alpha}\right)^{m_3+m_4} \int_0^{\alpha s} z^{m_3+m_4-1} K_{(m_3-m_4)}(z)\, dz \right\} + \left[\left\{ s^{m_3+m_4-1} K_{(m_3-m_4)}\left(2\sqrt{\frac{s^2 m_3 m_4}{\Omega_3\Omega_4}}\right) \times \left(\frac{1}{\beta}\right)^{m_1+m_2} \int_0^{\beta s} t^{m_1+m_2-1} K_{(m_1-m_2)}(t)\, dt \right\} \right] \tag{4.3.11}$$

where,

$$C = \frac{16}{\prod_{i=1}^{4}\Gamma(m_i)}\left(\frac{m_1 m_2}{\Omega_1\Omega_2}\right)^{\frac{m_1+m_2}{2}}\left(\frac{m_3 m_4}{\Omega_3\Omega_4}\right)^{\frac{m_3+m_4}{2}}$$

$$\alpha = 2\sqrt{\frac{m_3 m_4}{\Omega_3 \Omega_4}}$$

$$\beta = 2\sqrt{\frac{m_1 m_2}{\Omega_1 \Omega_2}}$$

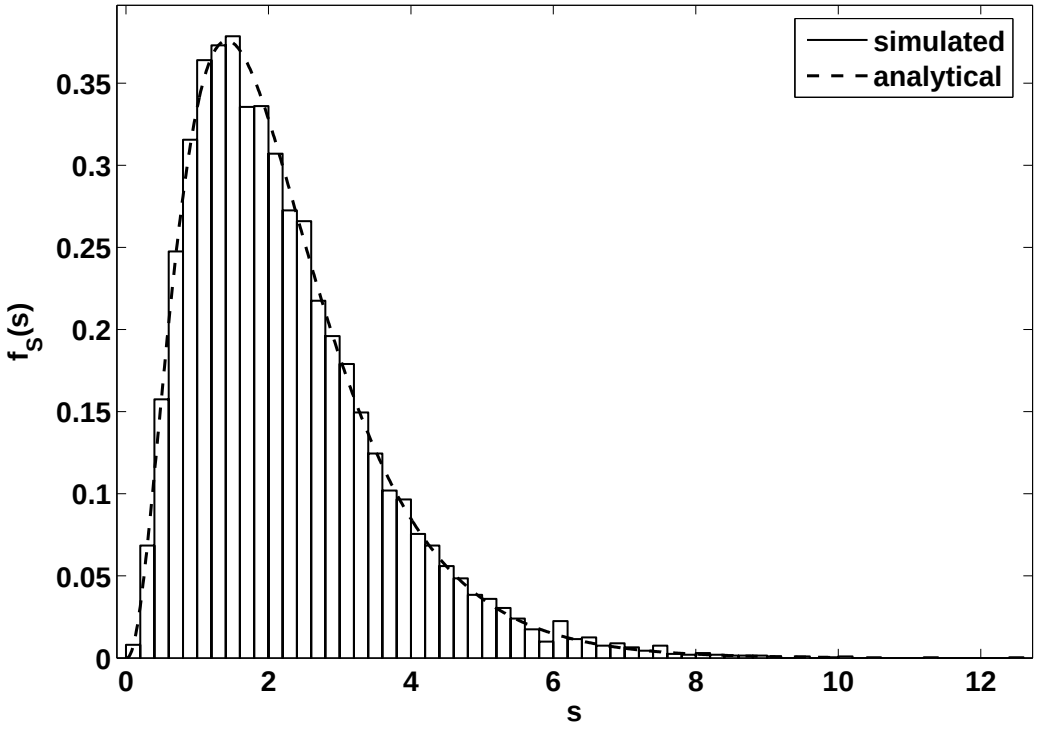

Figure 4.10: pdf of the envelope at the output of a selection combiner.

The density function at the output of the selection combiner given by equation 4.3.11 has been plotted in Fig. 4.10 and compared with those obtained through simulation of the system. The m-parameters of all the four links, of the two branches, were set to unity. Ω_1, Ω_2, Ω_3 and Ω_4 were taken to be 2. The simulations were done using MATLAB. The Nakagami-m distributed random variables were generated following the procedure given in [BC05] and described in section 4.2. $f_S(s)$ gives the voltage signal to noise ratio at the output of the selection combiner assuming the noise power to be unity, the power signal to noise ratio is of more relevance and can be obtained from $f_S(s)$ by substitution of variables.

The power signal to noise ratio (w) and the voltage signal to noise ratio (s) are related as,

$$SNR_P|_{N=1} = (SNR_V|_{N=1})^2 \tag{4.3.12}$$

$$w = s^2 \tag{4.3.13}$$

The probability density function of w can be obtained from that of s [RS00]

$$f_W(w) = \frac{1}{2\sqrt{w}} f_S\left(\sqrt{w}\right) + \frac{1}{2\sqrt{w}} f_S\left(-\sqrt{w}\right) \tag{4.3.14}$$

Since the pdf of s exists only for the positive values, hence the second term of equation 4.3.14 is zero.

$$f_W(w) = \frac{1}{2\sqrt{w}} f_S\left(\sqrt{w}\right) \tag{4.3.15}$$

All the above pdfs have been derived for unity noise power. But the pdf of the power signal to noise ratio for any arbitrary noise power is of theoretical importance and can be derived from equation 4.3.15. If w_N represents the signal to noise ratio for any arbitrary power N,

$$w_N = \frac{w}{N} \tag{4.3.16}$$

The pdf of w_N is related to that of w by [RS00]

$$f_{W_N}(w_N) = N f_W(N w_N) \tag{4.3.17}$$

Substituting 4.3.15 in 4.3.17

$$f_{W_N}(w_N) = \frac{\sqrt{N}}{2\sqrt{w_N}} f_S\left(\sqrt{N w_N}\right) \tag{4.3.18}$$

on further simplification,

$$f_{W_N}(w_N) = \frac{N}{2\sqrt{w}} f_S\left(\sqrt{w}\right) \tag{4.3.19}$$

Combining 4.3.19 and 4.3.11,

$$\begin{aligned} f_{W_N}(w_N) = \frac{C\sqrt{N}}{2\sqrt{w_N}} \Bigg[\Bigg\{ & \left(\sqrt{N w_N}\right)^{m_1+m_2-1} \\ & \times K_{(m_1-m_2)}\left(2\sqrt{\frac{N w_N m_1 m_2}{\Omega_1 \Omega_2}}\right) \\ & \times \left(\frac{1}{\alpha}\right)^{m_3+m_4} \int_0^{\alpha\sqrt{N w_N}} t^{m_3+m_4-1} K_{(m_3-m_4)}(t)\, dt \Bigg\} \\ & + \Bigg\{ \left(\sqrt{N w_N}\right)^{m_3+m_4-1} K_{(m_3-m_4)}\left(2\sqrt{\frac{N w_N m_3 m_4}{\Omega_3 \Omega_4}}\right) \\ & \times \left(\frac{1}{\beta}\right)^{m_1+m_2} \int_0^{\beta\sqrt{N w_N}} t^{m_1+m_2-1} K_{(m_1-m_2)}(t)\, dt \Bigg\} \Bigg] \end{aligned} \tag{4.3.20}$$

where, the constants C, α, and β are same as given in equation 4.3.11.

For m_1=m_2=m_3=m_4=1 and Ω_1=Ω_2=Ω_3=Ω_4=2, the power signal to noise ratio at the output of the selection combiner can be written as,

$$f_{W_N}(w_N) = \frac{\sqrt{N}}{2\sqrt{w_N}} \left[\left\{ \left(\sqrt{Nw_N}\right) K_0\left(\sqrt{Nw_N}\right) \times \int_0^{\sqrt{Nw_N}} tK_0(t)\,dt \right\} + \left\{ \left(\sqrt{Nw_N}\right) K_0\left(\sqrt{Nw_N}\right) \times \int_0^{\sqrt{Nw_N}} tK_0(t)\,dt \right\} \right] \tag{4.3.21}$$

4.3.2 Maximal ratio combining

In this subsection, the probability density function of the SNR at the output of a maximal ratio combiner at the destination node of Fig. 4.5 has been evaluated. The individual links have been assumed to be Nakagami-m faded as stated earlier. The density functions for both voltage signal to noise and power signal to noise ratio have been derived. The voltage signal to nose ratio and power signal to noise ratio are denoted as $SNR_{V_{MRC}}$ and $SNR_{P_{MRC}}$ respectively. The two signal to noise ratios are related to each other and to the input signals of the two diversity branches as,

$$SNR_{V_{MRC}} = \sqrt{SNR_{P_{MRC}}} = \frac{1}{\sqrt{N}}\sqrt{z_1^2 + z_2^2} \tag{4.3.22}$$

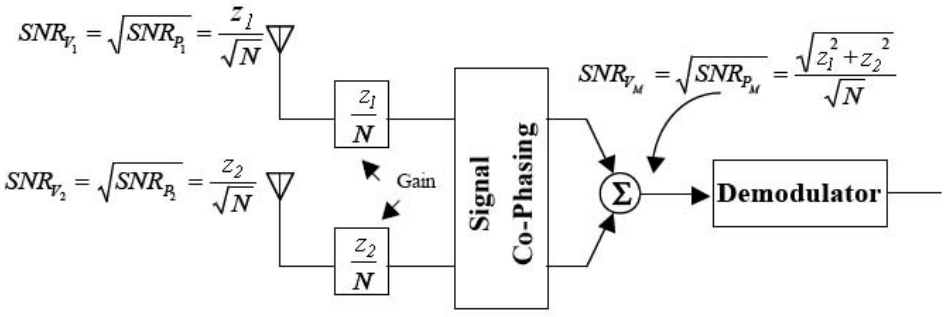

Figure 4.11: Block diagram of a two-branch maximal ratio combiner having equal noise power in both the branches.

The joint probability density function of two independent relay channels is as given in equation 4.3.4. It needs to be integrated to find the probability density function at the output of the maximal

ratio combiner. But in Cartesian coordinates the evaluation of the integral becomes very involved. Changing into polar coordinates makes the analytical formulation easily tractable. The variables are transformed as,

$$z_1 = m\cos\phi \tag{4.3.23}$$

$$z_2 = m\sin\phi \tag{4.3.24}$$

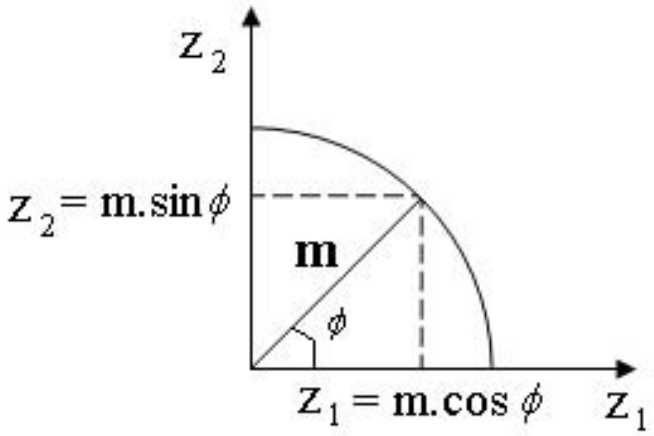

Figure 4.12: Combination of values of z_1 and z_2 that forms an envelope m at the output of the maximal ratio combiner.

As, $z_1 \geq 0$ and $z_2 \geq 0$, so $0 \leq \phi \leq \frac{\pi}{2}$ as shown in Fig. 4.12. The new probability density function can be deduced from equation 4.3.4, by change of variables and introduction of the Jacobian of the transformation. The new density function is defined as,

$$f_{M\Phi}(m,\phi) = \left|\tilde{J}\right| \cdot f_{Z_1Z_2}(z_1, z_2) \tag{4.3.25}$$

where, $\tilde{J}$ represents the Jacobian.

$$\tilde{J} = \begin{vmatrix} \frac{\partial z_1}{\partial m} & \frac{\partial z_1}{\partial \phi} \\ \frac{\partial z_2}{\partial m} & \frac{\partial z_2}{\partial \phi} \end{vmatrix} \tag{4.3.26}$$

Therefore, equation 4.3.25 gets modified to,

$$f_{M\Phi}(m,\phi) = m \cdot f_{Z_1Z_2}(z_1, z_2)\Big|_{\substack{z_1 = m\cos\phi \\ z_2 = m\sin\phi}} \tag{4.3.27}$$

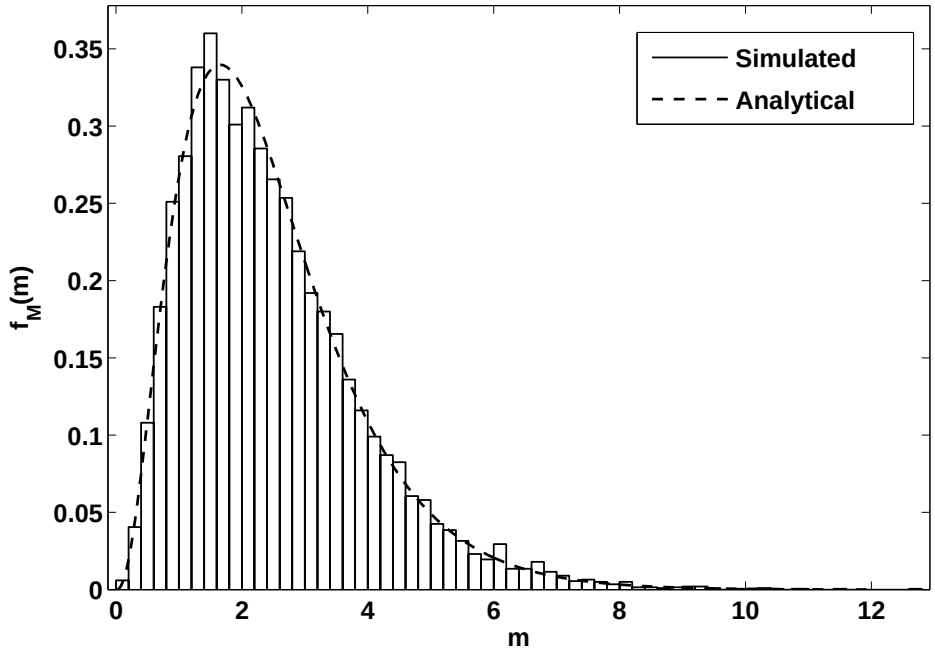

Figure 4.13: pdf of the envelope at the output of the maximal ratio combiner.

In equation 4.3.27 ϕ varies from 0 to $\frac{\pi}{2}$. So, $f_M(m)$ may be written as,

$$f_M(m) = \int_0^{\pi/2} f_{M\Phi}(m, \phi)\, d\phi \tag{4.3.28}$$

Substituting equation 4.3.27 into equation 4.3.28,

$$\begin{aligned} f_M(m) &= C m^{m_1+m_2+m_3+m_4-1} \\ &\quad \times \int_0^{\pi/2} \frac{1}{\sin\phi\cos\phi} \cos^{m_1+m_2}(\phi) \sin^{m_3+m_4}(\phi) \\ &\quad \times K_{(m_1-m_2)}\left(2\sqrt{\frac{m^2\cos^2(\phi)\, m_1 m_2}{\Omega_1\Omega_2}}\right) \\ &\quad \times K_{(m_3-m_4)}\left(2\sqrt{\frac{m^2\sin^2(\phi)\, m_3 m_4}{\Omega_3\Omega_4}}\right) d\phi \end{aligned} \tag{4.3.29}$$

where,

$$C = \frac{16}{\prod_{i=1}^{4}\Gamma(m_i)} \left(\frac{m_1 m_2}{\Omega_1\Omega_2}\right)^{\frac{m_1+m_2}{2}} \left(\frac{m_3 m_4}{\Omega_3\Omega_4}\right)^{\frac{m_3+m_4}{2}}$$

The density function at the output of the MRC given by equation 4.3.29 requires to be evaluated numerically for specific values of m_i and Ω_i , where i=1,2,..,4 .

For a specific case when m_i=1 and Ω_i = 2 for i = 1,...4. equation 4.3.29 reduces to [PB07a]

$$f_M(m) = C \cdot m^3 \cdot \int_0^{\pi/2} \cos(\phi) \cdot \sin(\phi) \cdot K_0(m\cos(\phi)) \times K_0(m\sin(\phi))\, d\phi \tag{4.3.30}$$

The above integral has been computed numerically to obtain the final density function at the output of maximal ratio combiner and shown in Fig. 4.13.

4.3.3 Bit error rate performances

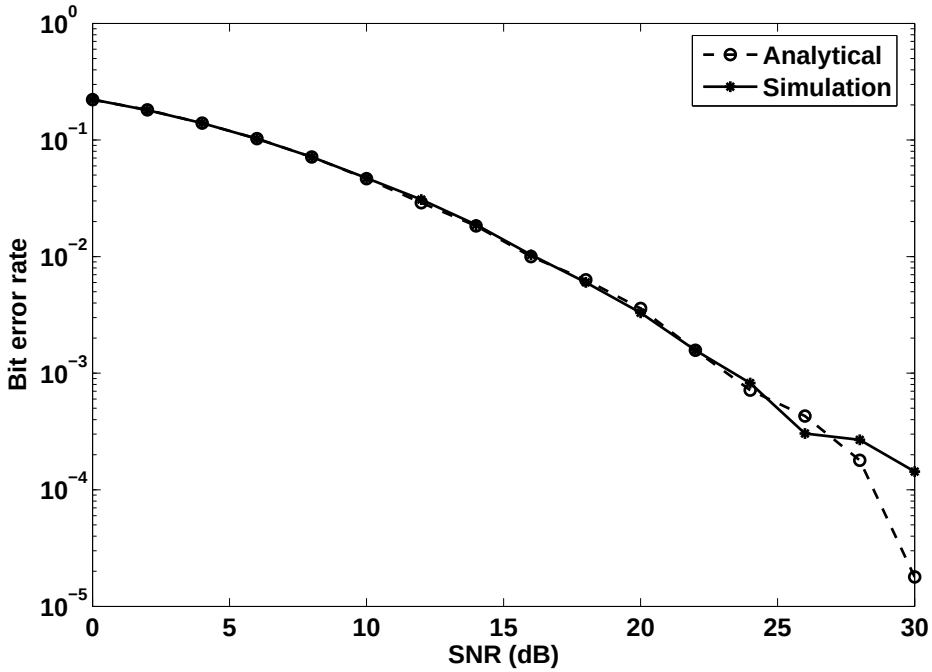

Figure 4.14: Comparison of bit error rate obtained analytically and through simulation at the output of the selection combiner.

The bit error rate for the system described in Fig. 4.5 and having selection combining at the output has been plotted in Fig. 4.14. The Nakagami parameters, m and Ω for all the individual links were assumed to be 1 and 2 respectively. The BER obtained for the channel having pdf given by equation 4.3.11 is same as the BER obtained through simulation of the individual channels,

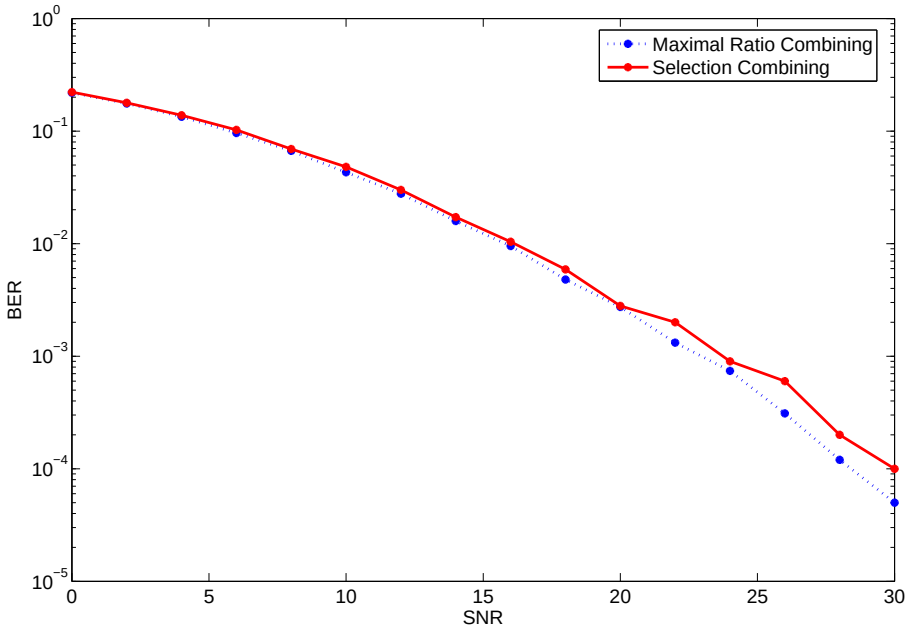

Figure 4.15: Comparison of bit error rate for selection and maximal ratio combinig.

generated according to the methods described in [BC05], and performing selection combining at the output. The validity of equation 4.3.11 is thus verified.

In Fig. 4.15 the bit error rate performances for selection and maximal ratio combining in the cooperative diversity scheme under consideration have been compared. The simulations have been carried out by generating random variables having the density functions given by equation 4.3.11 and equation 4.3.29. The random variables have been generated by the method of rejection [TSRK04]. It may be observed that the improvement in BER performance is not significant on application of maximal ratio combining with comparison to the BER performance for a selection combiner at the destination node for the system depicted in Fig. 4.5.

While evaluating the analytical expressions for the pdf of the two hop relay link, the relay node has been assumed to be noise free. Such an assumption of an ideal relay has been made to reduce the mathematical complexity in derivation of the pdf expression. In practice the SNR at the relay, what so ever large, is a finite quantity. It is therefore necessary to estimate the error introduced in computation of BER using the pdf in equation 4.2.5 and find some lower limit on the relay SNR above which the error in BER will be reasonably small. To study the behaviour of error in link BER as a function of SNR at the relay, the BER Vs SNR performances at the destination node with SNR

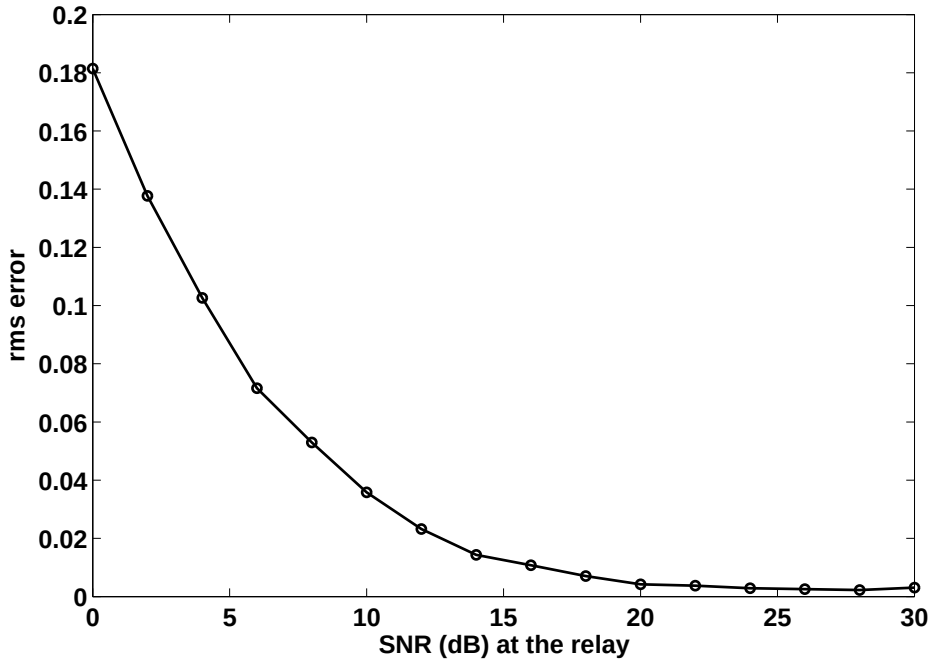

Figure 4.16: Root mean square error Vs SNR.

at the relay as a parameter have been computed . The range of destination SNR has been taken as 0 - 30 dB and the same range has been used for the relay SNR as well. From the knowledge of BER values at different destination SNRs, for a given SNR at the relay and comparing the same with the BER values for those destination SNRs for an ideal relay; the root mean square (rms) error in BER at the given relay SNR have been computed. Figure 4.16 shows the variation of the rms error as a function of the SNR at the relay. From Fig. 4.16 it can seen that for the values of relay SNR $\geq$ 20 dB, the equation 4.2.5 can be used for computation of BER without making significant error.

4.4 Conclusion

In this chapter the expressions for the probability density function of the signal envelope at the output of a selection combiner and maximal ratio combiner, having signals from two independent relay channels as inputs has been presented. The channel statistics of the individual hops of a relay diversity branch have been assumed to be Nakagami-m faded. The end-to-end density function of a two hop relay branch, with each hop being Nakagami-m distributed has also been evaluated. The analytical results have been verified through simulation for particular values of the Nakagami pa-

rameter, m. The bit error rates for the two combining schemes (selection combining and maximal ratio combining) have also been evaluated for the system under consideration.

Chapter 5

Conclusions

This thesis has addressed certain issues related to channel modelling for multi-antenna systems and also investigated the performance of relay based communication scenarios. MIMO system design for realistic environment needs to take into account the effect of array geometry and mutual coupling between the antenna elements as these factors affect the capacity of MIMO channels. Such issues have been addressed in this thesis using a geometrically based single bounce scattering model representing the propagation environment. A new method based on $S-$parameter has also been developed for evaluation of the channel matix **H**, when the channel is modelled from a microwave perspective. Direct communication between the mobile nodes known as mobile-to-mobile communication is prevalent in many recent wireless networks. By extending geometrically based channel models, analytical expressions for the angle of arrival and time of arrival probability density functions have been derived for M2M channels. In another form of communication, virtual MIMO systems are formed using node cooperation and relaying. Performance of a relay based diversity system has also been analysed here in detail. The main contributions are summarized in the Section 5.1 and a few tracks for extending the present works are outlined in Section 5.2.

5.1 Summary of Contributions

In Chapter 2 of the thesis, the following three problems related to MIMO systems have been addressed:

- The effects of array geometry on the capacity of a MIMO system

- Determination of channel matrix **H** for a MIMO channel modelling from microwave perspective and
- The effect of mutual coupling on MIMO channels.

The effect of array geometry on the capacity of a MIMO system has been investigated in the framework of geometry based single bounce modelling technique. Four different arrays namely, uniform linear array, uniform circular array, rhombic array and star array each having four elements have been considered for this purpose. For the different array combinations considered, it has been observed that for a properly aligned fixed MIMO link, use of linear arrays at both the transmitter and the receiver end gives the best performance in terms of the maximum achievable capacity. If the rotational motion of the mobile station array is taken into consideration which results due to mobility of the mobile stations, the combination of linear and star shaped antenna array has been found to give better performance. The mean capacity for the said array combination has been found to be maximum with minimum standard deviation.

MIMO channel modelling from microwave perspective has been considered and a scattering matrix based approach has been developed for obtaining channel matrix **H** for such modelling approach.

Studies have been performed on the effect of mutual coupling on MIMO system performance. It has been observed that for small inter-element separations (typically less than 1.5λ), mutual coupling has an effect on the estimated capacity of a MIMO system and hence such effects need to be included in MIMO channel models.

Chapter 3 of the thesis has dealt with geometrical modelling of M2M communication and using such models, analytical expressions for the TOA and AOA pdf have been derived. Uniformly distributed circular discs around the mobile station accounted for the scattering environment. The analysis has been extended to a more generalized dual annular strip model (DASM). The uniform circular scattering model can be considered to be a special case of DASM . DASM can also be used for circular scattering model with non uniform distribution of scatterers, for scenarios where scatterers are uniformly distributed along the angular direction and may have other distribution in the radial direction, with reference to a polar coordinate system. In doing so, the circular scattering region can be segmented into smaller annular strips and a circle of small radius over which the

scatterer distribution can be assumed to be uniform.

In Chapter 4 of the thesis, relay based communication system has been investigated and statistical models of the channels have been used to carry out analysis for:

- Selection diversity combining for a scheme having two diversity paths and each path having a non-regenerative relay
- Maximal ratio combining for the same scheme
- Bit-error-rate performances of both the schemes.

Expressions for the probability density function of the signal envelope at the output of a selection combiner and maximal ratio combiner, having signals from two independent relay channels as inputs have been derived. The channel statistics of the individual hops of a relay diversity branch has been assumed to be Nakagami-m faded. The end-to-end density function of a two hop relay branch, with each hop being Nakagami-m faded has also been evaluated. The bit error rates for the two combining schemes (selection combining and maximal ratio combining) have also been evaluated for the system under consideration.

5.2 Tracks for Future Work

Several issues related to MIMO, mobile-to-mobile and relay based communication systems still remain open. A few tracks for future research out of the present work are outlined below.

In this thesis the coupling matrix has been evaluated using dipole antennas. But in practical handheld devices planar or patch antennas are mostly used. Evaluation of coupling matrix for such planar antennas would help in more accurate geometrical modelling of MIMO channels.

While analysing M2M channels, the effect of far scatterers has not been taken into account. Far scatterers and presence of scatterer clusters modify the channel characteristics, the effect of such scattering may be studied in detail in the context of M2M channels.

This thesis has considered a single user multi-antenna system. Multi-user MIMO systems may be studied where interference from other users are also taken into consideration.

For the relay based system, the analysis has been kept limited to dual-hop two diversity path systems. Scopes exists in extending such analysis for relay path having more than two hops as well as systems having more than two diversity branches.

Appendix A

A.1 S-Parameter

Representation of microwave networks in terms of impedance or admittance matrix is not convenient. There is difficulty in defining voltages and currents for non-TEM (transverse electromagnetic) lines. Similarly, practical problem exists when trying to measure voltages and currents. Then equivalent voltages and currents and corresponding impedance and admittance matrices becomes somewhat abstraction in the microwave frequency range. The quantities that may be measured more easily and directly are reflection and transmission coefficient. This forms the basis of scattering matrix (S-matrix) formulation and such representation are more in accordance with direct measurement. Scattering parameters (S-parameters) are used to analyse N-port microwave networks in terms of the incident and reflected waves at different ports. Figure A.1 shows a N-port microwave network, where a_i and b_i respectively represent the incoming and outgoing traveling waves at the i^{th} port of the network and t_i's are the terminal planes. The a_i and b_i are defined as [Gup80]

$$a_i = Normalised\, incident\, wave\, at\, the\, i^{th}\, port = \frac{V_i^+}{\sqrt{Z_{0i}}} \tag{A.1.1}$$

$$b_i = Normalised\, reflected\, wave\, at\, the\, i^{th}\, port = \frac{V_i^-}{\sqrt{Z_{0i}}} \tag{A.1.2}$$

where, Z_{0i} gives the characteristic impedance of the i^{th} port and V_i^+ & V_i^- represents incident and outgoing waves at the terminal plane of the i^{th} port.

The S-parameter between any two ports, say the i^{th} and the j^{th} port is written as,

$$s_{ij} = \left.\frac{b_i}{a_j}\right|_{a_k=0} \qquad where\ k = 1, 2, 3 \ldots, N\, and\, k \neq j \tag{A.1.3}$$

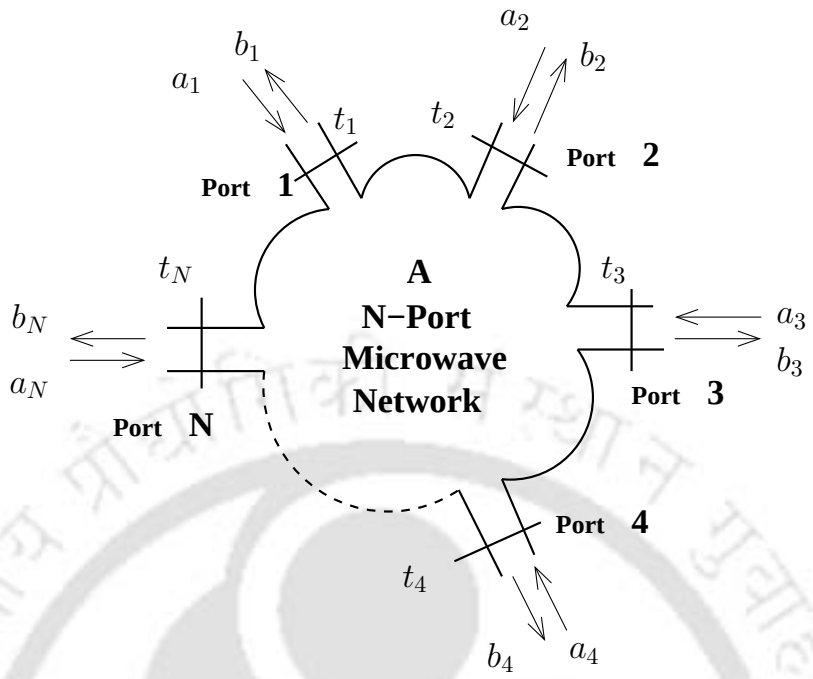

Figure A.1: A N-port microwave network.

Substituting equation A.1.1 and A.1.2 into equation A.1.3,

$$s_{ij} = \left.\frac{V_i^- / \sqrt{Z_{0i}}}{V_j^+ / \sqrt{Z_{0j}}}\right|_{V_k^+=0} \qquad where\ k = 1, 2, 3 \ldots, N\ and\ k \neq j \tag{A.1.4}$$

If the characteristic impedances of the i^{th} and j^{th} port of the microwave network are assumed to be equal, then equation A.1.4 can be written as,

$$s_{ij} = \left.\frac{V_i^-}{V_j^+}\right|_{V_k^+=0} \qquad where\ k = 1, 2, 3 \ldots, N\ and\ k \neq j \tag{A.1.5}$$

In matrix notation the relationship among the scattering parameters, the incoming and the outgoing traveling waves for N port microwave network can be written as,

$$\mathbf{b} = \mathbf{S}\,\mathbf{a} \tag{A.1.6}$$

$$\begin{bmatrix} b_1 \\ b_2 \\ \vdots \\ b_N \end{bmatrix} = \begin{bmatrix} s_{11} & s_{12} & \cdots & s_{1N} \\ s_{21} & s_{22} & \cdots & \vdots \\ \vdots & \vdots & \ddots & \vdots \\ s_{N2} & s_{N2} & \cdots & s_{NN} \end{bmatrix} \begin{bmatrix} a_1 \\ a_2 \\ \vdots \\ a_N \end{bmatrix} \tag{A.1.7}$$

where, $\mathbf{b}$ and $\mathbf{a}$ represents the $N \times 1$ vector constituting of the outgoing and the incoming traveling waves at the N-ports. $\mathbf{S}$ denotes the $N \times N$ scattering matrix. The outgoing traveling wave at the

i^{th} port can be written as,

$$b_i = \sum_{k=1}^{N} s_{ik} a_k \tag{A.1.8}$$

For a two port microwave network the relation between the incoming and outgoing waves at each ports can be written as,

$$b_1 = s_{11} a_1 + s_{12} a_2 \tag{A.1.9}$$

$$b_2 = s_{21} a_1 + s_{22} a_2 \tag{A.1.10}$$

When all the ports have the same characteristic impedance,

$$s_{11} = \left.\frac{b_1}{a_1}\right|_{a_2=0} = \left.\frac{V_1^-}{V_1^+}\right|_{V_2^+=0} \tag{A.1.11}$$

represents the reflection coefficient at port 1. If the port 2 is terminated to a load such that $V_2^+ = 0$, which implies that there is no reflected signal i.e. s_{11} gives the reflection coefficient at port 1 when port 2 is matched. In a similar manner other coefficients may be defined. s_{22} is the reflection coefficient at port 2 . s_{21} is the transmission coefficient from port1 to port 2 & s_{12} is the transmission coefficient from port 2 to 1.

Using the definitions of a_i and b_i:

$$V_i = V_i^+ + V_i^- = \sqrt{z_{oi}}(a_i + b_i) \tag{A.1.12}$$

$$I_i = \frac{1}{z_{oi}} \left(V_i^+ - V_i^-\right) \tag{A.1.13}$$

$$= \frac{1}{\sqrt{z_{oi}}} (a_i - b_i) \tag{A.1.14}$$

Power flow at the i^{th} port may be written as

$$P_i = \frac{1}{2}\mathrm{Re}\left(V_i I_i^*\right) \tag{A.1.15}$$

$$= \frac{1}{2}\mathrm{Re}\left((a_i + b_i)(a_i - b_i)^*\right) \tag{A.1.16}$$

$$= \frac{1}{2}\left(a_i a_i^* - b_i b_i^*\right) \tag{A.1.17}$$

Now $\frac{1}{2} a_i a_i^*$ is the power incident to i^{th} port and $\frac{1}{2} b_i b_i^*$ is the power reflected. Therefore P_i is the power carried into the port.

Some properties of $S-$ matrix :

Unitary Property : For any lossless network, the product of any column of the scattering matrix with the conjugate of this column equals unity. This property is referred as unitary property.

Zero Property : The product of any column of the scattering matrix with the complex conjugate of any other column is zero. This property is referred as zero property.

Change of reference plane : If $\theta_i = \beta_i l_i$ is the electrical length of the outward shift of the reference port of the i^{th} port the resultant scattering matrix may be written as:

$$[s'] = \begin{bmatrix} e^{-j\theta_1} & 0..... & 0 \\ 0 & e^{-j\theta_2}..... & 0 \\ 0 & 0..... & e^{-j\theta_N} \end{bmatrix} [s] \begin{bmatrix} e^{-j\theta_1} & 0..... & 0 \\ 0 & e^{-j\theta_2}..... & 0 \\ 0 & 0..... & e^{-j\theta_N} \end{bmatrix} \tag{A.1.18}$$

The effect of short circuiting a port is considered next. Equation A.1.10 can be written as,

$$a_2 = \frac{b_2 - a_1 s_{21}}{s_{22}} \tag{A.1.19}$$

If port 2 is terminated with a short circuit then $a_2 + b_2 = 0$, i.e. $a_2 = -b_2$. Equation A.1.19 can be modified to,

$$a_2 = \frac{-a_2 - a_1 s_{21}}{s_{22}} \tag{A.1.20}$$

$$a_2 = -a_1 \cdot \frac{s_{21}}{1 + s_{22}} \tag{A.1.21}$$

From equation A.1.9 and A.1.21 it can be written,

$$b_1 = a_1 s_{11} - a_1 \cdot \frac{s_{21} s_{12}}{1 + s_{22}} \tag{A.1.22}$$

s'_{11} is the reflection coefficient of the equivelent single port network obtained by short circuiting the second port.

$$s'_{11} = \left.\frac{b_1}{a_1}\right|_{port\,2\,short\,circuited} = s_{11} - \frac{s_{21} s_{12}}{1 + s_{22}} \tag{A.1.23}$$

Similar analysis can be extended to $N-$port network for which $M-$ports are short circuited and $M < N$.

Appendix B

B.1 Channel Capacity

A probabilistic experiment involving the observation at the output of a discreet source during every unit of time has been considered. The source output can be modelled as a discrete random variable S which takes symbols from a fixed finite alphabet given as,

$$S = \{s_0, s_1, s_2 \ldots, s_{K-1}\} \tag{B.1.1}$$

with probabilities

$$P(S = s_k) = p_k \qquad k = 0, 1, \ldots, K-1 \tag{B.1.2}$$

The information gained after observing the event $S = s_k$, which occurs with a probability p_k is defined as [Hay01],

$$I(s_k) = \log_2\left(\frac{1}{p_k}\right) \tag{B.1.3}$$

The mean of $I(s_k)$ over the source alphabet is given as

$$\begin{aligned} H(S) &= E[I(s_k)] \\ &= \sum_{k=0}^{K-1} p_k I(s_k) \\ &= \sum_{k=0}^{K-1} p_k \log_2\left(\tfrac{1}{p_k}\right) \end{aligned} \tag{B.1.4}$$

$H(\mathbf{S})$ is called the entropy of a discrete memoryless channel with source alphabet $\mathbf{S}$. Entropy gives the measure of the average information content per symbol.

A discrete memoryless channel can be modelled statistically as a system with input X and output Y which is a noisy version of X. For measuring the uncertainty in X after observing Y the

conditional entropy of X selected from the set of alphabet $\mathbf{X}$ given that $Y = y_k$ is defined as,

$$H\left(\mathbf{X}|\, Y = y_k\right) = \sum_{j=0}^{J-1} p\left(x_j|\, y_k\right) \log_2 \left[\frac{1}{p\left(x_j|\, y_k\right)}\right] \tag{B.1.5}$$

The mean of the entropy $H\left(\mathbf{X}|\, Y = y_k\right)$ over the output alphabet $\mathbf{Y}$ is given by,

$$H\left(\mathbf{X}|\, \mathbf{Y}\right) = \sum_{k=0}^{K-1} \sum_{j=0}^{J-1} p\left(x_j, y_k\right) \log_2 \left[\frac{1}{p\left(x_j|\, y_k\right)}\right] \tag{B.1.6}$$

$H\left(\mathbf{X}|\, \mathbf{Y}\right)$ is called the conditional entropy. It gives the uncertainty remaining about the channel input after the channel output has been observed. Hence, $H\left(\mathbf{X}\right) - H\left(\mathbf{X}|\, \mathbf{Y}\right)$ gives the uncertainty about the channel input that has been resolved by observing the channel output. This is known as the mutual information of the channel and is denoted by $I\left(\mathbf{X}; \mathbf{Y}\right)$

$$I\left(\mathbf{X}; \mathbf{Y}\right) = H\left(\mathbf{X}\right) - H\left(\mathbf{X}|\, \mathbf{Y}\right) \tag{B.1.7}$$

For the discrete memory less channel under consideration the mutual information of the channel can be written as,

$$I\left(X; Y\right) = \sum_{k=0}^{K-1} \sum_{j=0}^{J-1} p\left(x_j, y_k\right) \log_2 \left[\frac{p\left(y_k|\, x_j\right)}{p\left(y_k\right)}\right] \tag{B.1.8}$$

The input probability distribution $(p(x_j))$ is independent of the channel. Hence the mutual information can be maximised with respect to $p(x_j)$.

The channel capacity of a discrete memoryless channel is defined as the maximum mutual information $I\left(X; Y\right)$ in any signalling interval where the maximisation is over all possible input probability distributions $p(x_j)$ on $\mathbf{X}$. Hence,

$$C = \max_{\{p(x_j)\}} I\left(\mathbf{X}; \mathbf{Y}\right) \tag{B.1.9}$$

For formulating the information capacity for a band limited, power limited Gaussian channel, a zero mean stationary process $X(t)$ has been considered band limited to B Hertz. Let $X_k, k = 1, 2, ...K$ be the samples of the signal obtained on uniformly sampling $X(t)$ at the Nyquist rate of $2B$ samples per second. If the samples are transmitted in T seconds over a noisy channel bandlimited to B Hertz, then the number of samples K is given by,

$$K = 2BT \tag{B.1.10}$$

For any particular sample it can be written,

$$Y_k = X_k + w_k \qquad for\, k\, =\, 1, 2, ...K \tag{B.1.11}$$

w_k is the zero mean Gaussian noise sample with variance given by,

$$\sigma_w^2 = N_0 B \tag{B.1.12}$$

As the channel is power limited the information capacity of the channel can be defined as

$$C = \max_{f_{X_k}(x)} \left\{ I\left(X_k; Y_k\right) : E\left[X_k^2\right] = P \right\} \tag{B.1.13}$$

The maximization is attained by choosing the samples of the transmitted signal from a noise like process of average power P. Correspondingly, it may be written,

$$C = I\left(X_k; Y_k\right) : X_k\ Gaussian, \qquad E\left[X_k^2\right] = P \tag{B.1.14}$$

The variance of sample Y_k of the received signal equals $P + \sigma_w^2$. The differential entropy of Y_k can be written as

$$h\left(Y_k\right) = \frac{1}{2} \log_2 \left[2\pi e \left(P + \sigma_w^2\right)\right] \tag{B.1.15}$$

The differential entropy of w_k can be written as

$$h\left(w_k\right) = \frac{1}{2} \log_2 \left[2\pi e \sigma_w^2\right] \tag{B.1.16}$$

Hence, the information capacity in terms of bits per transmission can be written as,

$$C = \frac{1}{2} \log_2 \left(1 + \frac{P}{\sigma_w^2}\right) \tag{B.1.17}$$

Alternatively, information capacity of a real additive white Gaussian noise (AWGN) subject to the constraint of fixed transmit power P in terms of bits/sec can be written as,

$$C = B \log_2 \left(1 + \frac{P}{\sigma_w^2}\right) \qquad bits/\sec \tag{B.1.18}$$

where, B is the channel bandwidth and σ_w^2 gives the noise variance. For a wireless communication experiencing flat fading and the receiver having perfect knowledge of the channel state, the capacity is given by,

$$C = E\left[\log_2 \left(1 + \frac{|h|^2 P}{\sigma_w^2}\right)\right] \qquad bits/\sec/Hz \tag{B.1.19}$$

where, $h(n)$ gives the complex gain of the channel and is assumed to be stationary and ergodic.

For a MIMO flat faded channel the ergodic capacity is given by [HM05],

$$C = E\left[\log_2\left(\frac{\det\left(R_w + HR_sH^\dagger\right)}{\det\left(R_w\right)}\right)\right] \quad bits/\sec/Hz \tag{B.1.20}$$

subject to $\max_{R_s} \; tr\left(R_s\right) \leq P$ where, † represents Hermitian transpose. R_s & R_w are the correlation matrices of the transmitted signal vector s and the channel noise vector w.

When the signals are drawn from a white gaussian code book,

$$\begin{aligned} R_s &= E\left[ss^*\right] \\ &= \sigma_s^2 I_{N_t} \end{aligned} \tag{B.1.21}$$

N_r elements of the channel noise vector w are iid complex gaussian random variable,

$$\begin{aligned} R_w &= E\left[ww^*\right] \\ &= \sigma_w^2 I_{N_r} \end{aligned} \tag{B.1.22}$$

$$C = E\left[\log_2\left(I_{N_r} + \frac{\sigma_s^2}{\sigma_w^2}HH^\dagger\right)\right] \tag{B.1.23}$$

$$\rho = \frac{P}{\sigma_w^2} = \frac{N_t\sigma_s^2}{\sigma_w^2} \tag{B.1.24}$$

$$C = E\left[\log_2\left(\det\left(I_{N_r} + \frac{\rho}{N_t}HH^\dagger\right)\right)\right] \tag{B.1.25}$$

which gives the ergodic capacity for a MIMO flat faded channel, assuming $N_t > N_r$. For $N_t = N_r = N$ the capcity can be written as,

$$C = E\left[\log_2\left(\det\left(I_N + \frac{\rho}{N}HH^\dagger\right)\right)\right] \tag{B.1.26}$$

Bibliography

[ABB+07] P. Almers, E. Bonek, A. Burr, N. Czink, M. Debbah, V. Degli-Esposti, H. Hofstetter, P. Kyosti, D. Laurenson, G. Matz, A. F. Molisch, C. Oestges, and H. Ozcelik. Survey of channel and radio propagation models for wireless MIMO systems. *EURASIP Journal on Wireless Communications and Networking*, 2007(1):56–75, January 2007.

[AESVH06] A. A. Abouda, H. M. El-Sallabi, L. Vuokko, and S. G. Haggman. Performance of stochastic kronecker mimo radio channel model in urban microcells. In *Proceedings of 17th Annual IEEE International Symposium on Personal, Indoor and Mobile Radio Communications (PIMRC'06)*, 2006.

[AH86] A. S. Akki and F. Haber. A statistical model of mobile-to-mobile land communication channel. *IEEE Transactions on Vehicular Technology*, VT-35(1):2–7, 1986.

[AK02] A. Abdi and M. Kaveh. A space time correlation model for multelement antenna systems in mobile fading channels. *IEEE Journal on Selected Areas in Communications*, 20(3):550–560, 2002.

[Akk94] A. S. Akki. Statistical properties of mobile-to-mobile land communication channels. *IEEE Transactions on Vehicular Technology*, 43(4):826–831, 1994.

[BC05] N. C. Beaulieu and C. Cheng. Efficient Nakagami-m fading channel simulation. *IEEE Transactions on Vehicular Technology*, 54(2):413–424, March 2005.

[BDBU05] M. E. Bialkowski, S. Durrani, K. Bialkowski, and P. Uthansakul. Understanding and analyzing the performance of MIMO systems from the microwave perspective. In *Proceedings of IEEE MTT-S Microwave Symposium Digest*, volume 2, pages 2251–2254, June 2005.

[BUBD06] M. E. Bialkowski, P. Uthansakul, K. Bialkowski, and S. Durrani. Investigating the performance of mimo systems from an electromagnetic perspective. In *Proceedings of Microwave and Optical Technology Letters*, volume 48, pages 1233–1238, July 2006.

[DM05] M. Debbah and R. R. Muller. MIMO channel modeling and the principle of maximum entropy. *IEEE Transactions on Information Theory*, 51(5):1667–1690, 2005.

[ECS+01] R. B. Ertel, P. Carderi, K. W. Sowerby, T. S. Rappaport, and J. H. Reed. Overview of spatial channel models for antenna array communication systems. In *Proceedings of IEEE Vehicular Technology conference (VTC'01)*, volume 2, pages 1078–1082, October 2001.

[ER99] R. B. Ertel and J. H. Reed. Angle and time of arrival statistics for circular and elliptical scattering models. *IEEE Journal on Selected Areas in Commnunication*, 17(11):1829–1840, November 1999.

[FJ98] G. J. Foschini and M. J.Gans. On limits of wireless communications in a fading environment when using multiple antennas. In *Wireless Personal Communications*, volume 6, pages 311–335, March 1998.

[FMB98] J. Fuhl, A. F. Molisch, and E. Bonek. Unified channel model for mobile radio systems with smart antennas. In *IEEE Proceedings of Radar, Sonar and Navigation*, volume 145, pages 32–41, 1998.

[GK83] I. J. Gupta and A. K. Ksienski. Effect of mutual coupling on the performance of adaptive arrays. *IEEE Transactions on Antennas and Propagation*, 31(5):785–791, September 1983.

[Gol05] A. Goldsmith. *Wireless Communications*. Cambridge University Press, 2005.

[GR94] I. S. Gradshteyn and I. M. Ryzhik. *Tables of Integrals, Series, and Products*. CA: Academic, San Diego, 5th ed edition, 1994.

[GS05] A. B. Gershman and N. D. Sidiropoulo. *Space-Time Processing for MIMO Communications*. John Wiley & Sons, Ltd, 2005.

[GSS+03] D. Gesbert, M. Shafi, D. Shiu, P. J. Smith, and A. Naguib. From theory to practice: An overview of MIMO space-time coded wireless systems. *IEEE Journal on Selected Areas in Communications*, 21(3):281–302, April 2003.

[Gup80] K. C. Gupta. *Microwaves*. Wiley, 1980.

[HA04a] M. O. Hasna and M-S. Alouini. Harmonic mean and end-to-end performance of transmission systems with relays. *IEEE Transactions on Communications*, 52(1):132–135, January 2004.

[HA04b] M. O. Hasna and M-S. Alouini. A performance study of dual-hop transmissions with fixed gain relays. *IEEE Transactions on Wireless Communications*, 3(6):1963–1968, November 2004.

[Hay01] S. Haykin. *Communication Systems*. John Wiley & Sons, INC, 4th edition, 2001.

[HM05] S. Haykin and M. Moher. *Modern Wireless Communications*. Pearson Prentice Hall, 2005.

[HP04] B. O. Hogstad and M. Patzold. Capacity studies of MIMO channel models based on the geometrical one-ring scattering model. In *Proceedings of the 15th IEEE International Symposium Personal, Indoor and Mobile Radio Communications (PIMRC 2004)*, volume 3, pages 1613–1617, September 2004.

[HZF04] P. Herhold, E. Zimmermann, and G. Fettweis. A simple cooperative extension to wireless relaying. In *Proceedings of International Zuric Seminar on Communications*, pages 36–39, February 2004.

[Jak74] W. C. Jakes. *Microwave Mobile Communications*. IEEE Press, 1974.

[Jan01] R. Janaswamy. *Radiowave Propagation And Smart Antennas For Wireless Communications*. Kluwer Academic Publishers, 2001.

[Jan02] R. Janaswamy. Angle and time of arrival statistics for the gaussian scatter density model. *IEEE Transactions on Wireless Communications*, 1(3):488–497, July 2002.

[JT07] L. Jiang and S.Y. Tan. Geometrically based statistical channel models for outdoor and indoor propagation environments. *IEEE Transactions on Vehicular Technology*, 56(6):3587–3593, November 2007.

[KSM05] G.K. Karagiannidis, N.C. Sagias, and P.T. Mathiopoulos. The N* Nakagami fading channel model. In *Proceedings of 2nd International Symposium on Wireless Communication Systems*, September 2005.

[KSP+02] J. P. Kermoal, L. Schumacher, K. I. Pedersen, P. E. Mogensen, and F. Frederiksen. A stochastic MIMO radio channel model with experimental validation. *IEEE Journal on Selected Areas in Communications*, 20(6):1211–1226, 2002.

[KTM03] G. K. Karagiannidis, T. A. Tsiftsis, and R. K. Mallik. Bounds for multihop relayed communications in Nakagami-m fading. *IEEE Transactions on Communications*, 51(1):18–22, January 2003.

[Kuh06] Volker Kuhn. *Wireless Communications over MIMO Channels*. John Wiley & sons, 2006.

[Loy02] S. Loyka. MIMO channel capacity: electromagnetic wave perspective. In *Proceedings of the 27th URSI General Assembly*, Maastricht, Netherlands, August 2002.

[LR96] J. C. Liberti and T. S. Rappaport. A geometrically based model for line-of-sight multipath radio channels. In *Proceedings of IEEE 46th Vehicular Technology Conference (VTC '96)*, volume 2, pages 844–848, April-May 1996.

[LTW04] J. N. Laneman, D. Tse., and G.W. Wornell. Cooperative diversity in wireless networks: Efficient protocols and outage behavior. *IEEE Transactions on Information Technology*, 50(12):3062–3080, December 2004.

[LV07] Y. Liang and V. V. Veeravalli. Cooperative relay broadcast channels. *IEEE Transactions on Information Technology*, 53(3):900–928, March 2007.

[Nak60] M. Nakagami. The m-distribution - a general formula of intensity distribution of rapid fading. In *Statistical Methods in Radio WavePropagation*, pages 3–36. Oxford, U.K.: Pergamon, 1960.

[OAH04] M. K. Ozdemir, E. Arvas, and H.Arslan. Dynamics of spatial correlation and implications on mimo systems. *IEEE Communication Magazine*, 42(6):S14–S19, June 2004.

[OC07] Claude Oesteges and Bruno Clerckx. *MIMO Wireless Communications: From Real-World Propagation to Space-Time Code Design*. Academic Press, 2007.

[OEP03] C. Oestges, V. Erceg, and A. J. Paulraj. A physical scattering model for MIMO macrocellular broadband wireless channels. *IEEE Journal on Selected Areas in Communications*, 21(5):721–729, 2003.

[OEP04] C. Oestges, V. Erceg, and A.J. Paulraj. Propagation modeling of MIMO multipolarized fixed wireless channels. *IEEE Transactions on Vehicular Technology*, 53(3):644–654, May 2004.

[OHA04] M. K. Ozdemir, H.Arslan, and E. Arvas. On the correlation analysis of antennas in adaptive mimo systems with 3-d multipath scattering. In *Proceedings of IEEE Wireless Communications and Networking Conference*, volume 1, pages 295–299, March 2004.

[Pap91] A. Papoulis. *Probability, random variables and stochastic processes*. McGraw Hill, New York, 1991.

[PB06a] B. S. Paul and R. Bhattacharjee. Effect of array geometry on the capacity of outdoor MIMO communication: A study. In *Proceedings of IEEE Indicon*, pages 1–4, September 2006.

[PB06b] B. S. Paul and R. Bhattacharjee. Studies on the mutual coupling of one ring MIMO channel simulation model. In *Proceedings of the International Conference on Computers and Devices for Communication (CODEC-06)*, Kolkata, December 2006.

[PB07a] B. S. Paul and R. Bhattacharjee. Maximal ratio combining of two amplify-forward relay branches with individual links experiencing Nakagami fading. In *Proceedings of IEEE TENCON*, October 2007.

[PB07b] B. S. Paul and R. Bhattacharjee. Selection combining of two amplify-forward relay branches with individual links experiencing Nakagami fading. In *Proceedings of IEEE 2007 Asia Pacific Conference on Communication*, pages 449–452, October 2007.

[PB07c] B. S. Paul and R. Bhattacharjee. An S-parameter based modeling of a MIMO channel using half-wave dipole antennas. In *Proceedings of the Thirteenth National Conference on Communications (NCC)*, January 2007.

[PH04] M. Patzold and B. O. Hogstad. A space-time channel simulator for MIMO channels based on the geometrical one-ring scattering model. In *Proceedings of the Vehicular Technology Conference(VTC 2004)*, volume 1, pages 144–149, September 2004.

[PHYK05a] M. Patzold, B. O. Hogstad, N. Youssef, and D. Kim. A MIMO mobile-to-mobile channel model: Part-I The reference model. In *Proceedings of IEEE 16th International Symposium on Personal, Indoor and Mobile Radio Communications*, volume 1, pages 573–578, September 2005.

[PHYK05b] M. Patzold, B. O. Hogstad, N. Youssef, and D. Kim. A MIMO mobile-to-mobile channel model: Part II The simulation model. In *Proceedings of IEEE 16th International Symposium on Personal, Indoor and Mobile Radio Communications*, volume 1, pages 562–567, September 2005.

[PNG03] A. J. Paulraj, R. U. Nabar, and D. Gore. *Introduction to Space-Time Wireless Communications*. Cambridge University Press, 2003.

[PRR96] P. Petrus, J. H. Reed, and T. S. Rappaport. Geometrically based statistical channel model for macrocellular mobile environments. In *Proceedings of IEEE Globecom*, pages 1197–1201, 1996.

[PRR02] P. Petrus, J. H. Reed, and T. S. Rappaport. Geometrical-based statistical macrocell channel model for mobile environments. *IEEE Transactions on Communications*, 50(3):495–502, March 2002.

[PSP05] C. S. Patel, G. L. Stuber, and T. G. Pratt. Simulation of Rayleigh-faded mobile-to-mobile communication channels. *IEEE Transactions on Communications*, 53(11):1876–1884, 2005.

[PSP06] C. S. Patel, G. L. Stuber, and T. G. Pratt. Statistical properties of amplify and forward relay fading channels. *IEEE Transactions on Vehicular Technology*, 55(1):1–9, 2006.

[PWS+04] R. Pabst, B. H. Walke, D. C. Schultz, P. Herold, H. Yanikomeroglu, S. Mukherjee, H. Viswanathan, M. Lott, W. Zirwas, M. Dohler, H. Aghvami, D. D. Falconer, and G. P. Fettweis. Relay-based deployment concepts for wireless and mobile broadband radio. *IEEE Communication Magazine*, pages 80–89, September 2004.

[Rap01] T. S. Rappaport. *Wireless Communications: Principles and Practice*. Prentice Hall, 2001.

[RS00] V. K. Rohatgi and E. Saleh. *An Introduction to Probability and Statistics*. Wiley-Interscience, 2000.

[SEA03a] A. Sendonaris, E. Erkip, and B. Aazhang. User cooperation diversity part-I: System description. *IEEE Transactions on Communications*, 51(11):1927–1938, November 2003.

[SEA03b] A. Sendonaris, E. Erkip, and B. Aazhang. User cooperation diversity part-II: Implementation aspects and performance analysis. *IEEE Transactions on Communications*, 51(11):1939–1948, November 2003.

[SFGK00] D. Shiu, G. J. Foschini, M. J. Gans, and J. M. Kahn. Fading correlation and its effect on the capacity of multielement antenna systems. *IEEE Transactions on Communications*, 48(3):502–513, March 2000.

[SR01] T. Svantesson and A. Ranheim. Mutual coupling effects on the capacity of multielement antenna systems. In *Proceedings of the IEEE International Conference on Acoustics, Speech, and Signal Processing (ICASSP)*, volume 4, pages 2485–2488, May 2001.

[SV87] A. A. M. Saleh and R. A. Valenzuela. A statistical model for indoor multipath propagation. *IEEE Journal on Selected Areas of Communication*, SAC-5(2):128–137, February 1987.

[Tel99] I. E. Teletar. Capacity of multi-antenna gaussian channels. *European Transactions on Telecommunications*, 10(6):585–595, 1999.

[Tso06] George Tsoulos, editor. *MIMO System Technology for Wireless Communications*. CRC Press, 2006.

[TSRK04] W. H. Tranter, K. S. Shanmugan, T. S. Rappaport, and K. L. Kosbar. *Principles of Communications Systems Simulation With Wireless Applications*. Prentice Hall, 2004.

[VF97] F. Vatalaro and A. Forcella. Doppler spectrum in mobile-to-mobile communications in the presence of three-dimensional multipath scattering. *IEEE Transactions on Vehicular Technology*, 46(1):213–219, 1997.

[WHOB06] W. Weichselberger, M. Herdin, H. Ozcelik, and E. Bonek. A stochastic MIMO channel model with joint correlation of both link ends. *IEEE Transactions on Wireless Communications*, 1(6):90–99, 2006.

[Wir] WireMOM, http://www.sp.se/electronics/forms/eng/WireMoM.htm.

[WJ01] J. W. Wallace and M. A. Jensen. Statistical characteristics of measured MIMO wireless channel data and comparison to conventional models. In *Proceedings of the 54th IEEE Vehicular Technology Conference (VTC 01)*, volume 2, pages 1078–1082, Sidney, Australia, October 2001.

[WJ04] J. W. Wallace and M. A. Jensen. Mutual coupling in MIMO wireless systems: A rigorous network theory analysis. *IEEE Transactions On Wireless Communications*, 3(4):1317–1325, July 2004.

[WSW04] C. Waldschmidt, S. Schulteis, and W. Weisbeck. Complete RF system model for analysis of compact MIMO arrays. *IEEE Transactions On Vehicular Technology*, 53(3):579–586, May 2004.

[ZS06] A. G. Zajic and G. L. Stuber. A new simulation model for mobile-to-mobile Rayleigh fading channels. In *Proceedings of IEEE WCNC*, volume 3, pages 1266–1270, April 2006.